Mathematic Approaches for the Calibration of the CHAMP Satellite Magnetic Field Measurements

Von der Mathematisch-Naturwissenschaftlichen Fakultät
der Universität Potsdam
zur Erlangung des Grades eines Doktors
der Naturwissenschaften (Dr.rer.nat.)
genehmigte Dissertation

von Yin, Fan

1.Gutachter: Prof. Dr. Hermann Lühr
2.Gutachter: Prof. Dr. Matthias Holschneider

eingereicht am 25. Juni 2009
mündliche Prüfung (Disputation) am 14. Januar 2010

Published online at the
Institutional Repository of the University of Potsdam:
URL http://opus.kobv.de/ubp/volltexte/2010/4120/
URN urn:nbn:de:kobv:517-opus-41201
http://nbn-resolving.org/urn:nbn:de:kobv:517-opus-41201

Summary

CHAMP (CHAllenging Minisatellite Payload) is a German small satellite mission to study the earth's gravity field, magnetic field and upper atmosphere. Thanks to the good condition of the satellite so far, the planned 5 years mission is extended to year 2009. The satellite provides continuously a large quantity of measurement data for the purpose of Earth study. The measurements of the magnetic field are undertaken by two Fluxgate Magnetometers (vector magnetometer) and one Overhauser Magnetometer (scalar magnetometer) flown on CHAMP. In order to ensure the quality of the data during the whole mission, the calibration of the magnetometers has to be performed routinely in orbit. The scalar magnetometer serves as the magnetic reference and its readings are compared with the readings of the vector magnetometer. The readings of the vector magnetometer are corrected by the parameters that are derived from this comparison, which is called the scalar calibration. In the routine processing, these calibration parameters are updated every 15 days by means of scalar calibration. There are also magnetic effects coming from the satellite which disturb the measurements. Most of them have been characterized during tests before launch. Among them are the remanent magnetization of the spacecraft and fields generated by currents. They are all considered to be constant over the mission life.

The 8 years of operation experience allow us to investigate the long-term behaviors of the magnetometers and the satellite systems. According to the investigation, it was found that for example the scale factors of the FGM show obvious long-term changes which can be described by logarithmic functions. The other parameters (offsets and angles between the three components) can be considered constant. If these continuous parameters are applied for the FGM data processing, the disagreement between the OVM and the FGM readings is limited to $\pm 1nT$ over the whole mission. This demonstrates, the magnetometers on CHAMP exhibit

a very good stability. However, the daily correction of the parameter Z component offset of the FGM improves the agreement between the magnetometers markedly. The Z component offset plays a very important role for the data quality. It exhibits a linear relationship with the standard deviation of the disagreement between the OVM and the FGM readings. After Z offset correction, the errors are limited to $\pm 0.5nT$ (equivalent to a standard deviation of $0.2nT$).

We improved the corrections of the spacecraft field which are not taken into account in the routine processing. Such disturbance field, e.g. from the power supply system of the satellite, show some systematic errors in the FGM data and are misinterpreted in 9-parameter calibration, which brings false local time related variation of the calibration parameters. These corrections are made by applying a mathematical model to the measured currents. This non-linear model is derived from an inversion technique. If the disturbance field of the satellite body are fully corrected, the standard deviation of scalar error $\triangle B$ remains about $0.1nT$.

Additionally, in order to keep the OVM readings a reliable standard, the imperfect coefficients of the torquer current correction for the OVM are redetermined by solving a minimization problem. The temporal variation of the spacecraft remanent field is investigated. It was found that the average magnetic moment of the magneto-torquers reflects well the moment of the satellite. This allows for a continuous correction of the spacecraft field. The reasons for the possible unknown systemic error are discussed in this thesis. Particularly, both temperature uncertainties and time errors have influence on the FGM data. Based on the results of this thesis the data processing of future magnetic missions can be designed in an improved way. In particular, the upcoming ESA mission Swarm can take advantage of our findings and provide all the auxiliary measurements needed for a proper recovery of the ambient magnetic field.

Zusammenfassung

CHAMP(CHAllenging Minisatellite Payload) ist eine deutsche Kleinsatellitenmission für die Forschung und Anwendung in Bereich der Geowissenschaften und Atmosphärenphysik. Das Projekt wird vom GFZ geleitet. Mit seinen hochgenauen, multifunktionalen, sich ergänzenden Nutzlastelementen (Magnetometer, Akzelerometer, Sternsensor, GPS-Empfänger, Laser-Retroreflektor, Ionendriftmeter) liefert CHAMP erstmalig gleichzeitig hochgenaue Schwere- und Magnetfeldmessungen (seit Mitte 2000). Dank des bisherigen guten Zustandes des Satelliten ist die auf 5 Jahre ausgelegte Mission bis 2009 verlängert geworden. An Board befinden sich ein skalares Overhauser-Magnetometer(OVM) für Kalibrierungszwecke sowie zwei Fluxgate-Magnetometer(FGM) zur Messung des magnetischen Feldvektors. Die Messungen vom FGM werden immer verglichen mit denen vom OVM und korregiert im Fall von Widersprüche, das ist die sog. Skalar-Kalibrierung. Um eine zuverlässige Datenqualität während der 8 jährigen Mission zu garantieren, ist die Nachkalibrierung implementiert. Im Rahmen der standard mäßigen Datenverarbeitung werden die Instrumentenparameter des FGM alle 15 Tage neu bestimmt. Das Ziel der vorliegenden Arbeit ist es, eine Verbesserung der Vektormagnetfelddaten zu erzielen durch eine neue Methode der Kalibreirung, die die Eigenschaften der Sensoren und Störung vom Raumfahrzeug mit berücksichtigt. Die Erfahrung aus den zurückliegenden Jahren hat gezeigt, dass sich die Skalenfaktoren des FGM stark mit der Zeit ändern. Dieser Verlauf läßt sich gut durch eine Logarithmuskurve anpassen. Andere Parameter wie die Winkel und die Offsets scheinen stabil zu sein. Eine Ausnahme macht der Offset der Z-Komponent. Dieser bedarf einer regelmäßigen Korrektur. Während die Standardverarbeitung eine undifferenzierte Bestimmung aller 9 FGM Parameter durch nicht-lineare Inversion der skalar Daten vornimmt, beziehen wir jetzt die langzeitlichen Eigenschaften der Parameter in die Bestimmung mit ein. Eine weitere Verbesserung der CHAMP-Magnetfelddaten konnte erreicht werden durch geeignte Berücksichtigung von Störung vom Raumfahrzeug. Die verbleibenden Unsicherheiten konnten durch diese Massnahmen auf eine Standardabweichung von $0.1nT$ reduziert werden.

Contents

Chapter 1

Introduction

1.1 The Aim of the Thesis

CHAMP (CHAllenging Minisatellite Payload) is a German small satellite mission to study the earth's gravity field, magnetic field and upper atmosphere. The CHAMP satellite was launched into space with a Russian COSMOS launch vehicle on July 15, 2000 at the altitude of 454 km. This mission was scheduled to last for 5 years in order to provide a sufficiently long observation time to resolve long-term temporal variations primarily in the magnetic field, in the gravity field and within the atmosphere. Thanks to the good condition of the satellite so far the mission is extended to 2009 after three successful altitude maneuvers. The satellite as of Oct. 2008 flies at about 338 km altitude and still provides the scientists with reliable measurement data. The long time continuous observations of CHAMP enable us to learn more about the changes in the Earth system.

Launch Date	July 2000
Mission Duration	nominal 5 years (extended to 2010)
Altitude	470 km - 300 km
Inclination	87.3 deg
Eccentricity	< 0.001
Spatial Coverage	global
Temporal Coverage	all local times
Satellite Mass	522 kg (at launch)
Satellite Dimensions	1621 mm in width and 8333 mm in length (including 4044 mm for the boom)

In order to identify reliably long-term trends in the measured quantities the calibration of the on-board instruments has to be maintained over the mission life time. This thesis is focusing on the magnetometers. As part of the mission design a scalar magnetometer was assigned as the magnetic reference. The readings of the vector magnetometer were routinely compared with the data of the scalar instrument and corrected if inconsistencies occurred. The purpose of this thesis is to revisit the in-flight calibration and look for possible improvements of the magnetic field data.

The approach we are taking is considering also the characteristics of the sensors as revealed from the 8 years of operation in space. This concerns in particular the dependence on environmental conditions and temporal changes. Our aim is to reprocess all the magnetic field data using a common algorithm. This promises to provide a more consistent image of the geomagnetic field evolution.

1.2 Science instruments on the satellite CHAMP

The CHAMP mission focuses on geo-scientific research and applications. The effective payload of the satellite, consequently, is employed for the purposes of

- Earth's gravity field recovery
- Earth's magnetic field recovery
- global Earth's atmosphere sounding
- Earth's ionosphere sounding
- Complimentary tracking system with onboard GPS for precise orbit determination and gravity recovery
- Two-color laser ranging experiments

The following figure shows the science instruments carried by the CHAMP satellite and their locations on it. We now introduce more details about the instruments used to observe the Earth's magnetic field.

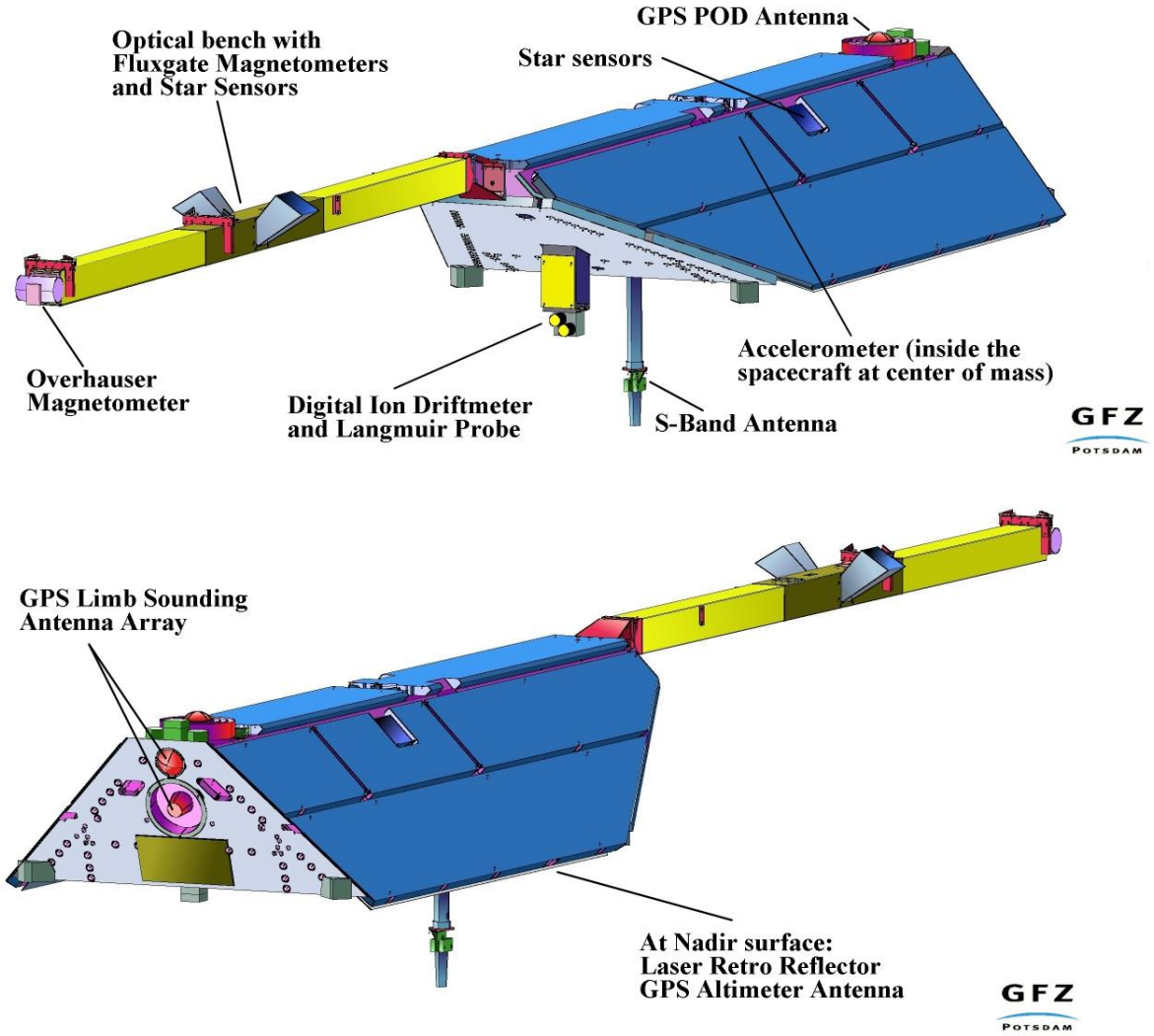

1.2.1 Fluxgate Magnetometer(FGM)

For redundancy reasons the CHAMP satellite carries two Fluxgate Magnetometers on the boom. Both are mounted together with the star cameras (ASC) on a common optical bench. They were developed and manufactured under contract by the DTU (Technical University of Denmark) Lyngby. The design is based on the CSC (Compact Spherical Coil) sensor which was newly developed for the Ørsted mission and presently demonstrates its outstanding per-

formance in orbit. Different to an absolute scalar magnetometer the FGM can provide us with the vector measurements of the Earth's magnetic field. This is very important for our global magnetic field model study and helps us to learn more about the currents in the ionosphere. The table below gives us the technical characteristics of the FGM.

Bit number of ADC	24 bit
Range	±65 000 nT
Resolution	10 pT
Deviation from linearity	±100 pT
Noise level	$<$ 100 pT (rms)
Sample rate	50 Hz (nominal), 10 Hz, 1 Hz
-3 dB bandwidth	13 Hz
Offset drift	$<$ 0.5 nT
Sensor weight dimensions	350 g (each) Ø 82 mm
Electronics box(for both sensors)	3.5 kg
Power Consumption dimensions	2 W (each) 204x194x101 mm^3

In the nominal operation mode the field vector is sampled by the FGM at a rate of 50Hz providing a spatial resolution along the orbit of approximately 150m. There are other modes which allow reducing the demands on data transmission. Both options, data compression and reduced sampling rates can be freely combined.

1.2.2 Overhauser Magnetometer(OVM)

The Overhauser Magnetometer is a type of magnetometer whose operational principle is based on measuring the frequency of the proton precession signals. The advantage of the Overhauser magnetometer is that the sensor is omnidirectional and shows no dead zones, it can provide precise absolute measurements of the ambient magnetic field strength without drift and dependency on temperature. In order to keep the influence of the magnetic stray field of the spacecraft as low as possible the OVM sensor is mounted at the tip of a 4 m long deployable boom. The electronics box is placed inside the satellite body to provide more comfortable environmental conditions. For these reasons the OVM is chosen to serve as the magnetic field standard for the CHAMP mission. Through the whole mission the OVM data are used to calibrate the readings of the FGM instrument.

Range	18,000 - 65,000 nT
Resolution	10 pT
Noise level	$<$ 50 pT (rms)
-3 dB bandwidth	0.28 Hz
Sample rate	1 Hz
Absolute accuracy	$<$ 0.5 nT
deviation from omnidirectionality	$<$ 0.2 nT
Sensor weight	1 kg
Electronics weight	2 kg
Power consumption	4.5 W
Sensor dimensions	Ø 90x180 mm
Electronics box dimensions	200x135x76 mm^3

From this table we can obtain more details about the OVM on the CHAMP satellite. There is only one operation mode: the ambient field strength is continuously sampled at a rate of 1 Hz. With the help of the GPS clock the instrument regularly checks the frequency of the internal crystal oscillator to ensure a precise measurement.

1.2.3 Advanced Stellar Compass(ASC)

Without the attitude information the vector measurements can provide the data only in the local spacecraft coordinates. There are two Advanced Stellar Compass (ASC) assemblies on the CHAMP satellite. The one on the boom provides the high precision attitude information needed for the magnetic field vector measurements and the other on the spacecraft body serves primarily the three component STAR accelerometer and the Digital Ion Drift Meter (DIDM). The common Data Processing Unit (DPU) of the ASC compares the digital star images acquired by the Camera Head Units (CHU) with an on-board stored star catalogue to calculate the high precision attitude information. This information is used also by the satellite attitude control system.

Attitude determination precision	4 arcsec (3σ , BOL)
Field of view	18.4° x 13.4°
Sampling rates	1 Hz (nominal), 0.5, 2 Hz
Magn. moment CHU	10^{-5} Am
Power consumption	8 W
CHU weight	200 g (exclusive baffles)
DPU weight	800 g
CHU dimensions	50x50x45 mm^3
DPU box dimensions	100x100x100 mm^3

Based on the measurement of the ASC, the data processing group can provide the final users with the magnetic field vector data in Earth-fixed coordinates.

1.3 The orbit of the CHAMP satellite

On 15th July 2000 the CHAMP satellite was launched with a Russian COSMOS launch vehicle into an almost circular, near polar (i=87°) orbit with an initial altitude of 454km. The orbit characteristics and the reason why we choose such an orbit can be summarized by these tables.

Circular and near polar
Homogeneous and complete global coverage of the Earth's sphere
Important to resolve gravitational and magnetic geo-potentials

Inclination of 87°
Local time variation of the satellite's ground track (24 hours in 260.5 days)
Separate constituents of periodic phenomena like tides, day-night and seasonal variations

Initial altitude of 454 km
Guarantee a planned 5-year observation period above 300 km
Adequate to observe the Earth's magnetic main field.
Compromise for both atmosphere/ionosphere study and the gravity field study

=

In one word, such an orbit ensures as much as possible a full spatial and temporal coverage of the geo-scientific observations undertaken by the CHAMP satellite. Due to atmospheric

drag and the solar activity the altitude of the satellite will decrease during the mission. After 2 orbit raise maneuvers in 2002 CHAMP was able to provide further highly valuable data. On 27th March 2006(MJD=2277) another orbit raise maneuvreer was successfully performed. The CHAMP mission is extend through 2009. Its lifetime is now much longer than it was designed.

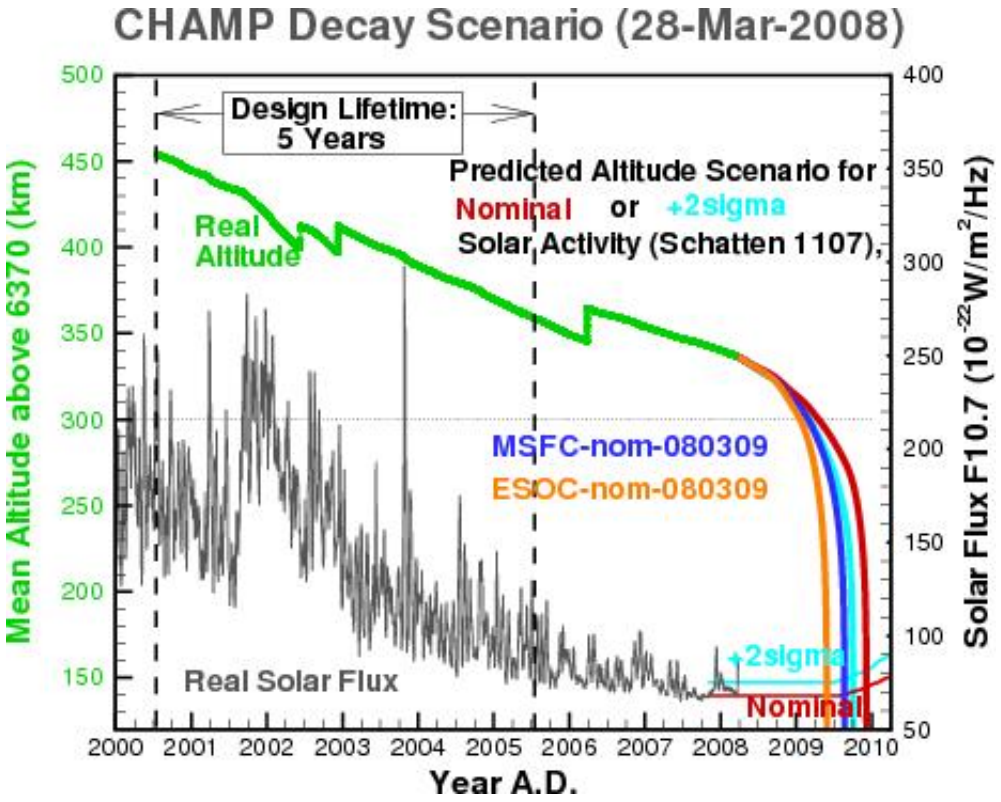

Chapter 2

The Calibration of CHAMP Magnetometers

The CHAMP satellite carries two Fluxgate Magnetometers (FGM), which measure the vector components of the Earth's magnetic field, and one Overhauser Magnetometer (OVM), which provides highly accurate absolute measurements of the magnitude and serves also as a reference instrument to calibrate the FGM vector magnetic field data. It can be imagined that no instrument is ideal, and although the structure of the satellite was very well designed, the local magnetic field of the spacecraft is still not zero at the magnetometers position. In this chapter we discuss all the sources that induce errors in the Earth's magnetic field measurements. The magnetic field at the FGM1 position is termed B_{fgm}, and at the OVM position B_{ovm}. The Earth's magnetic field, which we are interested in, is B_{em_fg} at FGM1 and B_{em_ov} at OVM. Because the distance (1.75m) between FGM1 and OVM is very short and the Earth's magnetic field on such small scale is homogeneous, B_{em_fg} is the same as B_{em_ov}.

$$B_{fgm} = B_{em\_fg} + B_{sc\_fg}$$

$$B_{ovm} = B_{em\_ov} + B_{sc\_ov}$$

where B_{sc_fg} and B_{sc_ov} are the spacecraft fields, respectively, at positions FGM1 and OVM. Many sources on the spacecraft can produce the disturbing magnetic fields, for example, the magneto-torquer currents. We will discuss more details later. If FGM and OVM are ideal instruments, that means the magnetometer outputs $E_{fgm} = B_{fgm}$ and $E_{ovm} = |B_{ovm}|$, and if we know exactly B_{sc_fg} and B_{sc_ov}, we can write,

$$B_{em\_fg} = E_{fgm} - B_{sc\_fg}$$
$$|B_{em\_ov}| = E_{ovm} - \frac{B_{em\_fg}}{|B_{em\_fg}|} \bullet B_{sc\_ov}$$

Figure 2.1

2.1 A linear vector magnetometer

However, no magnetometer is an ideal instrument. For the fluxgate magnetometers the pre-flight test has shown that it is almost a linear instrument. We now discuss the mathematical way to characterize the FGM.

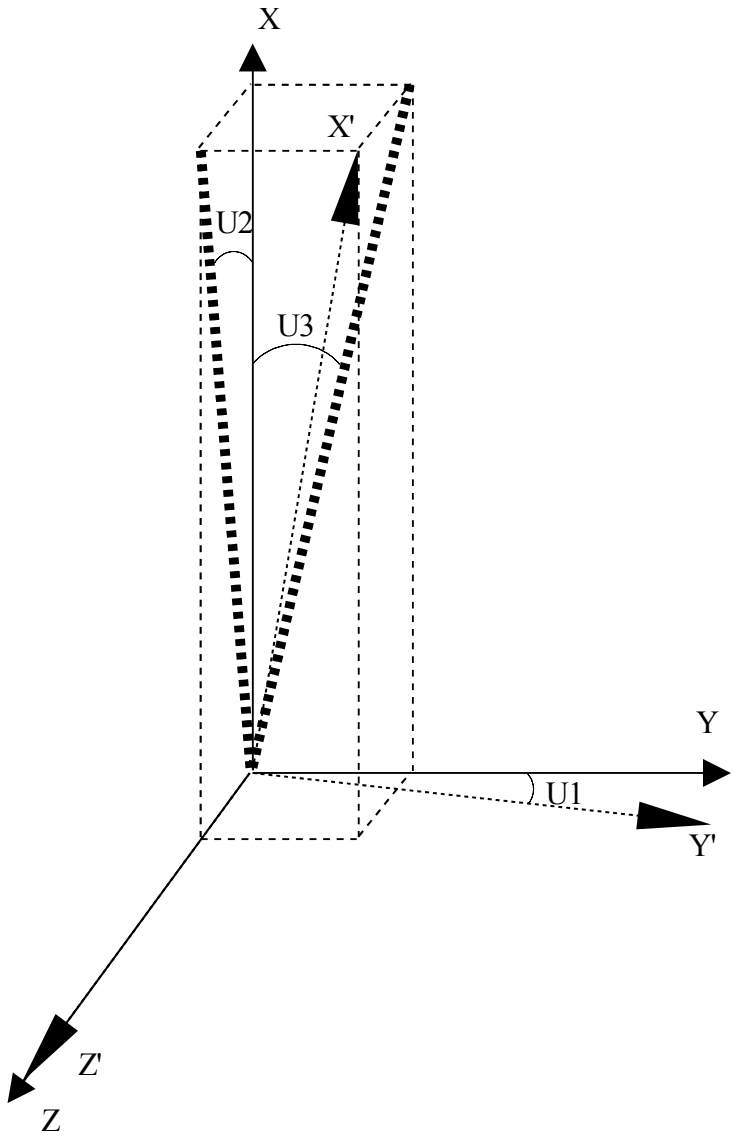

Figure 2.2

X', Y', Z' are the three sensor axes of the fluxgate magnetometer. Ideally, they are perpendicular to each other. However, it can't be technically realized, therefore the coordinate system based on these slightly skewed mechanical axes is non-orthogonal. As we will see, we can still build up a Cartesian reference frame from these non-orthogonal mechanical axes. We define the first principal axis (Z) which is totally aligned with the Z' mechanical axis.

The other component X is chosen to be perpendicular to the plane defined by the axes Z' and Y'. Consequently, the axis Y is defined to be perpendicular to both axes Z and X. Furthermore, it lies in the plane Z'Y'. There are unlimited options of definitions to build up an orthonormal basis from the sensor axes. But this definition is the simplest one. We will see, the transformation matrix involving three coefficients has a simple form. The relationship between the orthonormal basis and non-orthonormal basis can be described angles as follows:

$$\begin{pmatrix} E_x' \\ E_y' \\ E_z' \end{pmatrix} = A \begin{pmatrix} B_x \\ B_y \\ B_z \end{pmatrix} \tag{2.1}$$

Figure 2.2 illustrates the geometric relation between the two coordinate systems with misalignment angles U_1, U_2, U_3. So the transformation matrix A is expressed

$$A = \begin{pmatrix} a_1 & a_2 & a_3 \\ 0 & a_4 & a_5 \\ 0 & 0 & 1 \end{pmatrix} \tag{2.2}$$

with $a_1 = \frac{1}{W}$, $a_2 = \frac{\tan U_2}{W}$, $a_3 = \frac{\tan U_3}{W}$, $a_4 = \cos U_1$, $a_5 = \sin U_1$, $W = \sqrt{1 + (\tan U_2)^2 + (\tan U_3)^2}$. The angles U_1, U_2, U_3 are all close to zero. Notice that the FGM output of each component is affected also by the intrinsic offset and scale factor of the sensor. Therefore, these should be corrected first,

$$\begin{pmatrix} E_x \\ E_y \\ E_z \end{pmatrix} = \begin{pmatrix} S_x E_x' \\ S_y E_y' \\ S_z E_z' \end{pmatrix} + \begin{pmatrix} E_{x0} \\ E_{y0} \\ E_{z0} \end{pmatrix} \tag{2.3}$$

where E_{x0}, E_{y0}, E_{z0} are offsets and S_x, S_y, S_z are scale factors of the components. If we have the output readings of FGM, we can now calculate the observed magnetic field by FGM, which is expressed as:

$$\begin{pmatrix} E_x \\ E_y \\ E_z \end{pmatrix} = \begin{pmatrix} S_x a_1 & S_x a_2 & S_x a_3 \\ 0 & S_y a_4 & S_y a_5 \\ 0 & 0 & S_z \end{pmatrix} \begin{pmatrix} B_x \\ B_y \\ B_z \end{pmatrix} + \begin{pmatrix} E_{x0} \\ E_{y0} \\ E_{z0} \end{pmatrix} \tag{2.4}$$

Knowing S_x, S_y, S_z, U_1, U_2, U_3, E_{x0}, E_{y0}, E_{z0} and the output of the FGM we can derive the magnetic field. In this sense these nine parameters fully describe the character of the tri-axial sensor Fluxgate Magnetometer.

As we know, S_x, S_y, S_z are very close to 1 and U_1, U_2, U_3 are close to zero. Equation 2.4 can be written in this simplified inverse way,

$$\begin{pmatrix} B_x \\ B_y \\ B_z \end{pmatrix} = \begin{pmatrix} l_x & \cos a_{xy} & \cos a_{xz} \\ 0 & l_y & \cos a_{yz} \\ 0 & 0 & l_z \end{pmatrix} \left[\begin{pmatrix} E_x \\ E_y \\ E_z \end{pmatrix} - \begin{pmatrix} E_{x0} \\ E_{y0} \\ E_{z0} \end{pmatrix} \right]$$

where l_x, l_y, l_z represent approximately the scale factors and a_{xy}, a_{xz}, a_{yz} represent the angles between any two axes of the three sensor elements. However, the FGM is only almost a linear instrument. In ground tests it was found that it also shows some non-linearity. So we can rewrite 2.4 as flow

$$\begin{pmatrix} B_x \\ B_y \\ B_z \end{pmatrix} = \begin{pmatrix} l_x & \cos a_{xy} & \cos a_{xz} \\ 0 & l_y & \cos a_{yz} \\ 0 & 0 & l_z \end{pmatrix} \left[\begin{pmatrix} E_x \\ E_y \\ E_z \end{pmatrix} - \begin{pmatrix} E_{x0} \\ E_{y0} \\ E_{z0} \end{pmatrix} \right] + \begin{pmatrix} l_{2x}(E_x - E_{x0})^2 \\ l_{2y}(E_y - E_{y0})^2 \\ l_{2z}(E_z - E_{z0})^2 \end{pmatrix} + \begin{pmatrix} l_{3x}(E_x - E_{x0})^3 \\ l_{3y}(E_y - E_{y0})^3 \\ l_{3z}(E_z - E_{z0})^3 \end{pmatrix}$$

where l_2, l_3 are the non-linearity factors. Because they are very small, the effect of misalignment angles in the non-linearity parts can be neglected.

Experience and laboratory tests indicate that some of the parameters depend on time or other environmental influences, for example, temperature. The laboratory measurements have revealed the thermal drift of the scale factors of the three components. We can build a model to describe the thermal drift.

$$l_{x,y,z} = l_{0x,y,z} - l_{T_1 x,y,z}(T_{csc} - T_0) - l_{T_2}(T_{csc} - T_0)^2$$

Using data from laboratory tests the temperature dependent scale factors l_{T_1} are found to be $29.6 ppm/K$ for X, $30.37 ppm/K$ for Y and $30.46 ppm/K$ for the Z axis. l_{T_2} are found to be $4 \times 10^{-8}/K^2$ for all three components. T_0 is the reference temperature. l_0 is defined as the scale factor at the reference temperature. Here T_{csc} means the temperature at the CSC-

feedback coil of the FGM sensor. However, the temperature distribution in the magnetometer is not homogeneous. Due to this reason the temperature of the fluxgate sensor, CSC, and the ADC voltage reference in the electronics box are recorded individually. But the actual experience so far shows that for variations of the scale factors the temperature of the CSC coil plays a more important role than others. That is why we only choose the temperature of the CSC coil to modify the scale factors. Additionally, the temperature drift of the sensor non-linearity l_2, l_3 can be neglected because it is too small to be distinguished from other errors. Knowing the parameters (the angles a_{xy}, a_{xz}, a_{yz}; the scale factors of the three axes l_{0x}, l_{0y}, l_{0z}, l_{2x}, l_{2y}, l_{2z}, l_{3x}, l_{3y}, l_{3z} and their temperature coefficients l_{T_1x}, l_{T_1x}, l_{T_1z}, l_{T_2x}, l_{T_2y}, l_{T_2z}; the offsets of three axes E_{x0}, E_{y0}, E_{z0}) we can apply the output readings E_x, E_y, E_z of the FGM to obtain the true value of the measured magnetic field.

2.2 Scalar calibration of vector magnetometers

As mentioned above, if we know all parameters, we can use them to obtain the ambient magnetic field. These parameters of the vector magnetometers can be derived in laboratory tests before the satellite is launched. However, some of the parameters vary with time or due to other effects (e.g. vacuum or particle radiation). It is necessary to recalibrate the vector magnetometer during the mission. Based on its measurement principle the Overhauser magnetometer has no dependency on field direction, on temperature and on time. It can provide absolute readings of the magnetic field intensity. Furthermore, the Overhauser magnetometer on CHAMP satellite was mounted at the tip of a 4 m long deployable boom. Therefore the magnetic field of the spacecraft has less influence on the OVM than on the FGM. It is possible and also reliable to use the Overhauser magnetometer for calibrating the vector magnetometer. That is the so called scalar calibration. We now discuss the algorithms of this calibration in detail. We repeat Eq.(2.4) in such form,

$$\begin{pmatrix} B_x \\ B_y \\ B_z \end{pmatrix} = \begin{pmatrix} k_1 & k_2 & k_3 \\ 0 & k_4 & k_5 \\ 0 & 0 & k_6 \end{pmatrix} \begin{pmatrix} E_x - E_{x0} \\ E_y - E_{y0} \\ E_z - E_{z0} \end{pmatrix} \tag{2.5}$$

We only replace the parameter matrix K for reasons of convenience. We can calculate the field intensity $|B_{fgm}|$ from the vector magnetometer,

$$B_{fgm} = \sqrt{B_x^2 + B_y^2 + B_z^2}$$

$$= \sqrt{[k_1(E_x - E_{x0}) + k_2(E_y - E_{y0}) + k_3(E_z - E_{z0})]^2 + [k_4(E_y - E_{y0}) + k_5(E_z - E_{z0})]^2 + [k_6(E_z - E_{z0})]^2}$$

and compare it with the scalar measurements from the OVM, B_{ovm}, then we have

$$B_{ovm} = |B_{fgm}| + e \tag{2.6}$$

$$= \sqrt{[k_1(E_x - E_{x0}) + k_2(E_y - E_{y0}) + k_3(E_z - E_{z0})]^2 + [k_4(E_y - E_{y0}) + k_5(E_z - E_{z0})]^2 + [k_6(E_z - E_{z0})]^2} + e$$

where e means the residual error. We can choose uniform distributed data samples and using least-squares method to solve the function (2.6) for obtaining the nine parameters. The assumption is that the nine parameters are invariant over time of the considered data interval. Eq.(2.6) is a non-linear equation. In order to solve the function by iteration we may linearize it.

$$|B_{ovm}| = \sqrt{B_x^2 + B_y^2 + B_z^2}$$

$$E_{fgmx,y,z} = B_{x,y,z} + \triangle B_{x,y,z}$$

because $\triangle B_{x,y,z}$ are very small,

$$|E_{fgm}| = \sqrt{(B_x + \triangle B_x)^2 + (B_y + \triangle B_y)^2 + (B_z + \triangle B_z)^2} = |B_{ovm}| + \triangle B$$

where,

$$\triangle B \;\; = \;\; |E_{fgm}| - |B_{ovm}| = \frac{E_x}{|B_{ovm}|}\triangle B_x + \frac{E_y}{|B_{ovm}|}\triangle B_y + \frac{E_z}{|B_{ovm}|}\triangle B_z$$

$$\triangle B_x = E_x - B_x = E_x - k_1(E_x - E_{x0}) + k_2(E_y - E_{y0}) + k_3(E_z - E_{z0})$$
$$\triangle B_y = E_y - B_y = E_y - k_4(E_y - E_{y0}) + k_5(E_z - E_{z0})$$
$$\triangle B_z = E_z - B_z = E_z - k_6(E_z - E_{z0})$$

we rearrange the expression and find,

$$\triangle B = |E_{fgm}| - |B_{ovm}| = P \bullet M \tag{2.7}$$

where

$$P = \begin{pmatrix} 1-k_1 \\ 1-k_4 \\ 1-k_6 \\ -k_2 \\ -k_3 \\ -k_5 \\ k_1E_{x0} + k_2E_{y0} + k_3E_{z0} \\ k_4E_{y0} + k_5E_{z0} \\ k_6E_{z0} \end{pmatrix}' \approx \begin{pmatrix} 1-k_1 \\ 1-k_4 \\ 1-k_6 \\ -k_2 \\ -k_3 \\ -k_5 \\ E_{x0} \\ E_{y0} \\ E_{z0} \end{pmatrix}', \quad M = \begin{pmatrix} \frac{E_x^2}{|B_{ovm}|} \\ \frac{E_y^2}{|B_{ovm}|} \\ \frac{E_z^2}{|B_{ovm}|} \\ \frac{E_xE_y}{|B_{ovm}|} \\ \frac{E_xE_z}{|B_{ovm}|} \\ \frac{E_yE_z}{|B_{ovm}|} \\ \frac{E_x}{|B_{ovm}|} \\ \frac{E_y}{|B_{ovm}|} \\ \frac{E_z}{|B_{ovm}|} \end{pmatrix}$$

Since the condition (Condition(I))

- k_1, k_4, k_6 close to 1,
- k_2, k_3, k_5 close to zero,
- E_{x0}, E_{y0}, E_{z0} are small.

The parameters matrix P can be simplified as,

$$P \approx (1-k_1,\ 1-k_4,\ 1-k_6,\ -k_2,\ -k_3,\ -k_5,\ E_{x0},\ E_{y0},\ E_{z0})$$

Now we can use a linear least-squares procedure to estimate the nine parameters vector P to minimize the difference between the OVM output and the magnitude derived from the FGM components, i.e. $P = \triangle B/M$ is the solution in the least squares sense. In practice we use the FGM and OVM data of one day (sampling rate 1Hz, so we have 86400 equations $P = \triangle B_i/M_i$) to solve the overdetermined problem for the optimal result.

Moreover, another way to linearize Eq.(2.6) can be chose.

$$
\begin{aligned}
B_{ovm}^2 &= B_x^2 + B_y^2 + B_z^2 \\
&= [k_1(E_x - E_{x0}) + k_2(E_y - E_{y0}) + k_3(E_z - E_{z0})]^2 + [k_4(E_y - E_{y0}) + k_5(E_z - E_{z0})]^2 + [k_6(E_z - E_{z0})]^2 \\
&= P \bullet M + Q
\end{aligned}
$$

where

$$
P = \begin{pmatrix} k_1^2 \\ k_4^2 \\ k_6^2 \\ k_1k_2 \\ k_1k_3 \\ k_4k_5 \\ k_1E_{x0}^{'} \\ k_4E_{y0}^{'} \\ k_6E_{z0}^{'} \end{pmatrix}^{'} \approx \begin{pmatrix} k_1^2 \\ k_4^2 \\ k_6^2 \\ k_2 \\ k_3 \\ k_5 \\ E_{x0}^{'} \\ E_{y0}^{'} \\ E_{z0}^{'} \end{pmatrix}^{'}, \quad M = \begin{pmatrix} E_x^2 \\ E_y^2 \\ E_z^2 \\ 2E_xE_y \\ 2E_xE_z \\ 2E_yE_z \\ 2E_x \\ 2E_y \\ 2E_z \end{pmatrix}
$$

$$
Q = (2k_2k_3E_yE_z + k_2^2E_y^2 + k_3^2E_z^2 + k_5^2E_z^2) + (2k_2E_{x0}^{'}E_y + 2k_3E_{x0}^{'}E_z + 2k_5E_{y0}^{'}E_z) + (E_{x0}^{'2} + E_{y0}^{'2} + E_{z0}^{'2})
$$

We have used $E_{x0}^{'} = -k_1E_{x0} - k_2E_{y0} - k_3E_{z0}$, $E_{y0}^{'} = -k_4E_{y0} - k_5E_{z0}$, $E_{z0}^{'} = -k_6E_{z0}$ to reduce the equation to a simple form. For the same reason, $E_{x0}^{'} \approx -E_{x0}$, $E_{y0}^{'} \approx -E_{y0}$, $E_{z0}^{'} \approx -E_{z0}$, $P \approx (k_1^2,\ k_4^2,\ k_6^2,\ k_2,\ k_3,\ k_5,\ -E_{x0},\ -E_{y0},\ -E_{z0})$ and Q can be neglected compared with B_{ovm}^2. However, we can solve the function by iteration in the form of $B_{ovm}^2 - Q = P \bullet M$, if Condition(I) is not rigid. The solution of the parameter vector P is found to minimize the $B_{ovm}^2 - P \bullet M$ using a least-square method. If P was found, we can determine the matrix K and the offsets E_{x0}, E_{y0}, E_{z0} which are applied to calibrate the FGM readings.

The experience of the CHAMP mission showed that the parameters are usually valid for about a 15-day period. Consequently, the scalar calibration of vector magnetometer, as part of the routine CHAMP data processing, is performed every 15 days in order to keep the parameters updated.

2.3 Torquer correction

As mentioned in the beginning of this chapter, the FGM measured, B_{fgm}, is not only the Earth's magnetic field, B_{em_fg}, but in addition the stray field of the spacecraft, B_{sc_fg}. On the CHAMP satellite a set of three magneto-torquers, as a part of the satellite attitude control unit, generate a magnetic moment which interacts with the ambient field in order to keep the satellite at right attitude because most measurements of the CHAMP mission require an exact attitude. So one of the main sources of B_{sc_fg} are the torquer coils. Their influnce on the measurement of the Earth's magnetic field has to be corrected. Fortunately, the influence can be predicted exactly from the applied current on the basis of the Biot-Savart Law. Suppose that the components of the generated magnetic field are proportional to the strength of the current in the torquer coils, it can be formulated by the equation:

$$B_{tqr\_fg} = \alpha \bullet I_{tqr} = \begin{pmatrix} a_{11} & a_{12} & a_{13} \\ a_{21} & a_{22} & a_{23} \\ a_{31} & a_{32} & a_{33} \end{pmatrix} \begin{pmatrix} I_{tqrx} \\ I_{tqry} \\ I_{tqrz} \end{pmatrix}$$

where B_{tqr_fg} is the magnetic field vector which is generated by the torquer current at the position of the FGM. I_{tqrx}, I_{tqry}, I_{tqrz} denote the magnitude of the current throuth the three sets of the coils. The coefficients of the matrix α were derived from laboratory tests and confirmed in orbit.

$$\begin{pmatrix} a_{11} & a_{12} & a_{13} \\ a_{21} & a_{22} & a_{23} \\ a_{31} & a_{32} & a_{33} \end{pmatrix} = \begin{pmatrix} 15.000, & -9.600, & -13.400 \\ 0.000, & -27.100, & 0.100 \\ -1.300, & 1.000, & -35.950 \end{pmatrix}, \; nT/A$$

These coefficients are considered to never change during the whole CHAMP mission.

2.4 Magnetic field vector data processing

Before we summarize the whole magnetic field vector data processing, yet two things should be discussed. We compare the vector output with the output of the scalar magnetometer

to obtain the nine FGM calibration parameters. But we should know that a 100% time synchronization of sampling between the scalar and vector magnetometers is not guaranteed. A time-lag, for example, of 10ms delay between the measurements of two instruments will cause a 0.5nT error at a background magnetic field gradient of 50nT/s in scalar calibration. The sampling rate of FGM and OVM are, respectively, 50Hz and 1Hz, so it is believed that the timing errors between them are not larger than 20ms. We compared the two magnetometer data under the introduction of different time-lags. A 15ms shift was usually identified because it showed the best result. Another time shift we have to pay attention to is related to the CSC coil temperature correction. Inside the satellite there is vacuum. The thermal conduction may not be homogeneous. That means, the recorded temperature by the CSC coil thermistor is not the temperature that influences the scale factors, it may well reach the sensor coils a little later (on average 100s). Practical experience showed that this effect cannot be neglected. Furthermore, these time-lags seem not to be constant. They are determined every 15 days as well as the nine internal vector magnetometer parameters.

Now we can summarize the whole magnetic field vector data processing in the sequential course of events.

1	Time correction
2	Non-linearity correction.
3	CSC time shift of temperature correction.
4	Apply the nine intrinsic FGM sensor parameters: 3 scale factors, 3 misalignment angles, 3 offsets
5	Torquer correction.

We express the steps using the mathematical formulation in program syntax.

1. $t_{gps\_fg} = t_{gps\_fg} + \mathbf{t_{shift\_fg}}$

2. $$\begin{pmatrix} B_x \\ B_y \\ B_z \end{pmatrix} = \begin{pmatrix} \mathbf{l_x}(E_x - E_{x0}) \\ \mathbf{l_y}(E_y - E_{y0}) \\ \mathbf{l_z}(E_z - E_{z0}) \end{pmatrix} + \begin{pmatrix} \mathbf{l_{2x}}(E_x - E_{x0})^2 \\ \mathbf{l_{2y}}(E_y - E_{y0})^2 \\ \mathbf{l_{2z}}(E_z - E_{z0})^2 \end{pmatrix} + \begin{pmatrix} \mathbf{l_{3x}}(E_x - E_{x0})^3 \\ \mathbf{l_{3y}}(E_y - E_{y0})^3 \\ \mathbf{l_{3z}}(E_z - E_{z0})^3 \end{pmatrix}$$

3. $T_{csc} = interpol(t_{gps\_csc} + \mathbf{t_{shift\_csc}},\ t_{gps\_csc},\ T_{csc})$

4. (a) $$\begin{pmatrix} l_{Tx} \\ l_{Ty} \\ l_{Tz} \end{pmatrix} = \begin{pmatrix} 1 - \mathbf{l_{T1x}}(T_{csc} - \mathbf{T_0}) - \mathbf{l_{T2x}}(T_{csc} - \mathbf{T_0})^2 \\ 1 - \mathbf{l_{T1y}}(T_{csc} - \mathbf{T_0}) - \mathbf{l_{T2y}}(T_{csc} - \mathbf{T_0})^2 \\ 1 - \mathbf{l_{T1z}}(T_{csc} - \mathbf{T_0}) - \mathbf{l_{T2z}}(T_{csc} - \mathbf{T_0})^2 \end{pmatrix}$$

(b) $$\begin{pmatrix} B_x \\ B_y \\ B_z \end{pmatrix} = \begin{pmatrix} l_{Tx} B_x \\ l_{Ty} B_y \\ l_{Tz} B_z \end{pmatrix}$$

(c) $$\begin{pmatrix} B_x \\ B_y \\ B_z \end{pmatrix} = \begin{pmatrix} B_x - \mathbf{E_{x0}} \\ B_y - \mathbf{E_{y0}} \\ B_z - \mathbf{E_{z0}} \end{pmatrix}$$

(d) $$\begin{pmatrix} B_x \\ B_y \\ B_z \end{pmatrix} = \begin{pmatrix} 1 & \cos \mathbf{a_{xy}} & \cos \mathbf{a_{xz}} \\ 0 & 1 & \cos \mathbf{a_{yz}} \\ 0 & 0 & 1 \end{pmatrix} \begin{pmatrix} B_x \\ B_y \\ B_z \end{pmatrix}$$

5. $$\begin{pmatrix} B_x \\ B_y \\ B_z \end{pmatrix} = \begin{pmatrix} B_x \\ B_y \\ B_z \end{pmatrix} - \begin{pmatrix} \mathbf{a_{11}} & \mathbf{a_{12}} & \mathbf{a_{13}} \\ \mathbf{a_{21}} & \mathbf{a_{22}} & \mathbf{a_{23}} \\ \mathbf{a_{31}} & \mathbf{a_{32}} & \mathbf{a_{33}} \end{pmatrix} \begin{pmatrix} I_x \\ I_y \\ I_z \end{pmatrix}$$

The boldfaces indicate all the needed parameters for the corrections before we start the whole processing. Except for the nine intrinsic FGM sensor parameters we think that the other parameters are constant over the whole mission and they were already derived in the pre-flight tests. As for these nine intrinsic parameters of the FGM, we have mentioned, during the mission we perform a scalar calibration every 15 days to update them. That is the so called in-flight scalar calibration. So we can use the following scheme to illustrate the FGM data procedure.

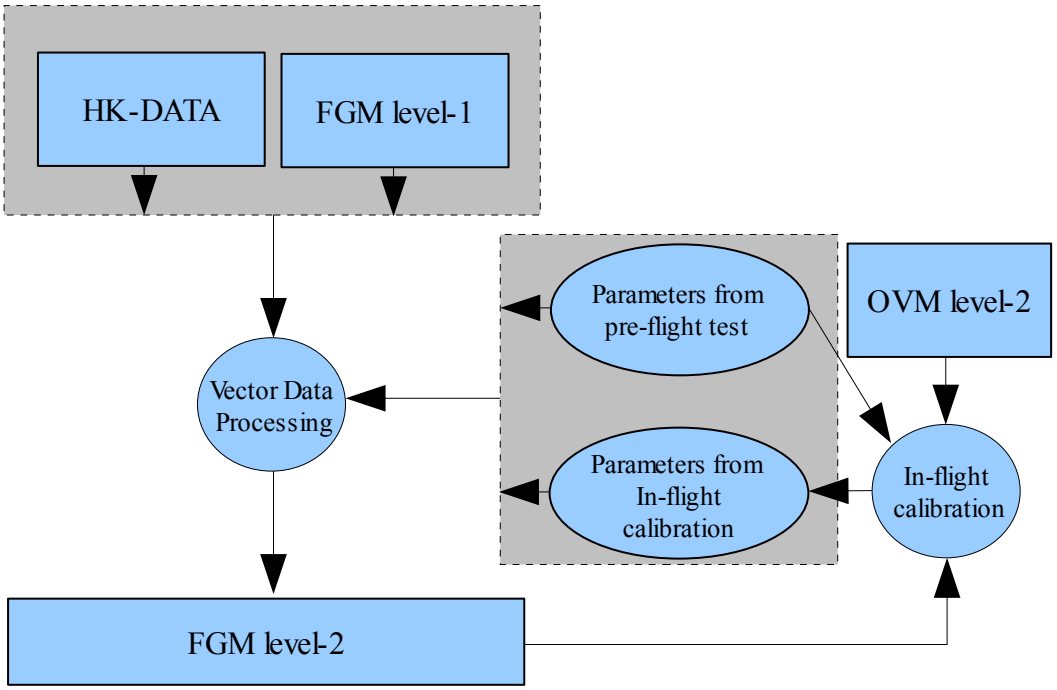

Figure 2.3

2.5 OVM data processing

Due to the advantage of the Overhauser Magnetometer, the data processing for its measurements is relatively simpler than for the Fluxgate Magnetometers. The magnetic field at the OVM position is B_{ovm}. The Earth's magnetic field, which we want to know, is B_{em_ov}. B_{d_ov} is the disturbing field at OVM position. We have,

$$B_{ovm} = B_{em\_ov} + B_{d\_ov}$$

If B_{d_ov} is very small on a background of strong ambient field strength B_{em_ov}, the correction of the OVM readings can be described as:

$$
\begin{aligned}
|B_{em\_ov}| &= E_{ovm} - \frac{B_{fgm}}{E_{ovm}} \bullet B_{d\_ov} \\
&= E_{ovm} - \frac{B_{xfgm}B_{xd\_ov} + B_{yfgm}B_{yd\_ov} + B_{zfgm}B_{zd\_ov}}{E_{ovm}}
\end{aligned}
$$

However, for the correction we need vector data. So far the source of the B_{d_ov} can include both additive portions and multiplicative portions:

- Additive(similar to offset)
  - the sensor heading error
  - the static magnetic field of the spacecraft
  - the stray field from electric currents on the spacecraft(so far mostly, torquer coils)
- Multiplicative(similar to scale factor)
  - cross-talk of the fluxgate magnetometer on the OVM
  - static induced magnetic field due to the soft magnetic material of the spacecraft

So we have,

$$
\begin{aligned}
B_{d\_ov} &= B_{h\_ov} + B_{sc\_ov} + B_{tqr\_ov} + B_{m1\_ov} + B_{m2\_ov} \\
&= \begin{pmatrix} B_{xh\_ov} \\ B_{yh\_ov} \\ B_{zh\_ov} \end{pmatrix} + \begin{pmatrix} B_{xsc\_ov} \\ B_{ysc\_ov} \\ B_{zsc\_ov} \end{pmatrix} + \begin{pmatrix} a_{11} & a_{12} & a_{13} \\ a_{21} & a_{22} & a_{23} \\ a_{31} & a_{32} & a_{33} \end{pmatrix} \begin{pmatrix} I_{tqrx} \\ I_{tqry} \\ I_{tqrz} \end{pmatrix} + \begin{pmatrix} q_{xm1}B_{xfgm} \\ q_{ym1}B_{yfgm} \\ q_{zm1}B_{zfgm} \end{pmatrix} + \begin{pmatrix} q_{xm2}B_{xfgm} \\ q_{xm2}B_{yfgm} \\ q_{xm2}B_{zfgm} \end{pmatrix}
\end{aligned}
$$

where the parameters B_{h_ov}, B_{sc_ov}, q_{sci_ov}, q_{soc_ov}, α_{tqr} are determined in the laboratory test before the launch. They are respectively.

$$
\begin{pmatrix} B_{xh\_ov} \\ B_{yh\_ov} \\ B_{zh\_ov} \end{pmatrix} = \begin{pmatrix} -0.178 \\ -0.138 \\ 0.035 \end{pmatrix} nT, \quad \begin{pmatrix} B_{xsc\_ov} \\ B_{ysc\_ov} \\ B_{zsc\_ov} \end{pmatrix} = \begin{pmatrix} 0.000 \\ -0.300 \\ 0.000 \end{pmatrix} nT
$$

$$\begin{pmatrix} a_{11} & a_{12} & a_{13} \\ a_{21} & a_{22} & a_{23} \\ a_{31} & a_{32} & a_{33} \end{pmatrix} = \begin{pmatrix} 7.40 & -2.60 & -2.40 \\ 0.00 & -10.70 & 0.00 \\ -0.40 & 0.30 & -11.60 \end{pmatrix} nT/A$$

$$\begin{pmatrix} q_{xm1} \\ q_{ym1} \\ q_{zm1} \end{pmatrix} = \begin{pmatrix} 0.0000140 \\ -0.0000060 \\ -0.0000050 \end{pmatrix}, \begin{pmatrix} q_{xm2} \\ q_{xm2} \\ q_{xm2} \end{pmatrix} = \begin{pmatrix} -0.00000884 \\ 0.00000544 \\ 0.00000590 \end{pmatrix} \; no\ unit$$

Although we think these parameters will not change over the whole mission, the experience tells us that B_{sc_ov} and α_{tqr} show a little change. We will discuss in more details about how to correct them in the next chapter. In year 2004, we have even introduced furthermore a time shift and a bias correction. That is,

$$|B_{ovm}| = |B_{ovm}| + \mathbf{t_{shift\_ov}} \frac{\triangle |\mathbf{B_{ovm}}|}{\triangle \mathbf{t}}$$

and

$$|B_{ovm}| = E_{ovm} + BIAS_{ovm}$$

where $\mathbf{t_{shift\_ov}}$ is determined every 15 days during the mission and $BIAS_{ovm}$ is adopted as $-0.4nT$. Before all these correction the OVM reading is rescaled based on the OVM housekeeping data reading f_{ovm}(of the internal oscillator), where f_{ref} is the nominal frequency of the oscillator.

$$B_{ovm} = B_{ovm} \frac{f_{ovm}}{f_{ref}}$$

Chapter 3

Using Continuous Parameters to Improve the Processing

Our purpose of the calibration of the Fluxgate Magnetometer with respect to the Overhauser magnetometer is to make the vector magnetic field measurements precise and reliable as far as possible. However precision and reliability of the data are sometimes in conflict. As far as our scalar calibration which is based on the least squares principle, that means, the more parameters and the shorter sample data we introduce into the calibration, the better fit of the data we can get but with lower reliability. We consider, that errors of each channel in the FGM can be given by a function of measured signal,

$$\triangle E_{x',y',z'} = f(B_{fgmx',y',z'})$$

as well as, the output readings of the FGM $E_{x',y',z'}$ are function of the measured signal,

$$E_{fgmx',y',z'} = B_{fgmx',y',z'} + \triangle E_{x',y',z'} = F(B_{fgmx',y',z'})$$

We use a polynomial approximation to expand the inverse function $F^{-1}(E_{fgmx',y',z'})$,

$$\begin{aligned} B_{fgmx',y',z'} &= F^{-1}(E_{fgmx',y',z'}) \\ &= q_{x'0,y'0,z'0} + q_{x'1,y'1,z'1}E_{fgmx',y',z'} + q_{x'2,y'2,z'2}E^2_{fgmx',y',z'} + q_{x'3,y'3,z'3}E^3_{fgmx',y',z'} + \dots \end{aligned}$$

So we can see that q_0 can be regarded as offsets, q_1 are just scale factors and q_2, q_3 are the parameters to correct the non-linearity of the FGM. q_1 is also a function of the CSC

temperature,

$$q_1 = l_{T0} - l_{T1}(T_{csc} - T_0) - l_{T2}(T_{csc} - T_0)^2$$

We revisit Eq.(2.7) in chapter 2,

$$\triangle B = |E_{fgm}| - |B_{ovm}| = P \bullet M$$

We consider the OVM measurements as a reference for the FGM measurements. Therefore, the difference $\triangle B = |E_{fgm}| - |B_{ovm}|$ is the only criterion to evaluate the quality of the FGM measurements after the launch. If the calibration parameters we have found make the $\triangle B$ smaller, then we think, they are better, and the calibrated measurements of the FGM therefore are more precise. During the mission we have found that the $\triangle B$ varies a lot with time. This is the reason why we do the calibration every 15 days so that we can correct the existing parameters. That means, some of the parameters are functions of time as well. We certainly may think that all of them vary with time and we take all of them into account by scalar calibration, so we have to extend the parameters matrix P and variables matrix M. Although that brings less $\triangle B$, more terms of the variables lead to the problem of crosstalk because of the nonuniform distribution of data.

However, we can analyze the statistic of the $\triangle B$ to investigate which parameters play an important role in the variation of $\triangle B$. We know that the typical statistical quantities are median value and standard deviation. We have tried to use a group of FGM data and OVM data in 2005 to show directly the relation between the statistical behavior of the $\triangle B$ and the FGM parameters.

The FGM data and OVM data were processed using a set of fixed parameters during the first 175 days, and then another set of parameters for 44 days. At MJD 2083 and 2127 we have changed the parameters. Figure 3.1 shows the result of the recalibration. The blue, green curves indicate, respectively, the scale factors of the X, Z components based on the result of the recalibration. The black and magenta curves indicate the median value and the standard deviation of the $\triangle B$. We can see that the drift of $\triangle B$ (median) shows a strong correlation with the scale factors.

It appears, from all the parameters, the scale factors play a very important role. This

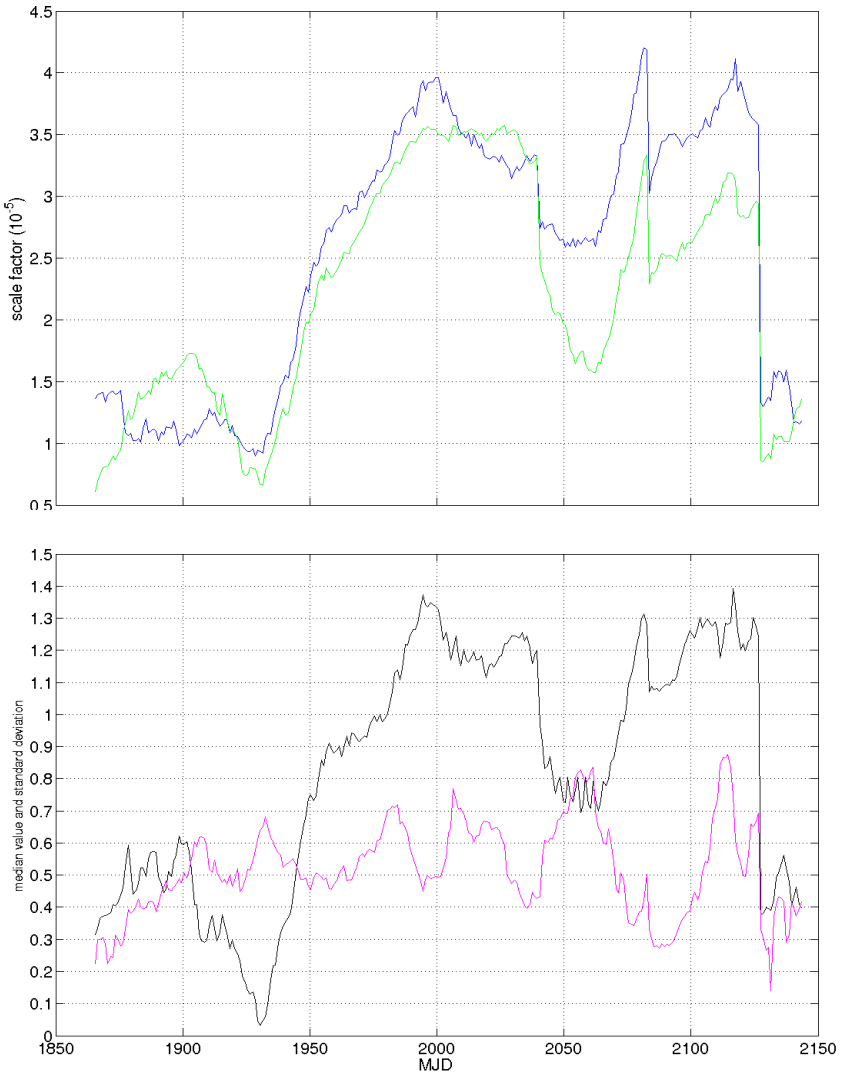

Figure 3.1: Parameter variation during the year 2005. The blue and green curve in the top panel show the X and Z scale factors, respectively. Below the median (black) and the standard deviation (magenta) are plotted

solid: applied scale factor ($l_0=l_a+l_b\ln(MJD-MJD_0)$)

dash: expected scale factor without OVM bias correction

magenta: modeling by a logarithm function

Figure 3.2: Temporal change of the FGM scale factors

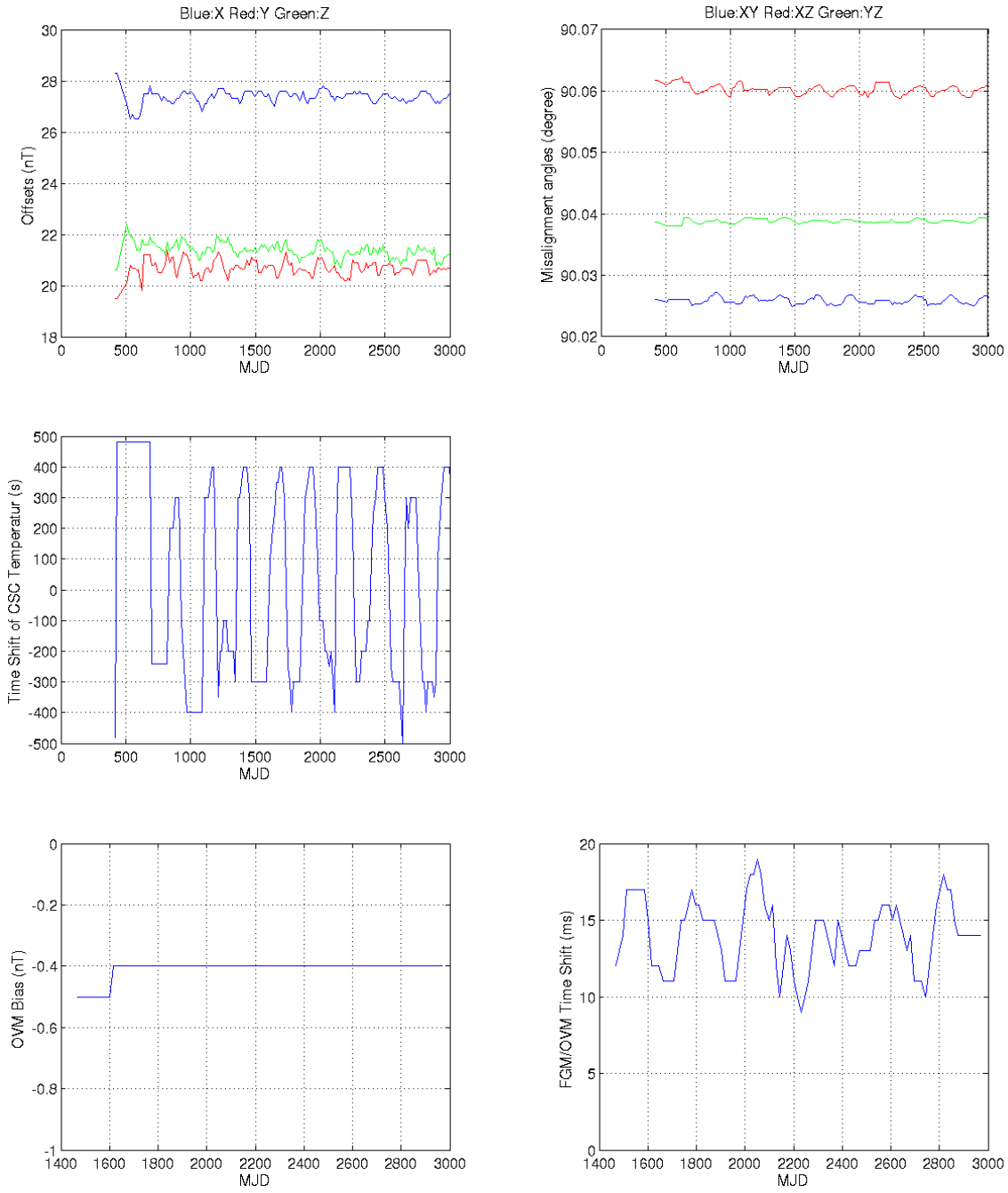

Figure 3.3: Temporal variations of the other 9 calibration parameters

example indicates that the drift of the mean $\triangle B$ comes mainly from the three scale factors.

$$\triangle B = |E_{fgm}| - |B_{ovm}| = P \bullet M$$

where

$$M = (\frac{E_x^2}{|B_{ovm}|}, \frac{E_y^2}{|B_{ovm}|}, \frac{E_z^2}{|B_{ovm}|}, \frac{E_x E_y}{|B_{ovm}|}, \frac{E_x E_z}{|B_{ovm}|}, \frac{E_y E_z}{|B_{ovm}|}, \frac{E_x}{|B_{ovm}|}, \frac{E_y}{|B_{ovm}|}, \frac{E_z}{|B_{ovm}|})'$$

From the view of statistics, the median value of $\triangle B$ is primarily determined by the three scale factors(p_1, p_2, p_3) because the first three terms E_x^2, E_y^2, E_z^2 are nonnegative and have strong mean constituent. Compared with them, the other terms, $E_x E_y$, $E_x E_z$, $E_y E_z$, E_x, E_y, E_z, are on average very close to zero due to their bipolar variations. The standard deviation of the $\triangle B$ mainly depends on the misalignment angles(p_4, p_5, p_6), offsets(p_7, p_8, p_9) and the time shift.

In addition, the existing parameters which we have updated every 15 days during the mission support the same conclusion. We can see no drift of the offsets and the misalignment angles but the scale factors. Hence two conclusions can be drawn:

- the long term drift of the three scale factors bring the drift of $\triangle B$.
- the standard deviation as well as the offsets and misalignment angles show no long term drift.

3.1 The disadvantage of the standard calibration

Different to the temperature correction and the torquer coil current correction the FGM calibration uses an inversion method. Some calibration parameters are in a sense not determined in a prelaunch test but by a least squares principle in the scalar calibration. In our standard calibration twelve parameters are introduced. As we have mentioned, they are three scale factors, three misalignment angles and three offsets, time shift of the CSC coil temperature, time shift between FGM and OVM, OVM bias. These twelve parameters are renewed every 15 days to keep the $\triangle B$ prolonged minimal. That is to say, if we have processed the FGM

data within 3000 days, we have used 200*12=2400 parameters to do that. Another problem is that using every 15 days a different parameter set causes discontinuities in the data, especially on the days when the parameters are renewed. This is because the parameters are determined independently each time, as we can see in Figure 3.4. The blue curve indicates $\triangle B$ on 28th May 2007 and the red one indicates $\triangle B$ on 29th May 2007. A new parameter set is applied on 29th. Therefore a jump in $\triangle B$ appears between the two days. This kind of jump occurs every 15 days when the new parameter sets are applied. Preferably, this artificial discontinuity shouldn't occur.

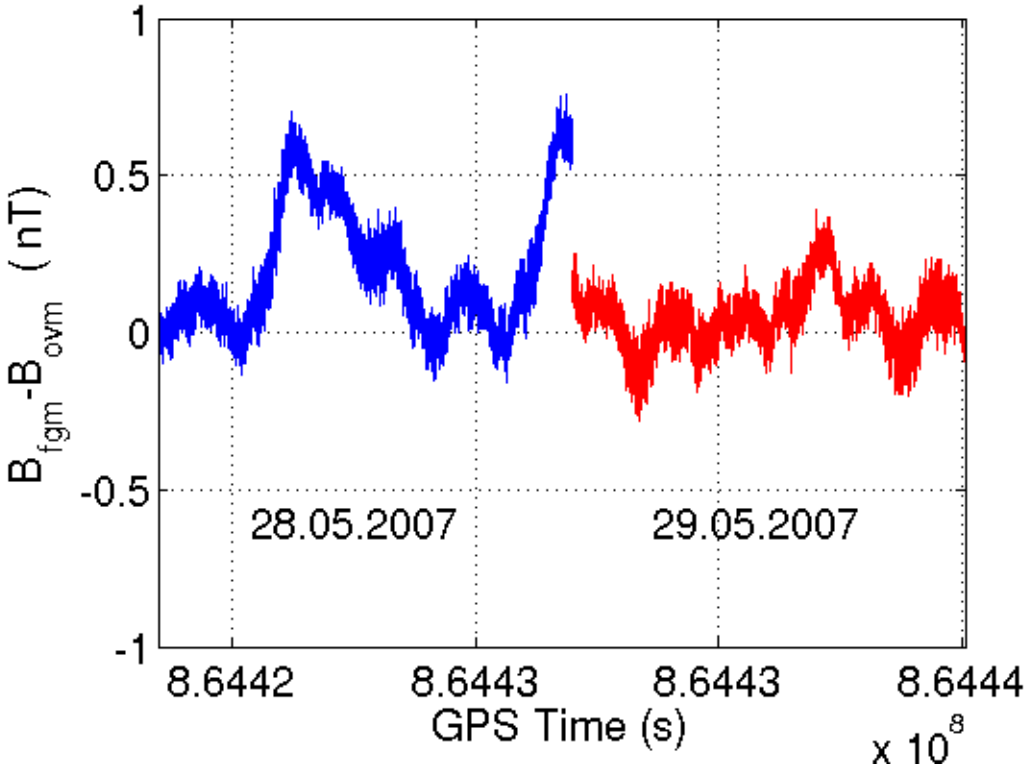

Figure 3.4: Variation of the difference between FGM and OVM measurements. At the time of FGM parameter update ΔB changes discontinuously (switch from blue to red curve)

3.2 The long time dependency of the scale factors

Based on the scale factors, we have updated every 15 days through the years, we can investigate the long-term behaviors of the FGM. Rother et al.(2003) had used a linear function to fit the drift of the scale factors. Olsen et al.(2001) had used a parabolic function to describe the time dependence of the scale factors of the FGM on the Ørsted satellite.

$$l_0 = l_a + l_b(t - t_{0_1}) + l_c(t - t_{0_2})^2$$

But their function is based on the variation of the scale factors only over several months. The CHAMP data covering eight years show that the long-term dependence of scale factor can be described much well by a logarithm function than by other functions (e.g. a parabolic function). Figure 3.2 shows the variation of the scale factors of the FGM on CHAMP. We have considered a function:

$$l_0 = l_a + l_b \ln(t - t_0)$$

where t is the time in Modified Julian Day(MJD, starting on 1.Jan 2000, 00:00UT). If we fit the time dependence of scale factors over eight years using a natural logarithm function, we can obtain a good result. The reason of the time dependence is probably related to aging of the electronic devices, e.g. radiation effects. The natural logarithm trend indicates that the long-term drift of the reference voltage in the Analog-to-Digital Conversion is possibly the cause. These devices tend to exhibit logarithmic aging curves.

3.3 Continuous parameters for the FGM data processing

So far from our analysis we can propose another way of processing the FGM data and OVM data. Compared with the standard processing we may use a much smaller set of continuous parameters but do not get a worse quality of the data. We have strong evidence that the drift of the scale factors is due to the aging of the reference voltage source for the AD convert of the fluxgate magnetometer. The temporal change can be described by a logarithm

function. We use this function to calculate the scale factors for each day and apply fixed misalignment angles and offsets value for all time. The parameters which were used in the standard processing can be used to derive the type of logarithm functions for the scale factors. And we take the average value of them as a good estimation of the fixed value.

$l_0 = l_a + l_b \ln(MJD - MJD_0)$, $MJD_0 = 150^*$

	X	Y	Z
l_a	1.00025304*	1.00111601*	1.00102659*
l_b	0.00028960*	0.00029990*	0.00029850*
Offsets	26.970 nT	19.843 nT	21.625 nT
Misalig angles	90.02613^o	90.05986^o	90.03873^o

Time shift of $Tcsc$	100 s
$t_{shift\_ov/fg}$	15 ms
$BIAS_{ovm}$	0 nT

**The value can be revised according to any new request.*

We consider that the remaining three parameters, the time shift of the correction for the CSC coil temperature, the time shift between FGM and OVM, and the OVM bias are constant as well. In order to get an overall better result we choose the time shift of the CSC coil temperature correction as 100s and the time shift between FGM and OVM as 15ms. Since we don't have experimental evidence for the OVM bias, we take it as null. For each scale factor of the X, Y, Z components we need two parameters to express the logarithm function. For the new approach we use in total 14 predetermined parameters to process the whole FGM data set over 8 years.

3.4 The correction of the disturbing magnetic fields from the satellite body

We have mentioned in the beginning of the first chapter that if there are B_{sc_fg} and B_{sc_ov} from the spacecraft itself, they will disturb the measurement of the space magnetic field. Many sources on the spacecraft can produce the disturbing magnetic fields, for example, currents in the cables and magnetic materials. However, the scalar calibration can't distinguish them from the offsets of the FGM. The correction of them is regarded as a direct problem. In other words, we use the available parameters to calculate the disturbing amplitude and take them off the measurements. For instance, we have done this for the torquer correction

in the standard processing.

Some currents in cabling and science instruments play a part in variable spacecraft magnetic fields. Although the layout of those loops and electrical units were well designed and their dynamic magnetic fields mostly compensate each other, we can still find some evidence from the result of the FGM and OVM measurements which indicated that such influences cannot be ignored. Nearly all the currents in the loops and instruments are recorded in spacecraft housekeeping data. Based on them we can analyze how strong the influences are.

3.4.1 Influences of the solar current from the satellite body

The power system on the satellite includes the solar arrays and the batteries. The satellite flies everyday alternatively in sunlight and in shadow. Hence the loops of power system carry the currents ranging from 17Amp to a few Amp, especially in the noon local time. If the battery is fully charged, the charge current will drop to zero in a very short time. However, this character provides us a good opportunity to identify whether the currents have an effect or not. We perform a superposed epoch analysis of the $B_{fgm} - B_{ovm}$ at the time around the solar current rapid drop. Figure 3.5 shows a result of 30.04.2007. The orbit local time was 03:20. We can see the solar current droped from 10.5A to 3A in 15 seconds. A small step (approximately 0.1 nT) in the difference $B_{fgm} - B_{ovm}$ can be clearly seen.

We have calculated all these small steps and found that they depend not only on the magnitude of the solar current and the external magnetic fields but also on the local time. That confirms our suspicion that one source of the dynamic magnetic field is the solar current because at different local time the body of the satellite is exposed to a different incident angle which leads to a different distribution of solar currents on the solar arrays.

The dynamic magnetic field at the FGM sensor location generated by the solar array currents contaminates the ambient magnetic field observations. However the field cannot be modeled directly using Biot-Savart's calculation because the precise distribution of the current loops is unknown. Moreover, the solar currents vary periodically along the orbit and many other effects vary similarly. Therefore we cannot simply use e.g. least square estimation to determine the coefficient due to the mismatch between the FGM and OVM.

Even though, the significant character of the solar currents changing allows us to dis-

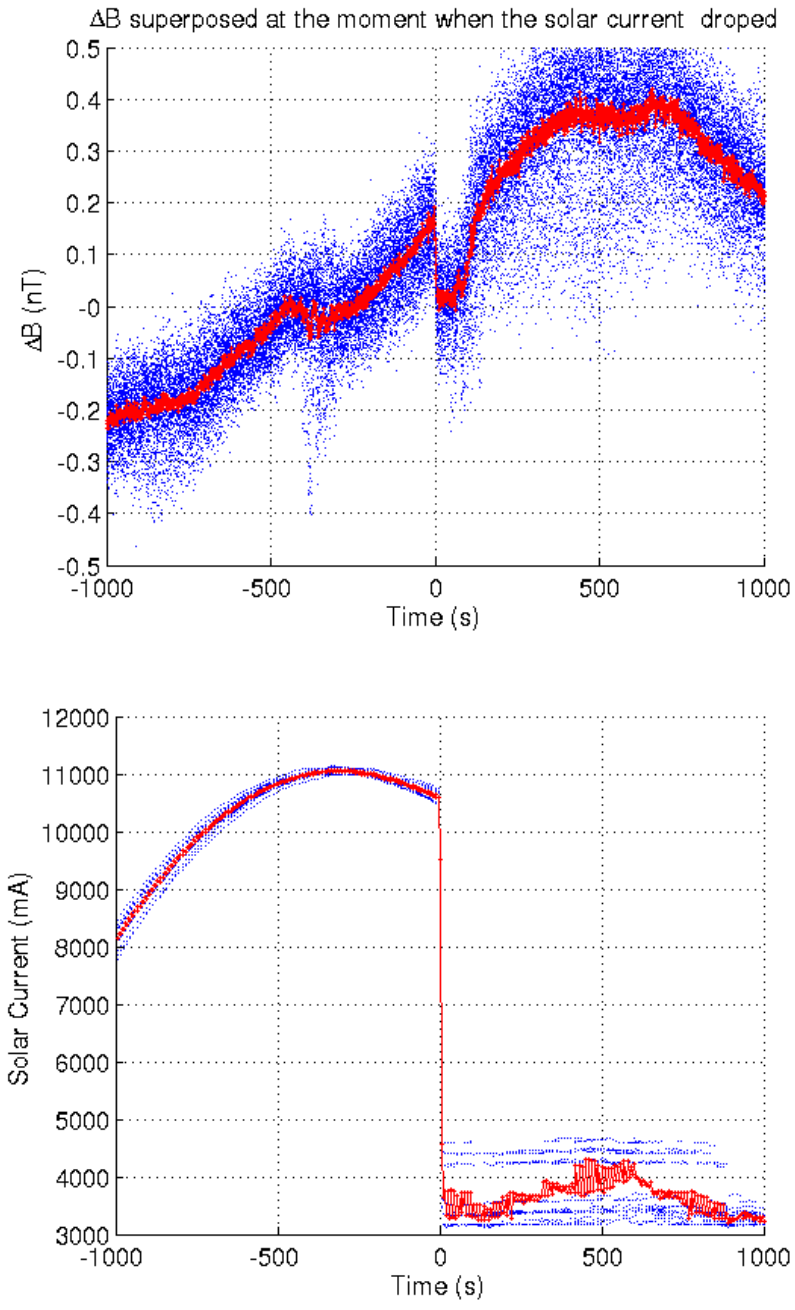

Figure 3.5: Jump in ΔB caused by the sudden drop of solar current strength

tinguish their magnetic field from the ambient magnetic field. As we have discussed, the charging current will drop to zero in a very short time when the battery is full. At this moment the change of the residuals between the FGM and the OVM are mainly from the rapid change of the solar currents. Therefore we can build an approximate model to determine the coefficients for the solar currents, which can be used to remove the disturbance field. We think, the contamination field at the sensor location is proportional to the solar current strength. So we have,

$$B_{solar\_fg} = I_{solar} \begin{pmatrix} \alpha_{fg} \\ \beta_{fg} \\ \gamma_{fg} \end{pmatrix} = I_{solar} A_{fg}$$

where I_{solar} is the measured solar currents and $(\alpha_{fg},\ \beta_{fg},\ \gamma_{fg})$ are the coefficients we want to determine for the solar current correction.

$$B_{fgm} = B_{em} + B_{sc\_fg} + B_{solar\_fg}$$

$$B_{ovm} = B_{em} + B_{sc\_ov} + B_{solar\_ov}$$

To simplify the equation we consider in a first approximation that B_{solar_ov} is very small because the OVM is mounted at the end of the boom. The distance between the OVM and the solar array is long enough.

$$B_{solar\_ov} = 0$$

$$\begin{aligned} \triangle B &= |B_{fgm}| - |B_{ovm}| \\ &= |B_{em} + B_{sc\_fg} + B_{solar\_fg}| - |B_{em} + B_{sc\_ov}| \\ &= |B_{em}| + \frac{B_{fgm}}{|B_{fgm}|} \bullet B_{sc\_fg} + \frac{B_{fgm}}{|B_{fgm}|} \bullet B_{solar\_fg} - |B_{em}| - \frac{B_{fgm}}{|B_{fgm}|} \bullet B_{sc\_ov} \\ &= \frac{B_{fgm}}{|B_{fgm}|} \bullet B_{solar\_fg} + \frac{B_{fgm}}{|B_{fgm}|} \bullet (B_{sc\_fg} - B_{sc\_ov}) \end{aligned}$$

The problem is that we don't know the term $\frac{B_{fgm}}{|B_{fgm}|} \bullet (B_{sc\_fg} - B_{sc\_ov})$ exactly. If we just use

least square estimation to determin the coefficient, the mismatch between the first term and the second term will surely come up. But at a certain moment the solar current suddenly drops (within 10 sec), the two terms can be approximately separated from each other because the $B_{sc\_fg} - B_{sc\_ov}$ changes very slowly compared to the solar currents. We can therefore assume that $B_{sc\_fg} - B_{sc\_ov}$ do not change within this 10 sec.

$$\begin{aligned}
\triangle B(t_1) - \triangle B(t_2) &\approx \frac{B_{fgm}(t_1)}{|B_{fgm}(t_1)|} \bullet B_{solar_fg}(t_1) + \frac{B_{fgm}(t_1)}{|B_{fgm}(t_1)|} \bullet (B_{sc_fg}(t_1) - B_{sc_ov}(t_1)) + e(t_1) \\
&\quad -[\frac{B_{fgm}(t_2)}{|B_{fgm}(t_2)|} \bullet B_{solar_fg}(t_2) + \frac{B_{fgm}(t_2)}{|B_{fgm}(t_2)|} \bullet (B_{sc_fg}(t_2) - B_{sc_ov}(t_2)) + e(t_2)] \\
&= [\frac{B_{fgm}(t_1)}{|B_{fgm}(t_1)|} \bullet [I_{solar}(t_1) \begin{pmatrix} \alpha_{fg} \\ \beta_{fg} \\ \gamma_{fg} \end{pmatrix}] - \frac{B_{fgm}(t_2)}{|B_{fgm}(t_2)|} \bullet [I_{solar}(t_2) \begin{pmatrix} \alpha_{fg} \\ \beta_{fg} \\ \gamma_{fg} \end{pmatrix}]] \\
&\quad +[\frac{B_{fgm}(t_1)}{|B_{fgm}(t_1)|} \bullet (B_{sc_fg}(t_1) - B_{sc_ov}(t_1)) - \frac{B_{fgm}(t_2)}{|B_{fgm}(t_2)|} \bullet (B_{sc_fg}(t_2) - B_{sc_ov}(t_2))] \\
&\quad +[e(t_1) - e(t_2)]
\end{aligned}$$

where e here means the difference of the measurment noise between the FGM and OVM. t_1, t_2 denote the times just before and after the solar current drop. Just as we have discussed, $\frac{B_{fgm}}{|B_{fgm}|}$ and $B_{sc\_fg} - B_{sc\_ov}$ are all slowly changing signals, in comparison with that, the solar current I_{solar} is a momentarily changing signal. So we can introduce,

$$\frac{B_{fgm}(t_1)}{|B_{fgm}(t_1)|} \bullet (B_{sc\_fg}(t_1) - B_{sc\_ov}(t_1)) \approx \frac{B_{fgm}(t_2)}{|B_{fgm}(t_2)|} \bullet (B_{sc\_fg}(t_2) - B_{sc\_ov}(t_2))$$

then we have,

$$\triangle B(t_1) - \triangle B(t_2) \approx \frac{B_{fgm}(t_1)}{|B_{fgm}(t_1)|} \bullet [I_{solar}(t_1) \begin{pmatrix} \alpha_{fg} \\ \beta_{fg} \\ \gamma_{fg} \end{pmatrix}] - \frac{B_{fgm}(t_2)}{|B_{fgm}(t_2)|} \bullet [I_{solar}(t_2) \begin{pmatrix} \alpha_{fg} \\ \beta_{fg} \\ \gamma_{fg} \end{pmatrix}] + e(t_1) - e(t_2)$$

So using this equation we can derive the coefficients $\alpha_{fg},\ \beta_{fg},\ \gamma_{fg}$. The principle to determine the coefficients is based on the assumption that the time variations of other errors are much slower at the moment when the solar current rapidly drops down. This special case allows

us to isolate the solar current signal from other systematic errors.

Now we assume that $e(t)$ is stationary Gaussian noise. In order to eliminate $e(t)$, we accumulate both sides of the equation for a period in the time domain.

$$\begin{aligned}\sum_{t_1-\triangle t}^{t_1+\triangle t} \triangle B(t) - \sum_{t_2-\triangle t}^{t_2+\triangle t} \triangle B(t) &= \sum_{t_1-\triangle t}^{t_1+\triangle t} \frac{B_{fgm}(t)}{|B_{fgm}(t)|} \bullet [I_{solar}(t) \begin{pmatrix} \alpha_{fg} \\ \beta_{fg} \\ \gamma_{fg} \end{pmatrix}] \\ &\quad - \sum_{t_2-\triangle t}^{t_2+\triangle t} \frac{B_{fgm}(t)}{|B_{fgm}(t)|} \bullet [I_{solar}(t) \begin{pmatrix} \alpha_{fg} \\ \beta_{fg} \\ \gamma_{fg} \end{pmatrix}] + \sum_{t_1-\triangle t}^{t_1+\triangle t} e(t) - \sum_{t_2-\triangle t}^{t_2+\triangle t} e(t)\end{aligned}$$

The average of stationary Gaussian noise in time can be regarded not to change. So the term $\sum_{t_1-\triangle t}^{t_1+\triangle t} e(t) - \sum_{t_2-\triangle t}^{t_2+\triangle t} e(t)$ can be neglected. Using this equation we can estimate the coefficients for the correction of solar current.

In a second step, we turn back to the equations,

$$B_{fgm} = B_{em} + B_{sc\_fg} + B_{solar\_fg}$$

$$B_{ovm} = B_{em} + B_{sc\_ov} + B_{solar\_ov}$$

if we consider that B_{solar_ov} is not zero, we have to find a way to estimate it.

$$\begin{aligned}\triangle B &= |B_{fgm}| - |B_{ovm}| \\ &= |B_{em} + B_{sc\_fg} + B_{solar\_fg}| - |B_{em} + B_{sc\_ov} + B_{solar\_ov}| \\ &= \frac{B_{fgm}}{|B_{fgm}|} \bullet (B_{solar\_fg} - B_{solar\_ov}) + \frac{B_{fgm}}{|B_{fgm}|} \bullet (B_{sc\_fg} - B_{sc\_ov})\end{aligned}$$

we have,

$$B_{solar\_ov} = I_{solar} \begin{pmatrix} \alpha_{ov} \\ \beta_{ov} \\ \gamma_{ov} \end{pmatrix} = I_{solar} A_{ov}$$

then,

$$\begin{aligned}\triangle B &= |B_{fgm}| - |B_{ovm}| \\ &= \frac{B_{fgm}}{|B_{fgm}|} \bullet (B_{solar\_fg} - B_{solar\_ov}) + \frac{B_{fgm}}{|B_{fgm}|} \bullet (B_{sc\_fg} - B_{sc\_ov}) \\ &= = \frac{B_{fgm}}{|B_{fgm}|} \bullet [I_{solar}(A_{fg} - A_{ov})] + \frac{B_{fgm}}{|B_{fgm}|} \bullet (B_{sc\_fg} - B_{sc\_ov})\end{aligned}$$

So we can still use the equations to derive the coefficients, but it is neither A_{fg} nor A_{ov}, but $A_{fg} - A_{ov}$. However, we assume that this local magnetic field of the solar currents, B_{solar}, at distances >2-3 times the satellite dimensions, approaches a dipole field. With this assumption and the known $A_{fg} - A_{ov}$, we can figure out the B_{solar_fg} and the B_{solar_ov} separately.

$$B_{solar\_fg} - B_{solar\_ov} = I_{solar}(A_{fg} - A_{ov}) \tag{3.1}$$

$$B_{solar\_fg} = \frac{\mu_0}{4\pi R_{fgm}^3}[3(r_{fgm} \bullet M)r_{fgm} - M]$$

$$B_{solar\_ov} = \frac{\mu_0}{4\pi R_{ovm}^3}[3(r_{ovm} \bullet M)r_{ovm} - M]$$

The descriptions of $B_{solar_fg}$and the B_{solar_ov} is based on a single magnetic dipole equation. M is the (vector) dipole moment. r is the unit vector parallel to the vector from the position of the dipole to the position where the field is being measured. To simplify the equation we assume that the center point of the dipole is located on the boom axis, that is to say,

$$M = [m_x \quad m_y \quad m_z], \;\; r_{fgm} = r_{ovm} = [1 \quad 0 \quad 0]$$

And then,

$$B_{solar\_fg} = \frac{\mu_0}{4\pi R_{fgm}^3}[2m_x \quad -m_y \quad -m_z]$$

$$B_{solar\_ov} = \frac{\mu_0}{4\pi R_{ovm}^3}[2m_x \quad -m_y \quad -m_z]$$

where $R_{fgm} = 4.75$m and $R_{ovm} = 6.5$m, so

$$B_{solar\_fg} = [0.0014850\mu_0 m_x \quad -0.0007425\mu_0 m_y \quad -0.0007425\mu_0 m_z]$$

$$B_{solar\_ov} = [0.0005796\mu_0 m_x \quad -0.0002898\mu_0 m_y \quad -0.0002898\mu_0 m_z]$$

Substitute them in Eq.(3.1),

$$\begin{aligned} B_{solar\_fg} - B_{solar\_ov} &= I_{solar}(A_{fg} - A_{ov}) \\ &= I_{solar}[\alpha_{fg} - \alpha_{ov} \quad \beta_{fg} - \beta_{ov} \quad \gamma_{fg} - \gamma_{ov}] \end{aligned}$$

Now , $B_{solar_fg}$and the B_{solar_ov} can be calculated.

$$B_{solar\_fg} = I_{solar}[1.64(\alpha_{fg} - \alpha_{ov}) \quad 1.64(\beta_{fg} - \beta_{ov}) \quad 1.64(\gamma_{fg} - \gamma_{ov})]$$

$$B_{solar\_ov} = I_{solar}[0.64(\alpha_{fg} - \alpha_{ov}) \quad 0.64(\beta_{fg} - \beta_{ov}) \quad 0.64(\gamma_{fg} - \gamma_{ov})]$$

We have used the FGM, OVM and the solar current(PCD) data for years 2006 and 2007 to calculate the $A_{fg} - A_{ov}$. Figure 3.6 shows the result.

From Figure 3.6 we can see that the coefficients α and γ show some time dependence on the local time of the satellite. This is expected due to the different solar aspect angles. Let's think about our correction model,

$$B_{solar\_fg} = I_{solar} \begin{pmatrix} \alpha_{fg} \\ \beta_{fg} \\ \gamma_{fg} \end{pmatrix} = I_{solar} A_{fg} \tag{3.2}$$

This model is based on Biot-Savart's equation. If the structure of the current loops and the postion of the FGM are never changed, the coefficients matrix A_{fg} is also defined without doubt. After all, how is this kind of time dependence produced, looking like Figure 3.6? The period of the satellite local time variation gives us a hint. We know the electrical energy source of the satellite are solar cells. The solar cells of CHAMP are located on the two sides and on the top of the main body surface. We know at different local times, the three panels of the solar cells are illuminated at different inclinations of sunlight, which causes the

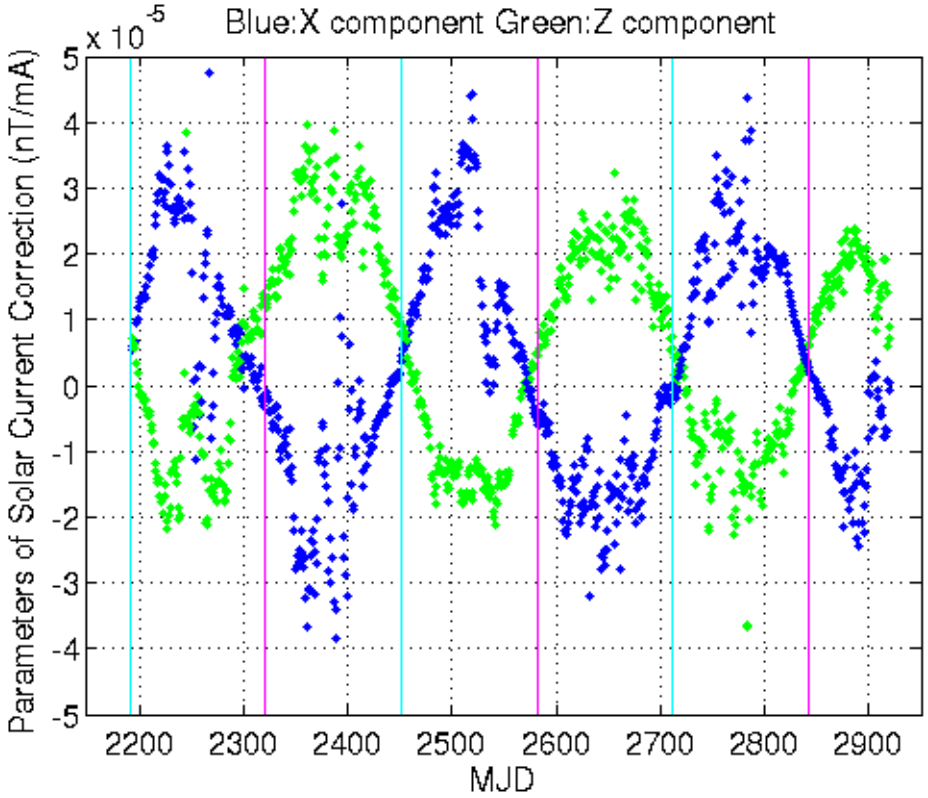

Figure 3.6: Local time dependence of the solar array magnetic disturbance in the X and Z component. The vertical lines indicate 12:00 LT(magenta) and 24:00 LT(cyan)

different distribution of the generated currents in the power supply loops. But our correction model applies only to the total solar current, I_{solar}, to describe the disturbance magnetic field, which doesn't represent this topological distribution of the currents in the loops caused by the change of the inclination. That means our correction model in Eq.(3.2) is too simple.

On the basis of the above analysis we try to separately describe the disturbance magnetic field of different solar cell panels. Since the panel on the top side has a small area, we first neglect it.

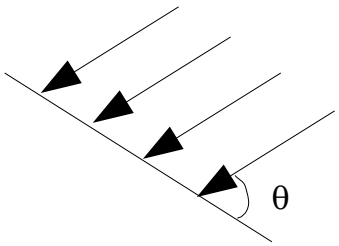

$$I_s = QS\sin(\theta) \tag{3.3}$$

This equation represents the magnitude of the current gener-

ated in the solar cell, where Q is the product of sunlight intensity and the conversion coefficient, S means the dimension of the illuminated area, θ means the inclination of the sunlight. So we have,

$$B_{s_1} = I_{s_1} A_1 = I_{s1} \begin{pmatrix} \alpha_1 \\ \beta_1 \\ \gamma_1 \end{pmatrix} = QS_1 \sin(\theta_1) \begin{pmatrix} \alpha_1 \\ \beta_1 \\ \gamma_1 \end{pmatrix}$$

$$B_{s_2} = I_{s_2} A_2 = I_{s_2} \begin{pmatrix} \alpha_2 \\ \beta_2 \\ \gamma_2 \end{pmatrix} = QS_2 \sin(\theta_2) \begin{pmatrix} \alpha_2 \\ \beta_2 \\ \gamma_2 \end{pmatrix}$$

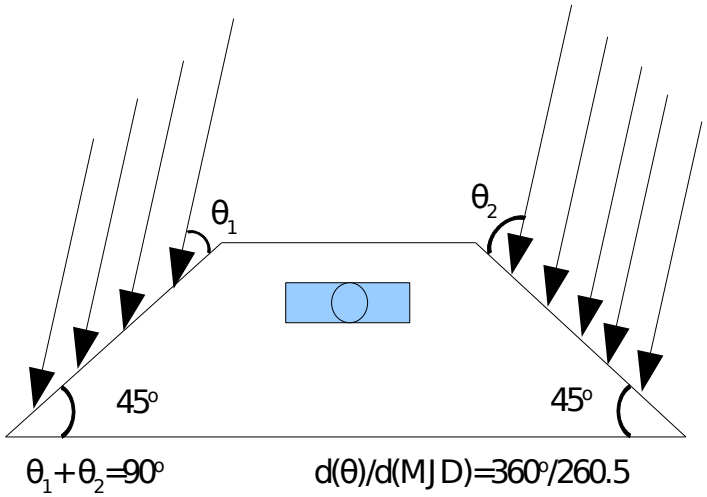

where B_{s_1} and B_{s_2} is, respectively, the magnetic field which is caused by the solar current in the left panel and right panel. We think the two panels have the same size, $S = S_1 = S_2$.

$$I_{solar} = I_{s_1} + I_{s_2} = QS \sin(\theta_1) + QS \sin(\theta_2) = QS(\sin(\theta_1) + \sin(\theta_2))$$

$$B_{solar\_fg} = B_{s1} + B_{s2}$$

$$= \quad QS \begin{pmatrix} \alpha_1 \sin(\theta_1) + \alpha_2 \sin(\theta_2) \\ \beta_1 \sin(\theta_1) + \beta_2 \sin(\theta_2) \\ \gamma_1 \sin(\theta_1) + \gamma_2 \sin(\theta_2) \end{pmatrix}$$

Consequently, if we go back to Eq.(3.2), and if both panels are illuminated, the coefficients A_{fg} should be,

$$A_{fg} = \begin{pmatrix} \alpha_{fg} \\ \beta_{fg} \\ \gamma_{fg} \end{pmatrix} = B_{solar\_fg}/I_{solar} = \frac{1}{\sin(\theta_1) + \sin(\theta_2)} \begin{pmatrix} \alpha_1 \sin(\theta_1) + \alpha_2 \sin(\theta_2) \\ \beta_1 \sin(\theta_1) + \beta_2 \sin(\theta_2) \\ \gamma_1 \sin(\theta_1) + \gamma_2 \sin(\theta_2) \end{pmatrix} \tag{3.4}$$

And if only one panel S_1 or S_2 is illuminated, then A_{fg} should be,

$$A_{fg} = \begin{pmatrix} \alpha_1 \\ \beta_1 \\ \gamma_1 \end{pmatrix} \text{ or } A_{fg} = \begin{pmatrix} \alpha_2 \\ \beta_2 \\ \gamma_2 \end{pmatrix}.$$

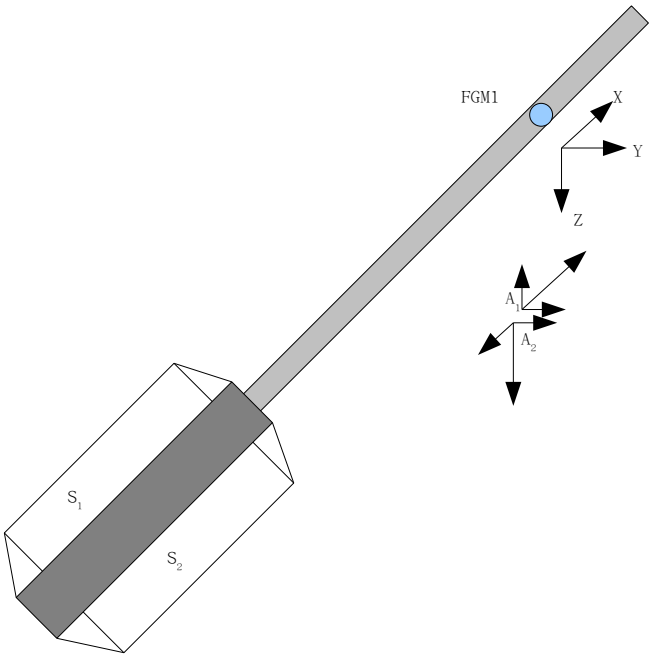

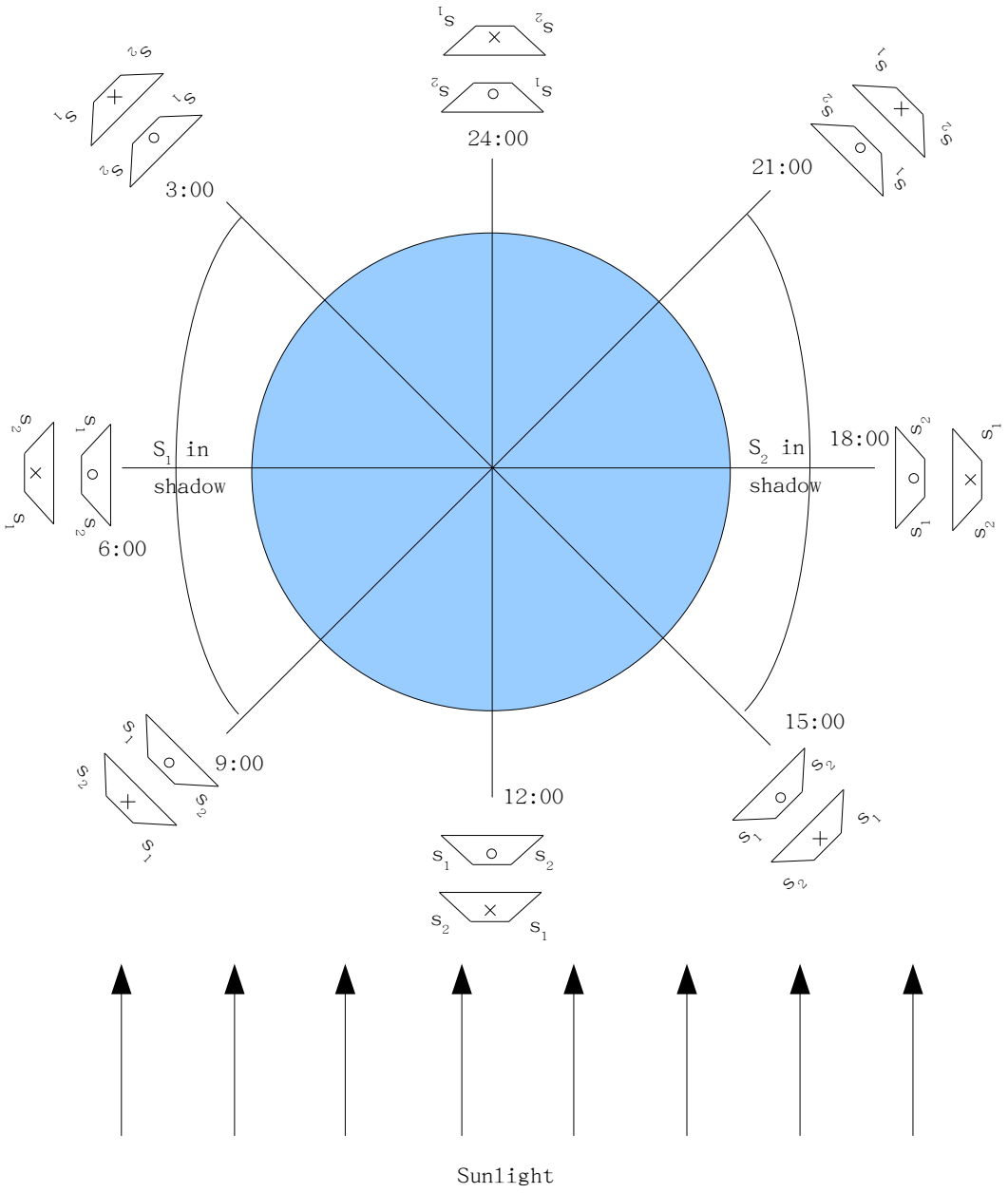
24:00
3:00
6:00
9:00
12:00
15:00
18:00
21:00
S1 in
shadow
S2 in
shadow
Sunlight

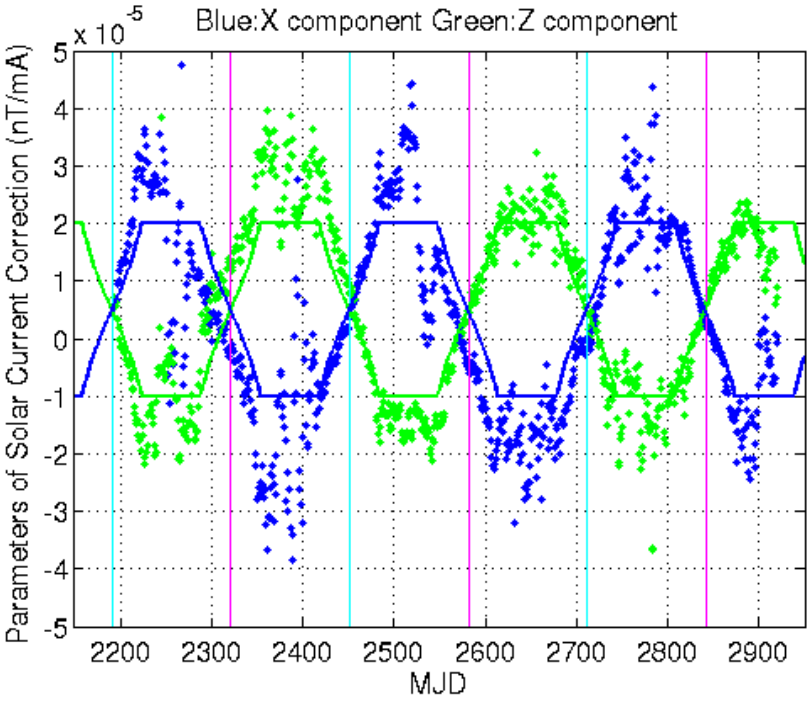

Figure 3.7: Local time dependence of the solar array magnetic disturbance in the X and Z component. The solid lines are the result of the model.

By summarizing the variation of A_{fg} in the 4 phases of a whole period, we have,

$$A_{fg} = \begin{cases} \begin{pmatrix} \alpha_2 \\ \beta_2 \\ \gamma_2 \end{pmatrix} & \begin{pmatrix} phase1(0 \leqslant p < 65) \\ 9:00 - 3:00\ S_1\ in\ shadow \end{pmatrix} \\ \frac{1}{\sin(\theta_1)+\sin(\theta_2)} \begin{pmatrix} \alpha_1 \sin(\theta_1) + \alpha_2 \sin(\theta_2) \\ \beta_1 \sin(\theta_1) + \beta_2 \sin(\theta_2) \\ \gamma_1 \sin(\theta_1) + \gamma_2 \sin(\theta_2) \end{pmatrix} & \begin{pmatrix} phase2(65 \leqslant p < 130) \\ 3:00 - 0:00(24:00) - 21:00 \\ \theta_1 = (p-65)\omega,\ \theta_2 = 90 - (p-65)\omega,\ \omega = \frac{360}{260.5} \end{pmatrix} \\ \begin{pmatrix} \alpha_1 \\ \beta_1 \\ \gamma_1 \end{pmatrix} & \begin{pmatrix} phase3(130 \leqslant p < 195) \\ 21:00 - 15:00\ S_2\ in\ shadow \end{pmatrix} \\ \frac{1}{\sin(\theta_1)+\sin(\theta_2)} \begin{pmatrix} \alpha_1 \sin(\theta_1) + \alpha_2 \sin(\theta_2) \\ \beta_1 \sin(\theta_1) + \beta_2 \sin(\theta_2) \\ \gamma_1 \sin(\theta_1) + \gamma_2 \sin(\theta_2) \end{pmatrix} & \begin{pmatrix} phase4(195 \leqslant p < 260) \\ 15:00 - 9:00 \\ \theta_1 = 90 - (p-195)\omega,\ \theta_2 = (p-195)\omega,\ \omega = \frac{360}{260.5} \end{pmatrix} \end{cases}$$

where p is the time difference between the actual MJD and the earlier MJD on which the

local time was 9:00. We now see that variation of the matrix A_{fg} is a function of the local time and implicitly of the day of mission. From the result in Figure 3.6, we take,

$$A_1 = \begin{pmatrix} \alpha_1 \\ \beta_1 \\ \gamma_1 \end{pmatrix} = \begin{pmatrix} 0.00002 \\ 0.00001 \\ -0.00001 \end{pmatrix} nT/mA, \quad A_2 = \begin{pmatrix} \alpha_2 \\ \beta_2 \\ \gamma_2 \end{pmatrix} = \begin{pmatrix} -0.00001 \\ 0.00001 \\ 0.00002 \end{pmatrix} nT/mA$$

and introduce them in to Eq.(3.4), Figure 3.7 shows the result of our simulation. After we used these simulation parameters to remove the disturbance of the solar current, we found better results in the phase 1 and 3 than in the phase 2 and 4. That means the situation when only one panel was illuminated is closer to the ideal correction model. In the other situation, for example, the top panel plays also a role and the recorded total current, I_{solar}, cannot represent the distribution of the magnetic field from the three panels.

3.4.2 The influences of the ASC-boom camera current

The Advanced Stellar Compass (ASC) on the satellite provides the high precision attitude needed for the magnetic field vector measurements. When the local time is around 21:00, 15:00, 09:00, 03:00, the sunlight will directly get into the ASC camera. The housekeeping data show that this leads to an extra current. The blue line in Figure 3.9 indicates the payload currents of the ASC on the boom. We can see a jerk of the current due to the incident sunlight. Corresponding to that, the $\triangle B = |B_{fgm}| - |B_{ovm}|$ shows a jerk as well.

Figure 3.8 shows how the relationship between the attitude of the satellite and the incident angle of sunlight. The maximal variation of this dynamic field is approximately 0.4nT and the corresponding proportion is 0.001nT/mA.

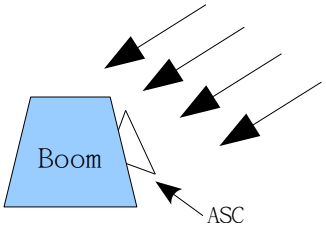

Figure 3.8:

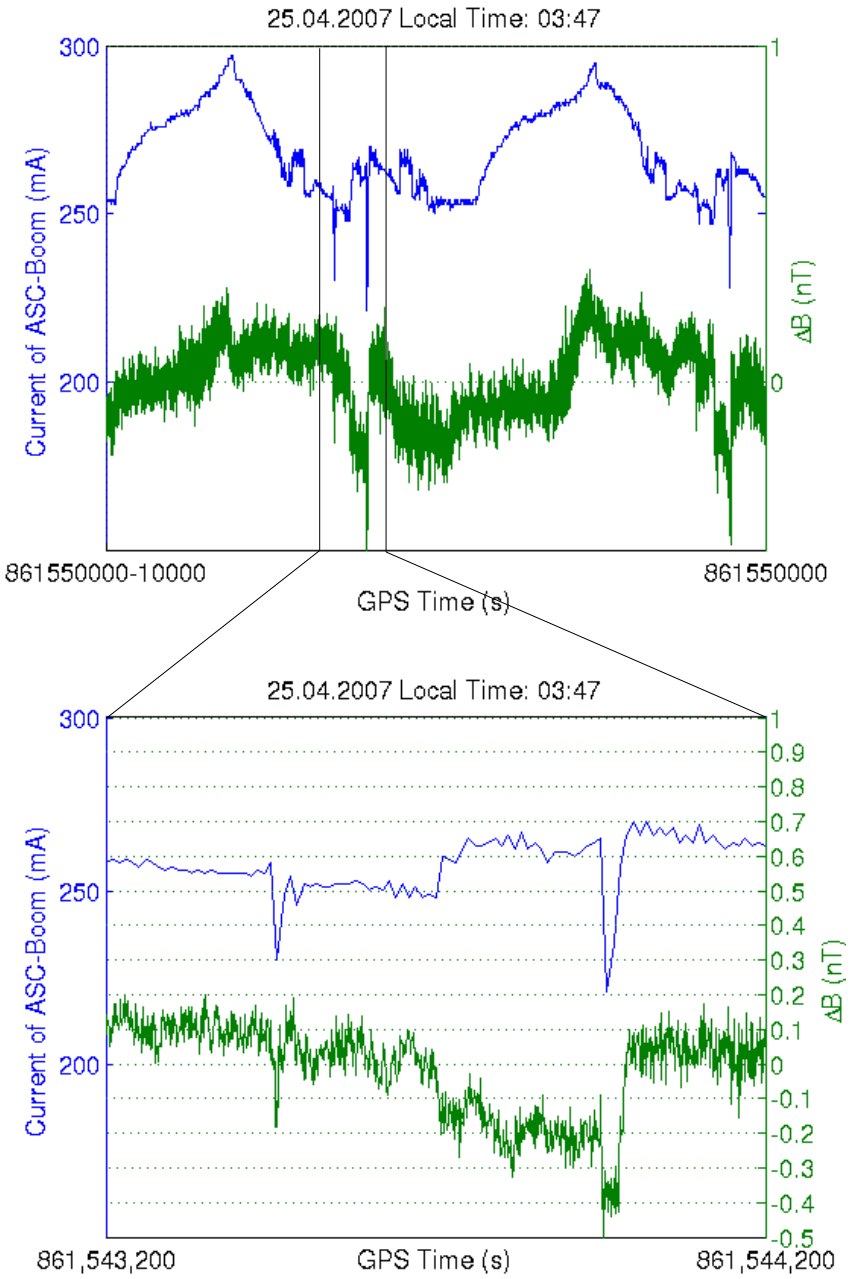

Figure 3.9: Influence of star tracker on the FGM readings

3.4.3 Redetermine the coefficients of the torquer correction

In Section 2.3 we have discuss the magneto-torquer correction. The correction is based on the coefficients which were determined in pre-flight test. The currents in the torquer coils generate the dynamic magnetic field. We use the following equation and the coefficients to remove it from the recorded magnetic field.

$$B = B - B_{tqr} = B - \alpha_{tqr} \bullet I_{tqr} = B - \begin{pmatrix} a_{11} & a_{12} & a_{13} \\ a_{21} & a_{22} & a_{23} \\ a_{31} & a_{32} & a_{33} \end{pmatrix} \begin{pmatrix} I_{tqrx} \\ I_{tqry} \\ I_{tqrz} \end{pmatrix}$$

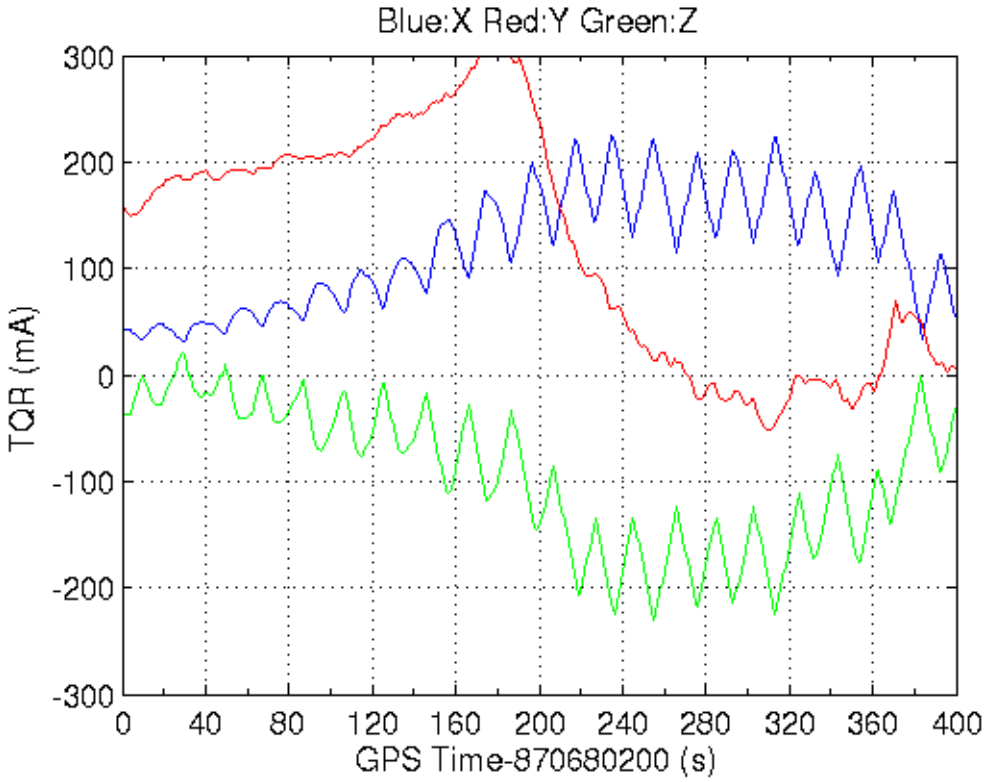

Figure 3.10: Example for the dynamic variations of the currents through the torquer coils

However, the in-flight measurements of the FGM and OVM show that the precision of the coefficients can be further improved. In order to isolate the torquer signal from the others,

the torquer currents are modulated by a 0.05Hz variation. From Figure 3.10 we can see the 20s periodical signal in the X and Z components of the torquer currents. Hence, we can analyze the spectrum of the residuals $\triangle B$ between B_{ovm} and B_{fgm} so that we can determine whether the torquer signal is completely removed.

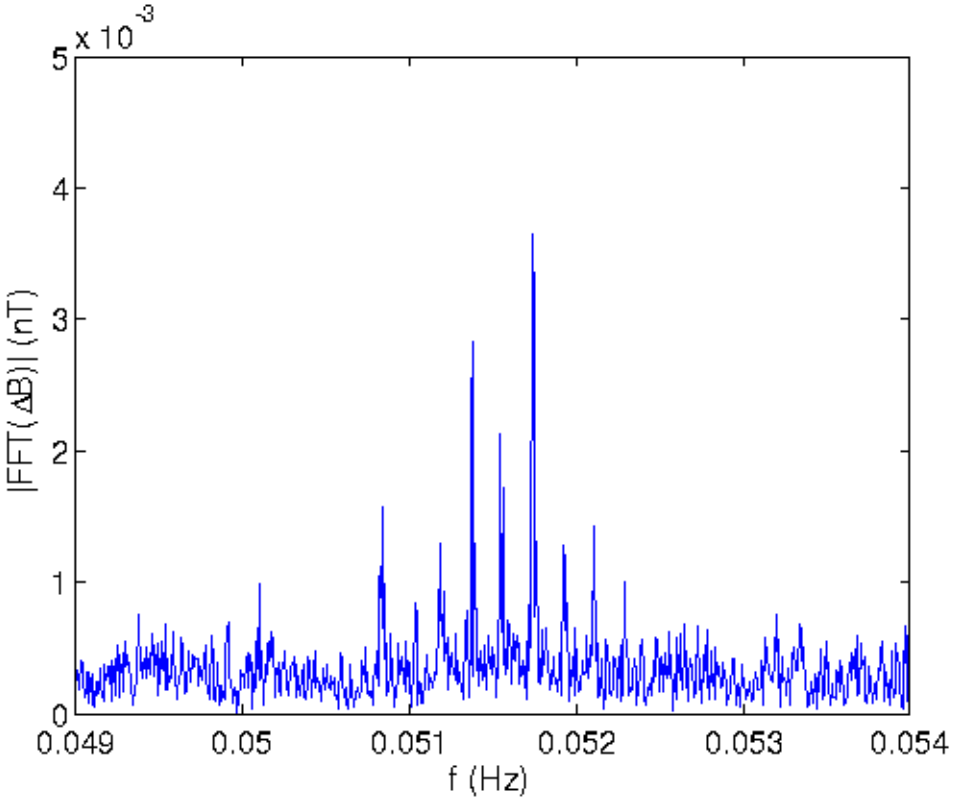

Figure 3.11: Signal spectra of ΔB. The spectral peaks mear 0.05Hz indicate imperfect torquer corrections

Figure 3.11 shows the FFT result of $\triangle B$ from the data of 09.08.2007. We can see peaks close to 0.05Hz. The peaks indicate that using the existing coefficients α_{tqr} the torquer signals are not completely removed from the FGM or OVM data.

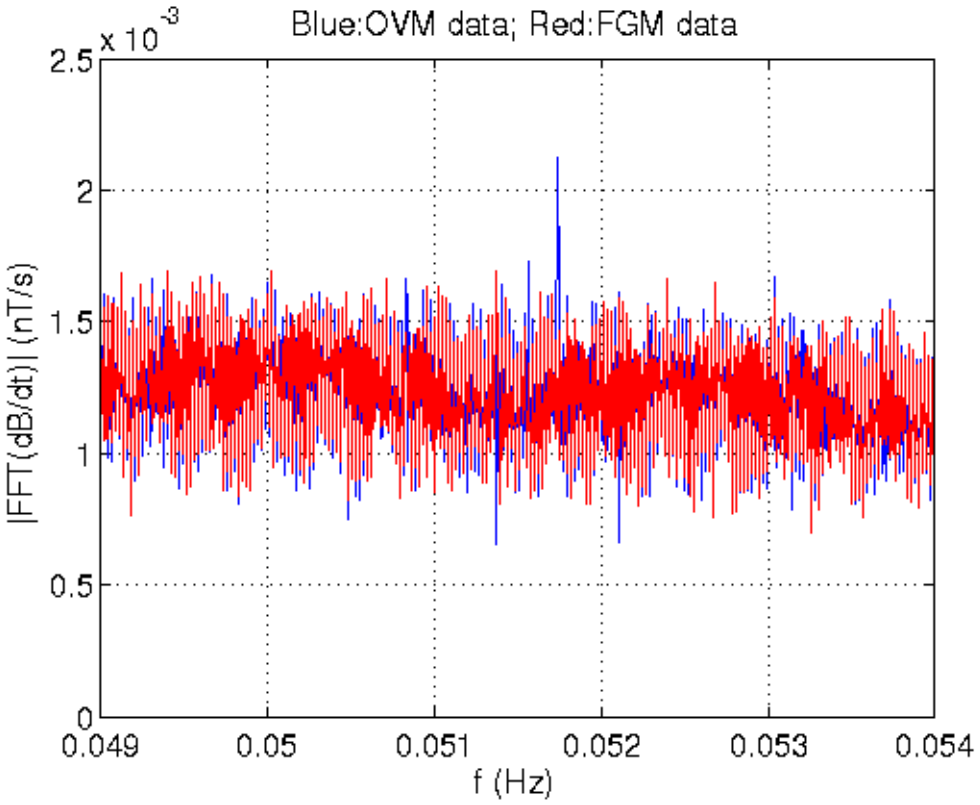

Figure 3.12: Individual signal spectra of the two magnetometers. Spectral peaks near 0.05Hz indicate imperfect torquer corrections

But how can we find out in which data set the 0.05Hz signal exist, in OVM data or FGM data? Because both B_{fgm} and B_{ovm} have strong low frequency signal(orbital period and its harmonic components) and the 0.05Hz torquer signal is very weak, it is difficult to distinguish it from the observed spectrum. We first use a high-pass FIR($D_i - D_{i-1}$) to filter, respectively, the FGM and OVM data and then analyze their spectra. The 0.05Hz peak exists in both FGM and OVM data. However, B_{ovm} has a stronger 0.05Hz signal than B_{fgm}. Figure 3.12 shows the result. So it can be concluded that the coefficients matrix of torquer correction for the OVM data requires more improvement.

We now discuss the method for improving the coefficients of the torquer correction. Our purpose is to find the new coefficients matrix α_{tqr}.

$$\alpha_{tqr} = \alpha'_{tqr} + \triangle\alpha_{tqr} = \begin{pmatrix} a_{11} & a_{12} & a_{13} \\ a_{21} & a_{22} & a_{23} \\ a_{31} & a_{32} & a_{33} \end{pmatrix} + \begin{pmatrix} \triangle a_{11} & \triangle a_{12} & \triangle a_{13} \\ \triangle a_{21} & \triangle a_{22} & \triangle a_{23} \\ \triangle a_{31} & \triangle a_{32} & \triangle a_{33} \end{pmatrix}$$

where α'_{tqr} is the old coefficient matrix which is supposed to be amended. $\triangle\alpha_{tqr}$ is the difference between the new one and the old one and the elements should not be very large.

$$\triangle B' = |B_{fgm}| - |B_{ovm}(\alpha'_{tqr})|$$

where $B_{ovm}(\alpha)$ doesn't mean $B_{ovm}\alpha$ but the OVM data corrected by the coefficients α, i.e B_{ovm} is function of the coefficients α. As mentioned above, due to the imperfection of the coefficients we have found a 0.05Hz peak in the spectrum of the $\triangle B'$. Since the error of each component is small, we can write,

$$\begin{aligned} |B_{ovm}(\alpha_{tqr})| &= |B_{ovm}(\alpha'_{tqr} + \triangle\alpha_{tqr})| \\ &= |B_{ovm}(\alpha'_{tqr})| + |B_{ovm}(\triangle\alpha_{tqr})| \\ &= |B_{ovm}(\alpha'_{tqr})| + \frac{B_x}{|B_{ovm}|}\triangle B_x + \frac{B_y}{|B_{ovm}|}\triangle B_y + \frac{B_z}{|B_{ovm}|}\triangle B_z \end{aligned}$$

where

$$\begin{pmatrix} \triangle B_x \\ \triangle B_y \\ \triangle B_z \end{pmatrix} = \begin{pmatrix} \triangle a_{11} & \triangle a_{12} & \triangle a_{13} \\ \triangle a_{21} & \triangle a_{22} & \triangle a_{23} \\ \triangle a_{31} & \triangle a_{32} & \triangle a_{33} \end{pmatrix} \begin{pmatrix} I_{tqrx} \\ I_{tqry} \\ I_{tqrz} \end{pmatrix}$$

So we have,

$$\begin{aligned} \triangle B &= |B_{fgm}| - |B_{ovm}(\alpha_{tqr})| \\ &= |B_{fgm}| - |B_{ovm}(\alpha'_{tqr} + \triangle\alpha_{tqr})| \\ &= |B_{fgm}| - |B_{ovm}(\alpha'_{tqr})| - |B_{ovm}(\triangle\alpha_{tqr})| \\ &= \triangle B' - (\triangle\alpha_{tqr} \bullet I_{tqr}) \bullet \frac{B_{ovm}}{|B_{ovm}|} \end{aligned}$$

If we can find the right $\triangle\alpha_{tqr}$, the 0.05Hz peak should disappear in the spectrum of $\triangle B$. In order to find the $\triangle\alpha_{tqr}$, we construct the following function,

$$E(\triangle\alpha_{tqr}) = \int_{f_1}^{f_2} |F(f)|df = \int_{f_1}^{f_2} F(f)F^*(f)df \tag{3.5}$$

where $F(f)$ is the continuous Fourier transform of $\triangle B$,

$$F(f) = \int \triangle B e^{-j2\pi ft}dt = \int (\triangle B' - (\triangle\alpha_{tqr} \bullet I_{tqr}) \bullet \frac{B_{ovm}}{|B_{ovm}|})e^{-j2\pi ft}dt$$

$\triangle B$ is a function of the parameters $\triangle\alpha_{tqr}$. The $\triangle f = f_2 - f_1$ may be chosen to cover a short bandwidth range around the 0.05Hz. If we discretize the function, we have

$$E(\triangle\alpha_{tqr}) = \sum_{f_1}^{f_2} F(f_i)F^*(f_i) \triangle f$$

where$F(f_i)$ is in this case the discrete Fourier transform of $\triangle B$. However, function E finally is a function of the parameters $\triangle\alpha_{tqr}$. So the problem is to find parameters $\triangle\alpha_{tqr}$ which make the function E minimal. In principle, this is a minimization problem.

$$min_{\triangle\alpha_{tqr}} E(\triangle\alpha_{tqr})$$

Because the coefficient array α'_{tqr} is very close to the right one, α_{tqr}, we can choose zero as an initial estimate of $\triangle\alpha_{tqr}$ to solve this minimax problem by using a sequential quadratic programming method.

We have done the calculation based on the data of all the years. From them the result of 2007 is taken as an example. Even though $\triangle\alpha_{tqr}$ are not the same from day to day and some of the elements(e.g. $\triangle\alpha_{22}$) show large uncertainties, their median value can be considered as a good estimation. The old coefficients are,

$$\alpha'_{tqr} = \begin{pmatrix} 7.40 & -2.60 & -2.40 \\ 0.00 & -10.70 & 0.00 \\ -0.40 & 0.30 & -11.60 \end{pmatrix} nT/A$$

and the $\triangle\alpha_{tqr}$ we have obtained are

$$\triangle\alpha_{tqr} = \begin{pmatrix} 0.385 & 0.134 & 0.162 \\ -0.402 & 1.452 & -0.199 \\ 0.237 & -0.247 & 0.232 \end{pmatrix} \pm \begin{pmatrix} 0.154 & 0.341 & 0.035 \\ 0.100 & 1.192 & 0.140 \\ 0.016 & 0.242 & 0.139 \end{pmatrix} nT/A$$

Thus we have the new coefficients for OVM torquer correction

$$\alpha_{tqr} = \alpha'_{tqr} + \triangle\alpha_{tqr} = \begin{pmatrix} 7.785 & -2.466 & -2.238 \\ -0.402 & -9.248 & -0.199 \\ -0.163 & 0.053 & -11.368 \end{pmatrix} \pm \begin{pmatrix} 0.154 & 0.341 & 0.035 \\ 0.100 & 1.192 & 0.140 \\ 0.016 & 0.242 & 0.139 \end{pmatrix} nT/A$$

Applying these new coefficients we can repeat the spectrum analyses in order to see how much better the torquer correction is.

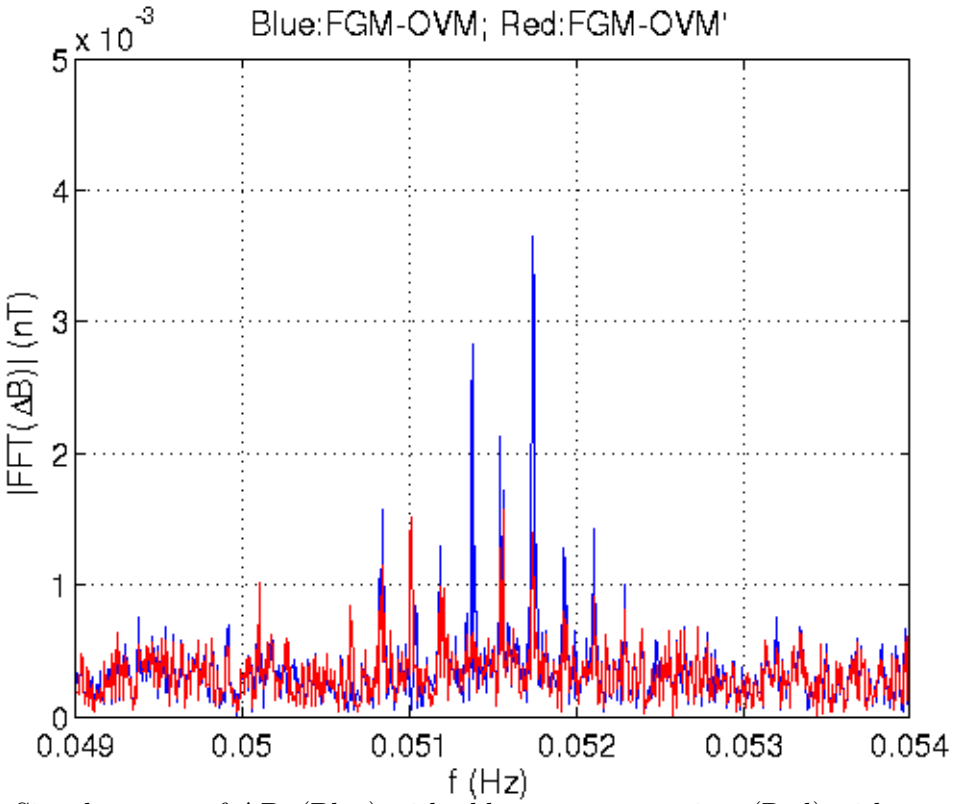

Figure 3.13: Signal spectra of ΔB, (Blue) with old torquer correction, (Red) with new coefficients

After comparing the two power spectra (the blue using the old coefficients and the red the new ones) we can see that the 0.05Hz peaks are reduced. It should be pointed out that $\triangle\alpha_{tqr}$ has a very small value, the changes of OVM data incurred by the new coefficients are not more than 0.1 nT.

3.4.4 The CHAMP remanent field correction of the OVM measurements

As we know, if an object with magnetic moment moves in an ambient magnetic field, a torque is exerted due to the interaction, and the attitude of the object will change. The same situation is valid for the CHAMP satellite. The body of the satellite carries the sources, such as the magnetic material and the fixed currents, which produced the magnetic moment. Hence a set of three magneto-torquers is employed by the Attitude and Orbit Control Subsystem (AOCS) in order to eliminate the effect of the satellite remanent field. Using the high precision attitude information from the advanced stellar compass the AOCS commands the torquer currents which produce the magnetic moment dynamically to compensate on average the satellite remanent field. So we have,

$$B_{tqr\_ov} + B_{sc\_ov} \approx 0$$

However, this brings another problem. The magnetic field at the sensor OVM is,

$$B_{ovm} = B_{em\_ov} + B_{tqr\_ov} + B_{sc\_ov} \approx B_{em\_ov}$$

where B_{em_ov} is the Earth's magnetic field at the OVM which we are finally interested in. But the torquer correction is also necessary. If we have only made a torquer correction, we obtain,

$$B'_{em\_ov} = B_{ovm} - B_{tqr\_ov} = B_{em\_ov} + B_{sc\_ov}$$

That means, the torquer correction and the remove of B_{sc_ov} should be jointly implemented. However, $B_{sc\_ov} \approx -B_{tqr\_ov}$ means, the magnetic field of the torquer currents are not always equal to the satellite remanent magnetic field. It is only compensation on average.

Nevertheless, we can still estimate the B_{sc_ov} according to the B_{tqr_ov}. To remove the quick variations and the effect depending on local time we calculate the 260 days average value of the torquer currents to estimate the B_{sc_ov} because of the linear relation between B_{tqr_ov} and I_{tqr}. Figure 3.14 shows our calculations.

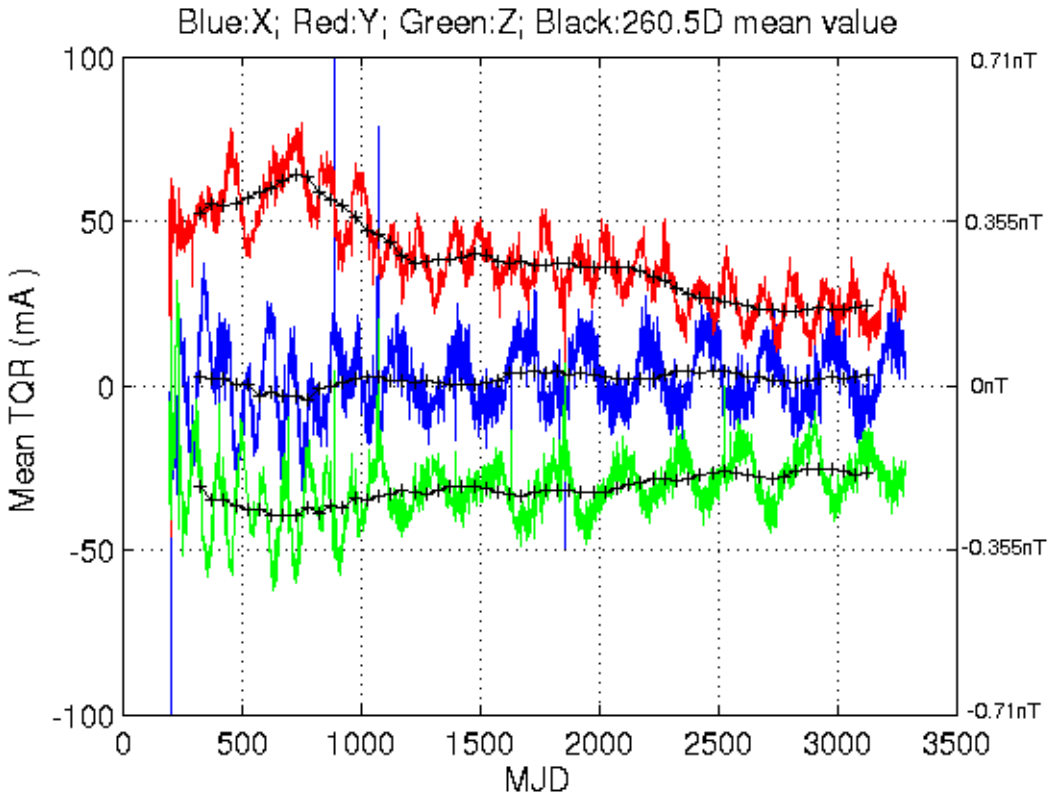

Figure 3.14: Daily averages of the torquer currents of the three components and 260-day moving averages of the currents

The crossed lines give the 260 days average torquer current values for each component. From which $\overline{I_{tqrX}}$ can be considered to be constant, $\overline{I_{tqrX}} = 0$. So we have,

$$\begin{pmatrix} B_{sc\_ovX} \\ B_{sc\_ovY} \\ B_{sc\_ovZ} \end{pmatrix} = \eta \begin{pmatrix} 0 \\ \overline{I_{tqrY}} \\ \overline{I_{tqrZ}} \end{pmatrix}$$

where η is 0.0071nT/mA for the position of OVM, which was obtained in the pre-flight test, $\overline{I_{tqrY}}$ and $\overline{I_{tqrZ}}$ are the average torquer currents of the Y and Z components.

3.5 The result of the new processing with continuous parameters

Different to the standard processing, we have in the new approach continuously varying parameters applied as well as improved corrections of the disturbing magnetic fields from the satellite body. We show some result in this section to evaluate the new processing.

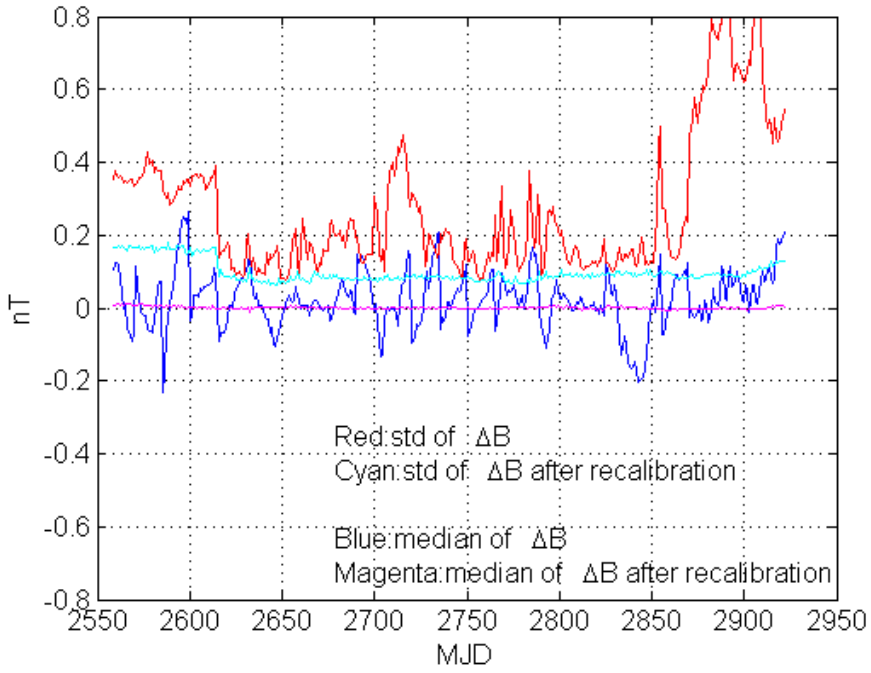

Figure 3.15: Temporal variation of several parameters after standard processing of 2007

As an indicator for the quality of the agreement between the data from the OVM and the FGM, we use the difference in total fields, $\triangle B$. Two parameters for characterizing $\triangle B$ are the standard deviation(std) and the median, both applied to the data of one day. Figure 3.15 shows for the year 2007 the standard deviation and median of $\triangle B$ in red and blue,

respectively, of the data routinely processed. Quite evident is the 15-day periodicity in some parts of the blue curve. This is the update rate of the FGM parameters. For test purposes the scalar calibration has been repeated and the nine parameters are updated on a daily case. After that the std of $\triangle B$ is markedly reduced(cyan line) and the median of $\triangle B$ is constantly zero(magenta).

Alternatively, we applied the new processing to the data of 2007. Figure 3.16 shows the results corresponding to those of Figure 3.15. Although we are using predetermined functions or constant values for the FGM parameter, the size of the standard deviation and median values of $\triangle B$ are not significantly larger. The absence of any long-term trend confirms the choice of functions for the parameters. Also in this case the magnetic field data were subjected to another scalar calibration on a daily case. When all the 9 FGM parameters are adjusted we obtain again a constantly small std of$\triangle B$(cyan) and a zero median(magenta).

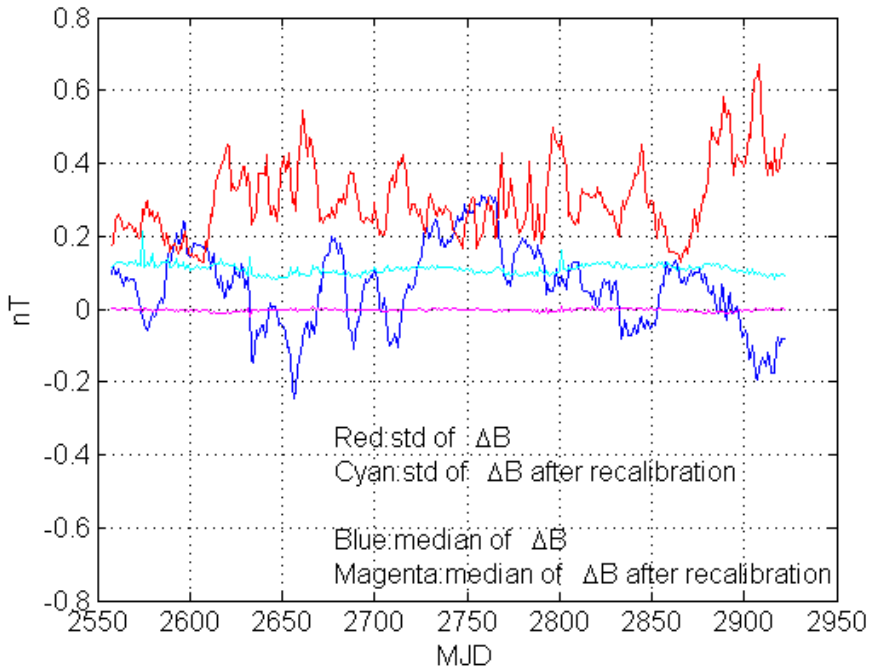

Figure 3.16: Temporal variation of several parameters after new processing of 2007

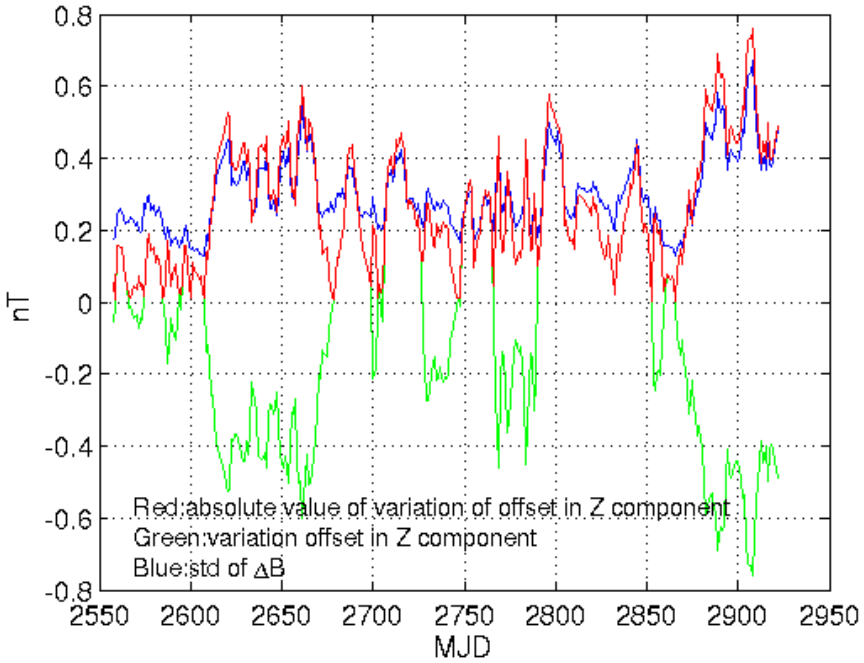

Figure 3.17: Comparison of the ΔB standard deviation with the Zcomponent offset

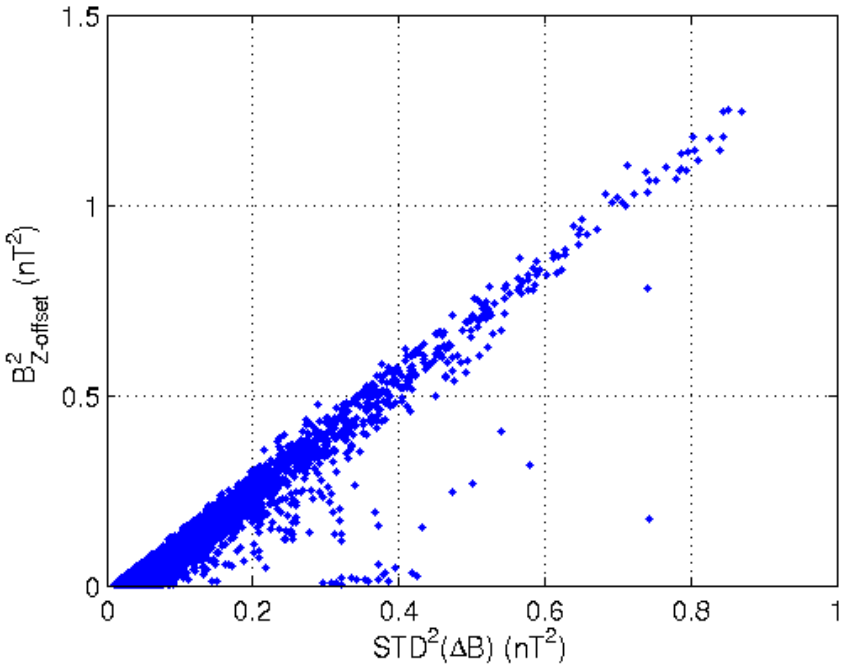

Figure 3.18: Linear correlation between the variance of ΔB and the squared Z offset

Since we want to avoid the scalar calibration in the new processing approach, we try to identify the reason for the temporal variations of the standard variation (red curve in Figure 3.16). In a previous section we had already presented some indications that the Z component offset plays an important role for $\triangle B$. In Figure 3.17 we repeat the std of $\triangle B$ as a red curve. In green the Z component offset, as determined in the daily scalar calibration, is plotted. For a better comparison the absolute value of the offset is drawn in blue. The synchronous variation of the red and blue curves provides strong evidence for the close relationship between the Z offset and the standard deviation.

For obtaining a more quantitative expression of the relation between the two quantities we assumed the following linear function.

$$std^2(\triangle B) = aZ_0^2 + noise^2$$

For testing this assumption we made use of the daily results of these two quantities for the years 2001 through 2008. Figure 3.18 shows a scatter plot of all the data points. As expected, a nice linear relation emerges. From a linear regression we obtain the coefficients and can write,

$$std^2(\triangle B) = 0.6655Z_0^2 + 0.0390nT^2 \tag{3.6}$$

For the physical interpretation of this result we make a short model calculation. The Earth's magnetic field can be approximated by a dipole with the components,

$$X = B_0 \sin\theta,\ Y = 0,\ Z = 2B_0 \cos\theta$$

where B_0 is the field strength at the equator and θ the angle of colatitude($\theta = 0^o$at North pole). The effect of a small disturbance field, b, on the field magnitude can be expressed in the form of a scalar product.

$$\triangle B = \frac{b \bullet B}{|B|} = \frac{Z_0(2B_0 \cos\theta)}{B_0\sqrt{1 + 3\cos^2\theta}}$$

For an average over an orbit of the squared function we obtain

$$\left\langle \triangle B^2 \right\rangle = \left\langle \frac{4Z_0^2 \cos^2\theta}{1+3\cos^2\theta} \right\rangle = \frac{2}{3} Z_0^2$$

The obtained orbital average can be compared with the squared standard deviation of $\triangle B$ in Eq.(3.6). It is interesting to note, that the proportionality factor of Z_0^2 obtained in the correlation analysis is very close to the one predicted from the simple dipole model(0.6655 vs 0.6667). This confirms the role of the Z offset for the std of $\triangle B$. The imperfection of all the other 11 parameters contribute to the noise floor of $\triangle B$ which amounts to $\sqrt{0.039} \approx 0.2nT$(See also Figure 3.17). Based on the analysis above, if an daily Z offset correction is necessary, we can use Eq.(3.6) to derive the Z offset from the std of $\triangle B$.

Regarding the remaining residuals, $\triangle B$, we can find a mathematical way to minimize the values. We have,

$$\triangle B = |B_{fgm}| - |B_{ovm}|$$

The residual $\triangle B$ can be distributed among the components of the FGM readings as follows,

$$\begin{pmatrix} B'_x \\ B'_y \\ B'_z \end{pmatrix} = \frac{|B_{ovm}|}{|B_{fgm}|} \begin{pmatrix} B_x \\ B_y \\ B_z \end{pmatrix} = (1 - \frac{\triangle B'}{|B_{fgm}|}) \begin{pmatrix} B_x \\ B_y \\ B_z \end{pmatrix} \tag{3.7}$$

The above equations forces that, $|[B'_x,\ B'_y,\ B'_z]|$is equal to $|B_{ovm}|$. Unfortunately, the obtained correction is not unique. As can be seen, its value is weighted by the amplitude of the component. Even though, we regard the correction as worth while, in order to make the OVM and FGM data consistent, in particular for correcting the B_z offset deviations.

In practice we find a short-period scatter in the $\triangle B = |B_{fgm}| - |B_{ovm}|$, which reflect the measurement noise of the OVM data. This is typical considering the principle of the Overhauser magnetometer. In order to avoid a contamination of the FGM vector data by this short-period noise of the OVM measurements we applied a low-pass filter with a cut-off period at 80 sec to the $\triangle B$ before computing the Eq.(3.7).

$$\triangle B' = filter(\triangle B) = filter(|B_{fgm}| - |B_{ovm}|)$$

As we can see, in Figure 3.19, the difference between the $|[B'_x \quad B'_y \quad B'_z]|$ and $|B_{ovm}|$ only shows the measurements noise of the OVM, and the amplitude of the OVM measurement noise is $\pm 0.1\, nT$. The peaks indicate a little stronger noise at locations where the intensity of the magnetic field is weak (over the equator).

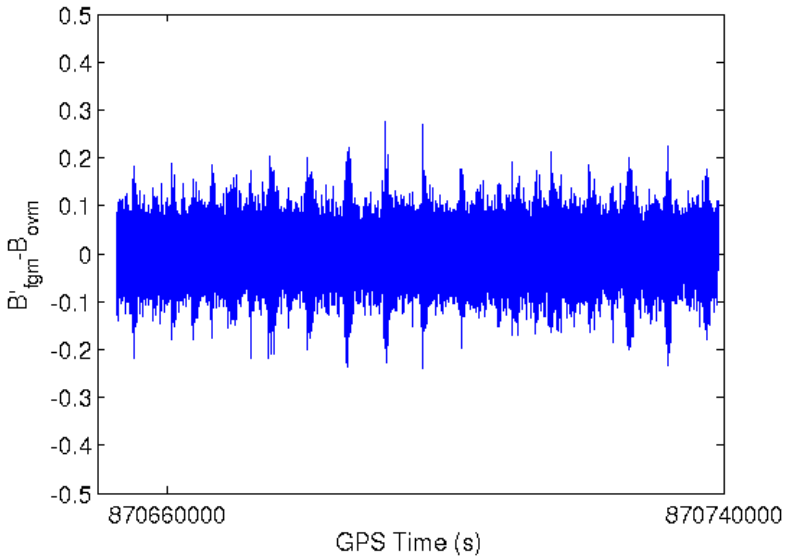

Figure 3.19: An example of one day. Difference between the magnitude of the field FGM data and the OVM readings, only the OVM noise remains, no systematic variation

Chapter 4

Time Variation of the FGM Calibration Parameters and Problem of Cross-talk

The 9-parameter scalar calibration has proved to be a very robust and practical solution in the presence of measurement noise in many missions for magnetic field investigations. However, its reliability depends on the degree of cross-talk between the involved error parameters and functions.

At the beginning of Chapter 3 we have discussed the form of the error for each component. We consider that the error of each component is a function of the measured signal(this means we think the error are only from the instrument itself),

$$\triangle E_{x,y,z} = f_{ins}(B_{fgmx,y,z})$$

With the error propagation function which we have frequently used, the error of the scalar value can be given,

$$\triangle B = |E_{fgm}| - |B_{ovm}| = \frac{B_x}{|B|}\triangle E_x + \frac{B_y}{|B|}\triangle E_y + \frac{B_z}{|B|}\triangle E_z$$

The idea of the 9-parameter scalar calibration is fundamentally a simplification of the error

function $f_{ins}(B_{fgmx,y,z})$ and to give relevant parameters concrete physical significance. That means, we consider an error function $f_{ins}(B_{fgmx,y,z})$ in the form(we take the X component for example),

$$\triangle E_x = f_{insx}(B_{fgmx,y,z}) = O_x + S_x B_{fgmx} + \cos(A_{xy}) B_{fgmy} + \cos(A_{xz}) B_{fgmz}$$

and then we name O offset of the component, S scale factor or sensitivity of the component, and A non-orthonormal angles between the components. Why do we take the $f_{ins}(B_{fgmx,y,z})$ in such form? It is because of our knowledge about the error of a vector magnetometer, which we have discussed in Chapter 2. Therefore we have this linear error model,

$$\triangle B = |E_{fgm}| - |B_{ovm}| = P \bullet M$$

We establish the right variable matrix M and solve for the right parameter vector P.

However, the actual errors of the magnetometers in the satellite are much more complicated than this error model. For example, if we consider some non-linearity errors of the X component or some error due to the temperature dependence of the scale factor, we have to take the additional terms(B^3_{fgmx} and $(T_{csc} - \mathbf{T_0})B^2_{fgmx}$) in matrix M to extend the model. Furthermore, if there are some disturbing magnetic fields from the satellite body, the component error function will be

$$\triangle E_x = f_{insx}(B_{fgmx,y,z}) + f_{satx}(t, I, T, P...)$$

The $f_{satx}(t, I, T...)$ is a function of the time t, current I, temperature T, position P and other possible variables which indicate the source of error. More generally, both error functions f_{ins} and f_{sat} can be described by non-linear functions or non-parameter functions rather than linear parameter functions. Therefore, we consider a generalized additive model for the scalar error,

$$\begin{aligned} \triangle B &= |E_{fgm}| - |B_{ovm}| \\ &= \frac{B_x}{|B|}(f_{insx} + f_{satx}) + \frac{B_y}{|B|}(f_{insy} + f_{saty}) + \frac{B_z}{|B|}(f_{insz} + f_{satz}) + f_{ovm} \end{aligned}$$

Where f_{ovm} is the error function of the OVM, if there is one.

Unfortunately, the information about these error functions is insufficient considering the in-flight calibration. The $\triangle B = |E_{fgm}| - |B_{ovm}|$ is only the criterion to estimate them. Moreover, due to the orbit of the satellite the measurements of the instruments are very nonuniform distributed. This leads to a problem of cross-talk or mis-coupling. This means, if we take a wrong error function or an error function in a wrong form, we invert the wrong error function or wrong parameter. For example, imagine that all the errors of $\triangle B$ were caused by the OVM, if we only consider the FGM and use the 9-parameter scalar calibration to derive the parameters, then the result is totally wrong. There are two types of cross-talk problem, one is that the error function in the model mismatches those that are not taken into account, the other is that both error functions are taken into the model, but due to the dependent or nonuniform distributed variables, they are not decoupled from each other.

The key issue is now to decide which error function in which form is the right. This we want to achieve with the help of our apriori knowledge about the error or other restrictive conditions. An important principle is that, if we want to calculate the main source of the error, then we take the corresponding error function. For example, if we know $f_{insx} \gg f_{satx}$, then we can neglect f_{satx} and take only f_{insx}. Another important idea is in case we cannot directly determine which error function to choose, we can take a simple form of the model, e.g. 9-parameter linear model, to estimate the parameters or functions. We analyze these parameters and functions to judge whether they agree with our expectation about the corresponding error or not. If they don't agree, we believe the error is coming from another source and consider the model corresponding to that form.

As a result, in Chapter 3 we have applied continuous descriptions of the parameters to produce the FGM and OVM data. We think that the major part of the error f_{ins} is already removed. However, if we do again the 9-parameter scalar calibration for every day, the derived parameters may give us more details of their time variations or an indication of other error sources. In this chapter we discuss the result of the calibration and the cross-talk problems we have found. For some of the before unknown errors we give a mathematical solution and corresponding physical explanation.

4.1 The variation of the recalibration parameters

If we do again a daily 9-parameter scalar calibration for the data which have been processed by the continuous parameters, namely logarithmically evolving scale factors, constant sensor offsets and misalignment angles, the derived parameters are losing their original physical significance. More probably they give information about their daily apparent variation. Thereby we can study whether the variation is due to the variation of the environment of the satellite in the space or due to some other reasons.

We know, the orbit(almost circular, near polar (i=87°)) of CHAMP leads to variation of the environment of the satellite in the space. The satellite flies everyday alternatively in sunlight and in shadow. How long in sunlight and how long in shadow depends on the local time of the satellite orbit. The local time of the orbit varies from 00:00 bis 24:00 and its repetition period is 260.5 days. So we can name 260.5 days one satellite year (SY). At different local time the satellite is exposed to sunlight for a different period. We name one orbital period (93min) of the satellite one satellite day (SD). Accordingly, SD has different length of daytime and nighttime. For example, around local time 24:00 or 12:00 the daytime of SD is about 45min and around 15:00 09:00 03:00 or 21:00 it is about 60min. Around 18:00 or 06:00 the satellite flies in the sunlight all the time, which is similar to polar summer in the polar region on the ground. The different sunshine duration results in a variation of the conditions onboard the satellite, especial the temperature. The maximum of the daily average temperature is around local time 18:00 and 06:00 and the minimum is around 24:00 and 12:00. If we define the days with daily average temperature higher than 10^oC hot satellite season(SS) and under 10^oC cold satellite season, then the pendulation of hot and cold SS has a 130D period. Approximately, we think, the environmental conditions of the satellite during the days in the same phase of SS are same. Figure 4.1 shows the relationship between these concepts about satellite day(SD), satellite season(SS) and satellite year(SY). In this section we discuss the variation of the recalibration parameters and the possible influence on them due to the variation of the environmental conditions. By means of that we can find some hints of other error sources, especially from the satellite body.

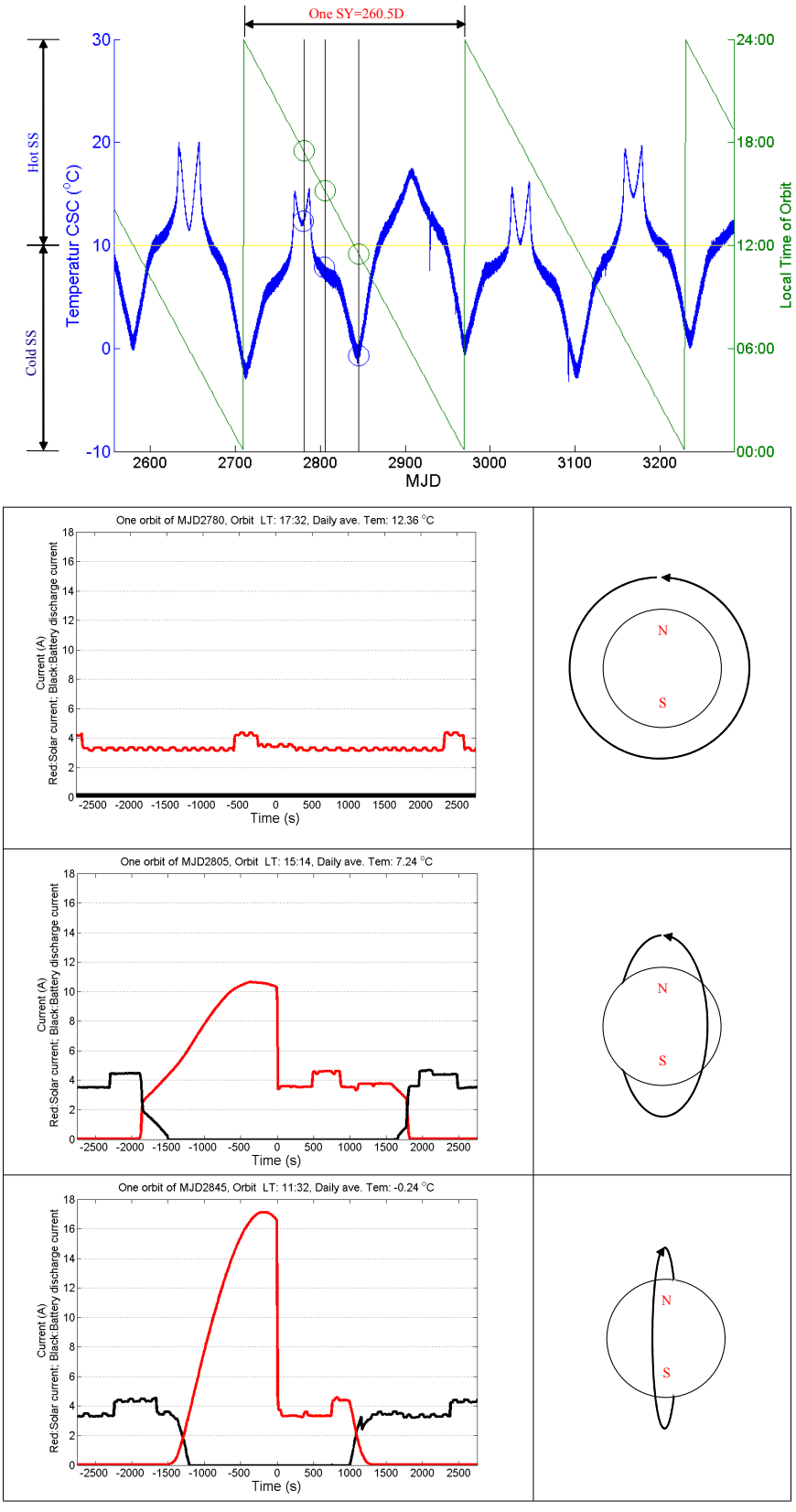

Figure 4.1: The relationship between local time, SD, SS and SY. The magnetometer coils temperature indicates the hot and cold SS. The presence of solar current and battery discharge current indicates respectively the nighttime and daytime of SD

4.1.1 The variation of the scale factors

The long-term time dependency of the scale factors is represented by a natural logarithm function in the processing. So in recalibration we can see more details, how they vary due to other effects. We can see that, as expected, the scale factor of the Y-axis shows larger variations than the X and Z-axis since the Y(eastward) component of the Earth's magnetic field has the smallest intensity($\pm 1 \times 10^4 nT$) compared to the other two components(X : $\pm 3 \times 10^4 nT$; $Z : \pm 6 \times 10^4 nT$). Therefore it is harder, to distinguish it from other effects or from noise. Obviously, the variations of the scale factors have a strong relationship with the local time of the CHAMP orbit. The signal of SS alternation emerges clearly in the scale factor variations. Such synchronous variations indicate a correlation to temperature. The most relevant temperature inside the satellite, which can affect the outputs of the FGM, is the temperature of the CSC sensor coils.

Figure 4.2 shows the scale factors of the X and Z components and the temperature of the CSC coils during 2006 and 2007. A strong correlation between temperature and scale factors can be seen. Special attention is paid to the period when the temperature variation curve of the CSC coils showed a unique double peaked structure. The variations of the scale factors also exhibit such a structure. The figure below shows an example at the beginning of the year 2006. We can clearly see that the variations of the scale factors exhibit a similar pattern as the CSC temperature.

Why does the temperature effect still exist in the data even though they have been corrected by the CSC temperature in data processing? There are maybe two possible reasons for these result. One is that possibly the CSC temperature correction alone is not enough. We know, not only the CSC temperature shows a double peaked variation, as well other temperatures, for example, the ADC voltage reference temperature(see in Figure 4.4). The influence of the temperature is, in most cases, so complicated that it is very hard to find a clear correspondence between the scale factors and the temperatures of the different parts inside the FGM instrument even in laboratory tests. The other possibility is that the correction of the CSC coil temperature we have made is not so correct. For this case there are also two possibilities. We can revisit our CSC coil temperature correction.

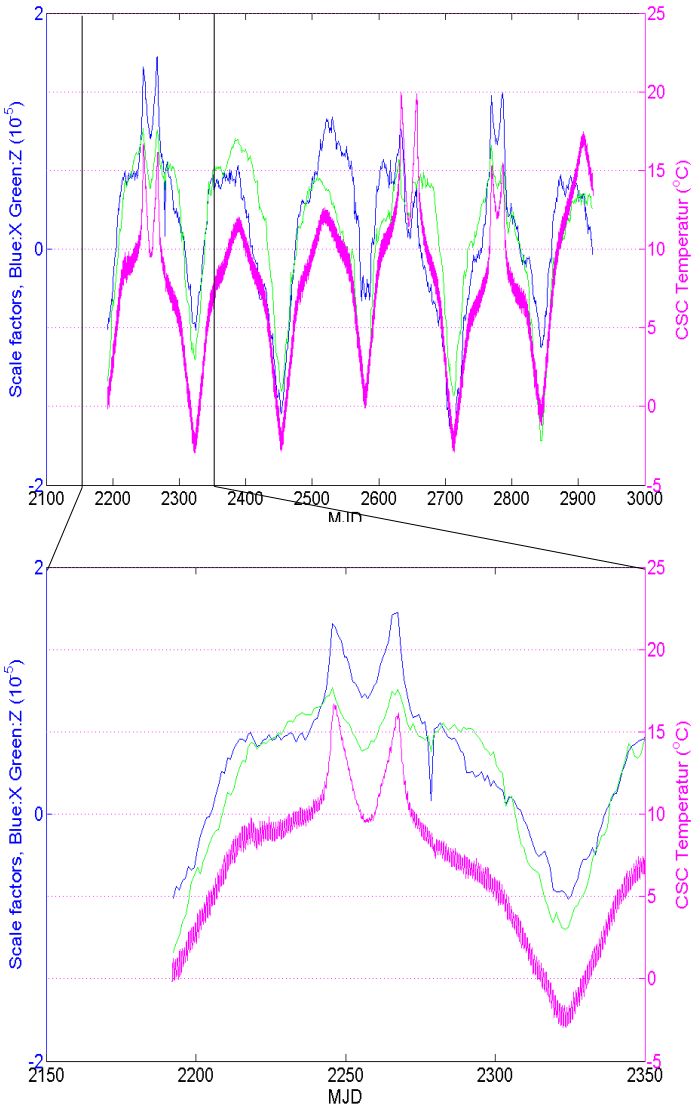

Figure 4.2: Relation between the FGM sensor temperature and the scale factors X and Z components

$$\begin{pmatrix} l_{Tx} \\ l_{Ty} \\ l_{Tz} \end{pmatrix} = \begin{pmatrix} \mathbf{l_0} - \mathbf{l_{T1x}}(T_{csc} - \mathbf{T_0}) - \mathbf{l_{T2x}}(T_{csc} - \mathbf{T_0})^2 \\ \mathbf{l_0} - \mathbf{l_{T1y}}(T_{csc} - \mathbf{T_0}) - \mathbf{l_{T2y}}(T_{csc} - \mathbf{T_0})^2 \\ \mathbf{l_0} - \mathbf{l_{T1z}}(T_{csc} - \mathbf{T_0}) - \mathbf{l_{T2z}}(T_{csc} - \mathbf{T_0})^2 \end{pmatrix}$$

The equations show how the scale factors are corrected by the CSC temperature data. Here are $\mathbf{l_{T1x}} = 29.6ppm/K$, $\mathbf{l_{T1y}} = 30.37ppm/K$, $\mathbf{l_{T1z}} = 30.46ppm/K$ and the quadratic term is $\mathbf{l_{T2}} = 4 \times 10^{-8}/K^2$ for all components. One possibility is that the parabolic correction model may not be accurate to describe the influences of the temperature.

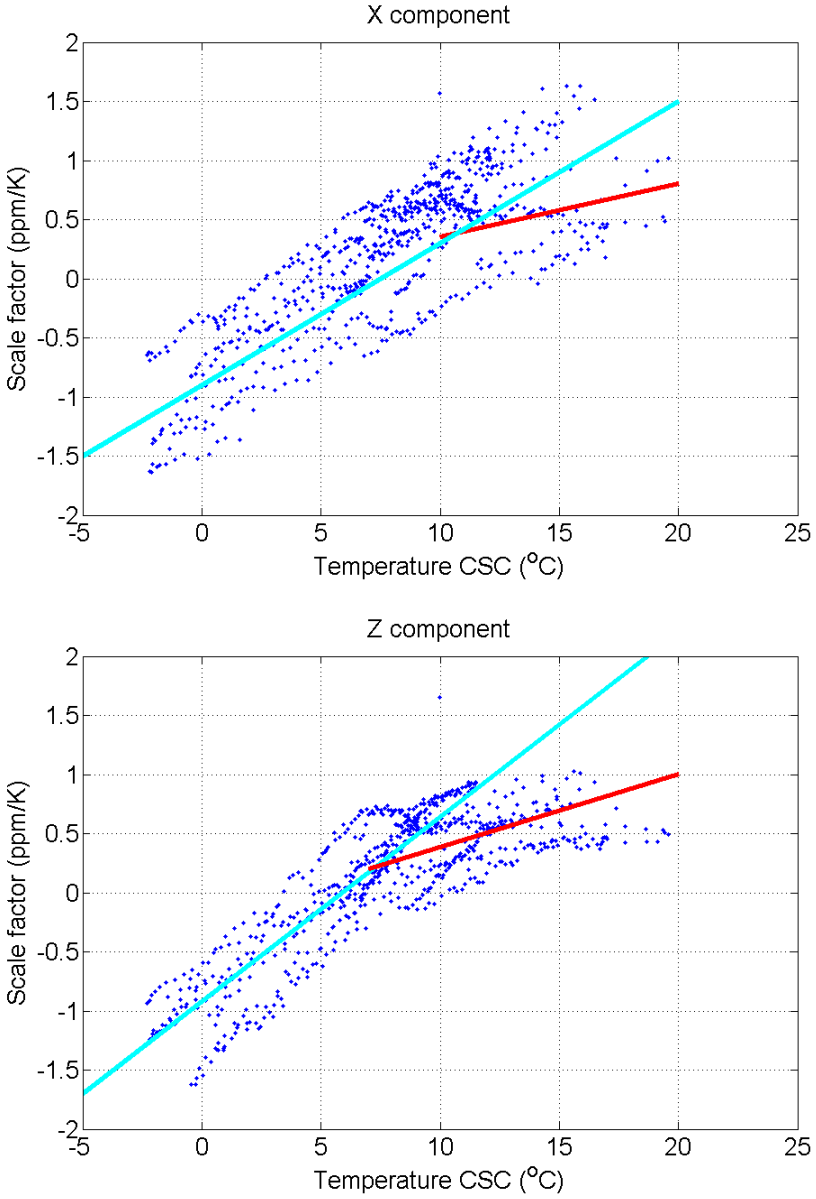

Figure 4.3: The temperature and scale factor plots show some thermal hysteresis.

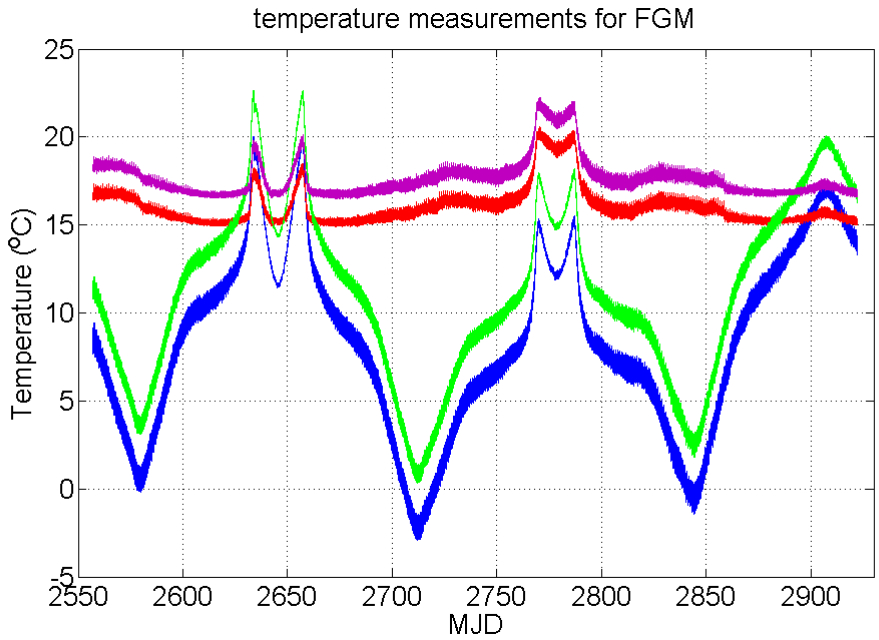

Figure 4.4: Blue: CSC feedback coil temperature; Red: ADC voltage reference temperature; Green: Fluxgate sensor temperature; Magenta: Magnetometer ADC bank temperature

The thermal effects are usually complicated and sometimes show thermal hysteresis (see in Figure 4.3). The other possibility is that the model itself is accurate enough, but the coefficients may have changed due to the space conditions after the satellite was launched. If this reason is supposed, we can do some small corrections on these three linear parameters $\mathbf{l_{T1x,y,z}}$, to see whether the temperature effect reduces.

We made a test using slightly different coefficients $\mathbf{l_{T1x,y,z}}$, respectively, $28.5ppm/K$, $29.2ppm/K$, $29.3ppm/K$(that means all coefficients are $1.1ppm/K$ smaller) to process the FGM data. After that we obtain recalibrated results.

It can be seen in Figure 4.5 that for the new coefficients the scale factors of X and Z components are becoming smoother at low temperature but on the hot days the scale factor of the Z component has a negative correlation with the CSC temperature. This is not significant for the X component. By comparison with the old coefficients, $\mathbf{l_{T1x,y,z}}$, the scale factors of both X and Z components at low temperatures have stronger positive correlation with the CSC temperature and also a little bit positive correlation at high CSC temperature.

This result points out that the thermal effects are really complicated and nonlinear and show some thermal hysteresis. Both the correction model and the coefficients are not fully accurate. But within the achievable range the new coefficients are more suitable than the old ones. Note that a signal at 260.5D period comes out, and it should probably not be caused by the temperature. We will come back to this point later.

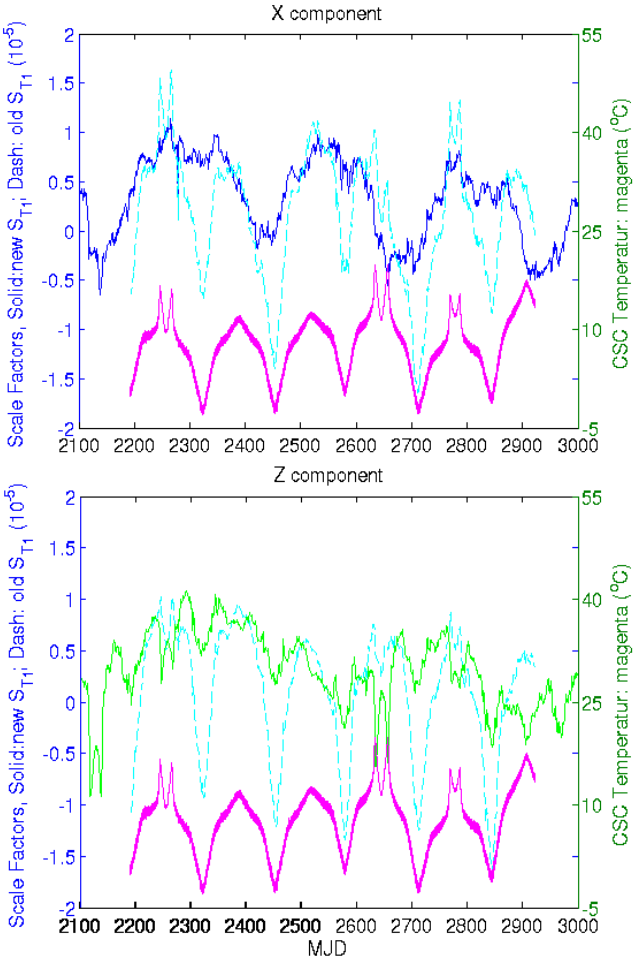

Figure 4.5: Improvement of the scale factor temperature dependence. The FGM sensor temperature is shown as magenta curve; the dashed and solid lines reflect the variation of the scale factors after correction with inital and new temperature coefficients, respectively.

To understand the medium-term ($> 260.5D$) behavior of the scale factors we can average the scale factors after the recalibration over 260 days to eliminate the effects due to local time. The logarithmic long-term time dependence was removed before the recalibration.

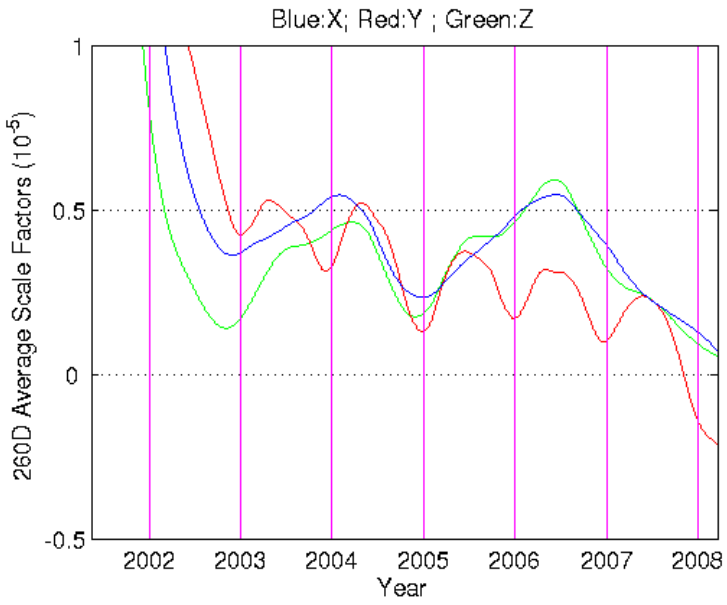

Figure 4.6: Temporal evolution of the scale factors after removal of the logarithmic trend

We can see that at the beginning of the mission the scale factors deviate a little from their logarithmic variation. This may be caused by the change of the environment conditions inside the satellite, for example, humidity and barometric pressure. There is a clear deflection between year 2004 and 2005. This probably illustrates that the applied logarithmic long-term time dependency does not capture the detailed variations.

$$l_0 = l_a + l_b \ln(MJD - MJD_0)$$

l_b may be influenced by some environmental factor. In addition, the Y and Z components exhibit a small cycle per solar year variation, but the X component shows no such a phenomenon. As far as X and Z components are concerned, it means a better temperature correction of X component than Z component. We know that the Y component is less precisely determined than the X and Z components. Our calibration model takes only 9 parameters into account. If there are any other unknown effects or inaccurate coefficients or measurement noise, they will strongly influence the result of the calibration, especially of the Y component. That means, there are some mixture of the error function f_{ins} and f_{sat} or

of the components. Due to this kind of cross-talk, the result of the recalibration may show some dependence on the magnetic field strength itself.

4.1.2 The variation of the offsets

Based on our experience the offsets of the FGM show no strong long-term drift. So we choose the long-term averages, $E_{xo} = 26.970nT$, $E_{yo} = 19.843nT$, $E_{zo} = 21.625nT$ as a standard for correcting the FGM data. After we recalibrate the data, however, the derived offsets are not only due to the FGM sensor but some mixture of the constant part of f_{ins} and f_{sat}. Figure 4.7 shows the variation of the offsets during the years. The day to day variation of the offsets looks more complicated. So we do some averaging and spectrum analysis. The offsets also show a signal correlated with local time. The phase of it starts approximately at 18:00 LT, as we can see from the Figure 4.9 where the data are smoothed by a 60-day moving box-car filter.

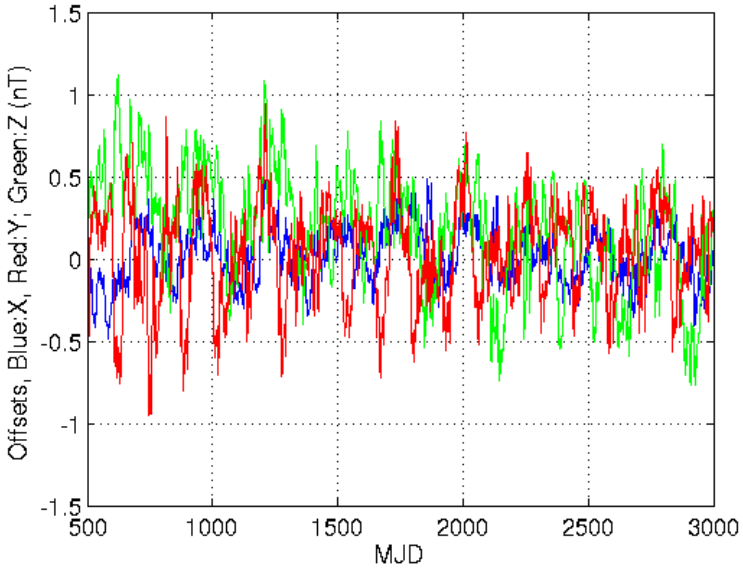

Figure 4.7: Daily averages of the FGM offsets. Mean values are subtracted.

However, the local time has different influences on each component. From FFT analysis we find that the X component opposed to the other two components shows no 130d spectral

peak and all components exhibit large peaks at 260d. The 130d period is much related to the period of the temperature variation. Furthermore, the Z component shows a signal with 365d period. For this component we also perform an averaging over 260 days. The period of one solar year can be seen well in the Z component. Peaks exist at the middle of the years. Obviously different to the X and Y component, a $-0.00024\,nT/d$ drift of the Z component is found. In the mathematical model of calibration the offsets are interpreted as a characteristic of the Fluxgate magnetometer. But practically, it can also be caused by the spacecraft magnetic field at the location of the FGM. These spacecraft fields become part of the offsets which are obtained in the scalar calibration. Therefore, there are three possible reason for the periodical annual signal, the cross-talk caused by unknown effects or the inaccurate instrument model, the variation of the FGM intrinsic offsets caused by the external environment(e.g. excentricity of Earth's orbit around the sun), or the magnetic field variation of the spacecraft caused by the external environment. However, the X and Y components show no such periodical signal, which indicates that, the first and the third suggestions are more reasonable.

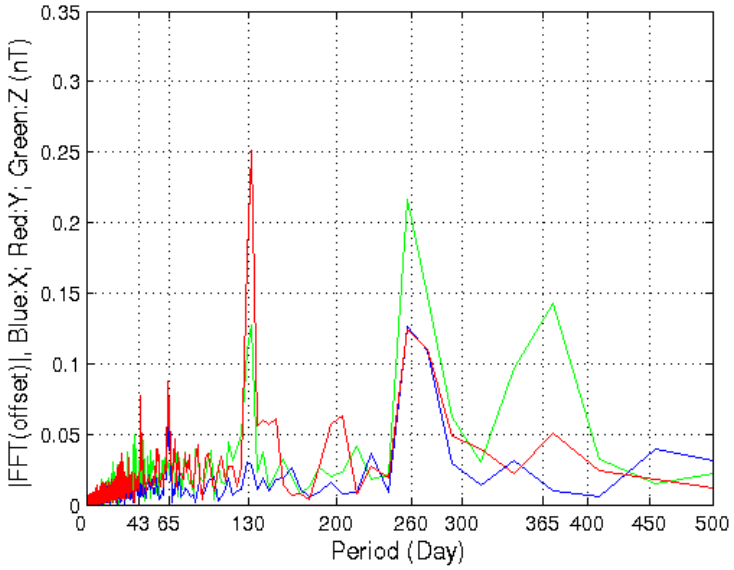

Figure 4.8: Spectra of the FGM offset variations

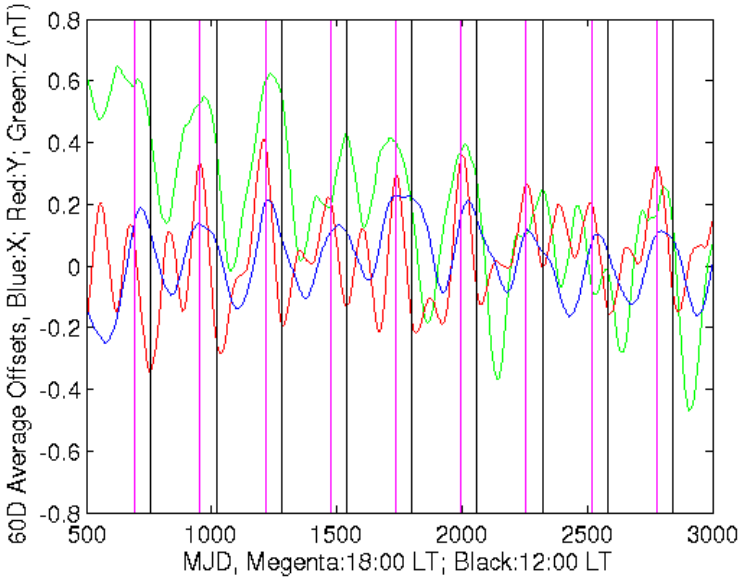

Figure 4.9: Daily average of the FGM offsets, 60-day smoothed. Vertical lines mark certain local times of the orbit plane

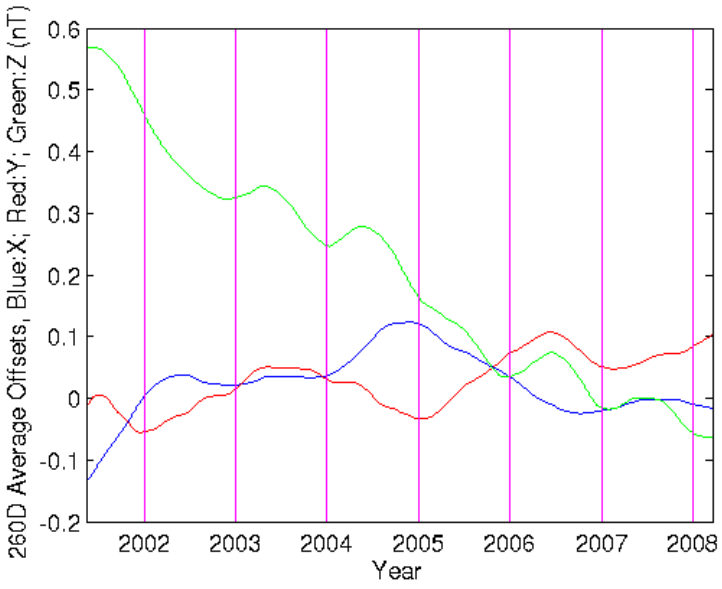

Figure 4.10: Long-term variation of the FGM offsets. Signals have been filtered by a 260d box-car.

Some evidence, we have found, suggests that the offsets are effected by the time standard on CHAMP. We know that every Wednesday the FGM instrument is reset in order to syn-

chronize it with the GPS time standard. From Figure 4.11 we reveal, on some Wednesdays the offsets of the X and Z components show a discontinuous variation. We looked into the FGM and OVM data of the two days, for example, MJD2516 and MJD2517. Visibly, there is a leap of the difference $\triangle B$ between the days, and the amplitude of $\triangle B$ on the two days is clearly different (see Figure 4.12).

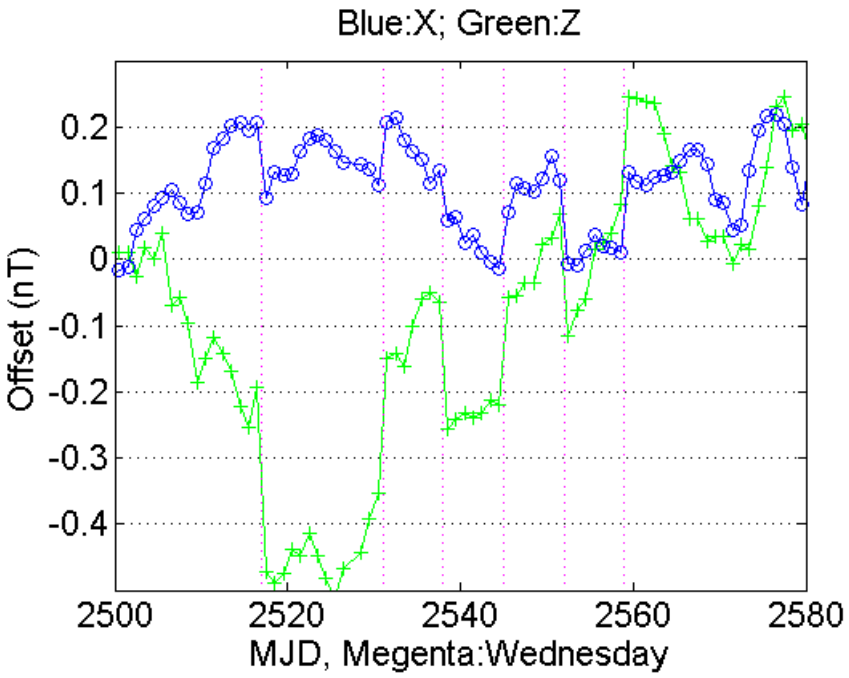

Figure 4.11: FGM offset shifts associated with the weekly reset of the instrument. Vertical magenta lines mark some Wednesdays.

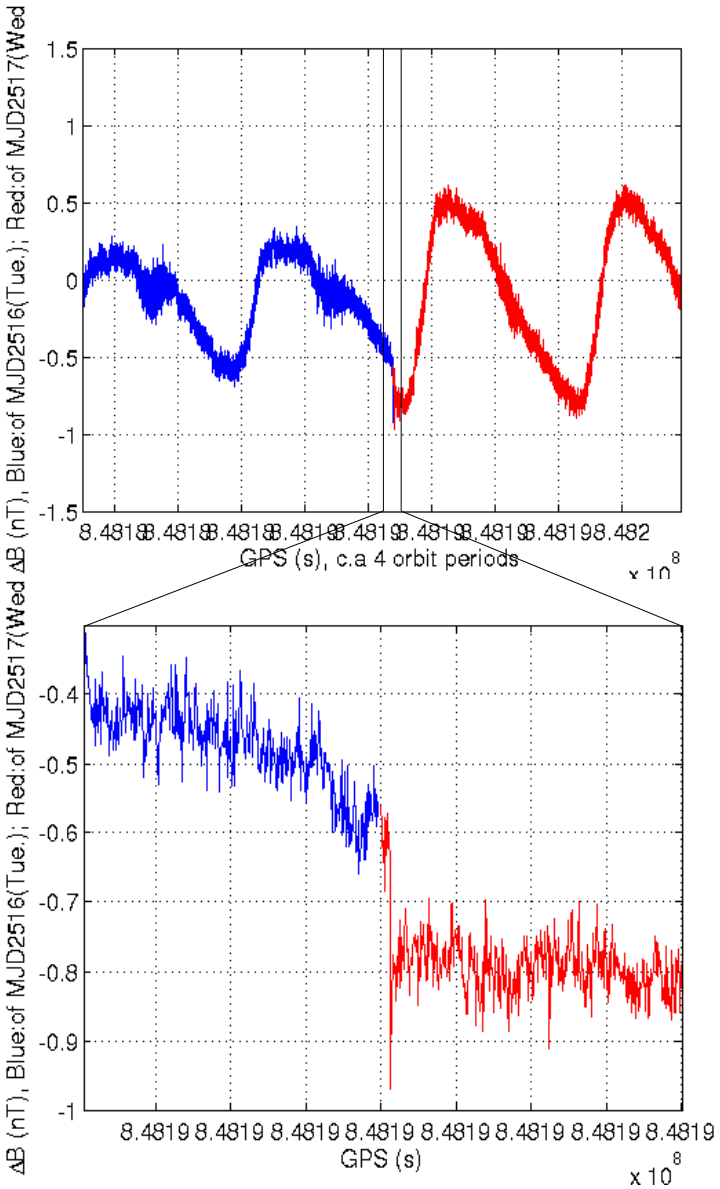

Figure 4.12: Sudden change of the ΔB amplitude at the transition from Tuesday to Wednesday

We find also the effect that the offsets have some relation to the temperature. However, we have found more CSC temperature related cases of Z component than X component. More puzzling is that, the offset of Z component shows sometime positive and sometime negative correlation with the temperature. For values below 13 $°C$ it is negative and for higher temperatures we find positive correlations.

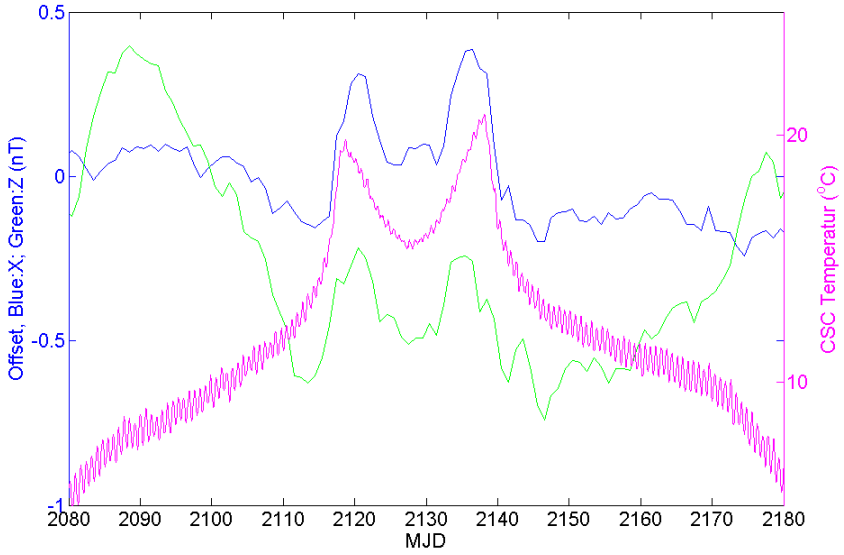

Figure 4.13: Temperature dependent variation of the FGM offsets

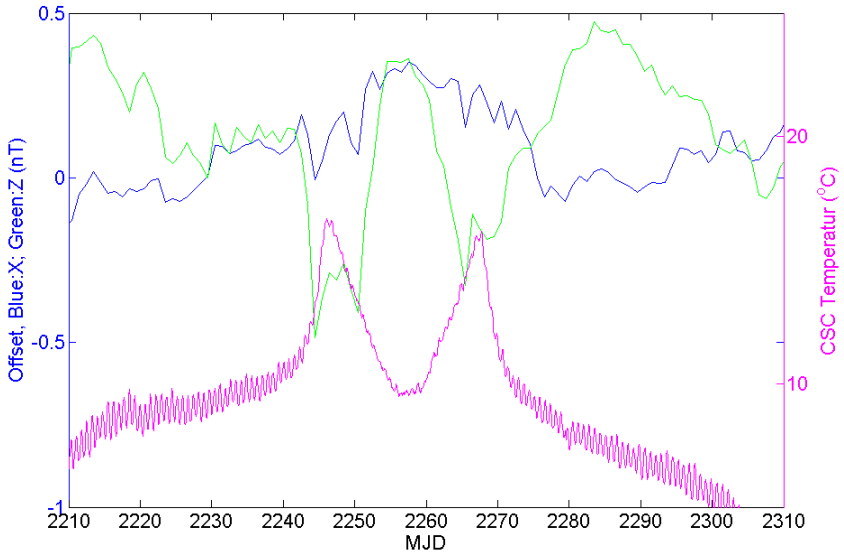

Figure 4.14: Temperature dependent variation of the FGM offsets

4.1.3 The variation of the misalignment angles

Similar to the offsets, the misalignment angles show no long-term drift. We choose for them fixed values, xy: 90.02613, xz: 90.05986, yz: 90.03873, as determined in ground calibrations before launch. After the recalibration we can also see clear signals with 260 days period. The apparent variations of the three components have about the same phase and amplitude, which indicates that the changes of the three angles are homogenous. The peaks appear always at noon. This is possibly due to different orbit local times. The satellite is subject to the different conditions of sunlight, which causes the different distribution of thermal conduction inside the satellite. Consequently, the different thermal expansion may lead to the variation of the sensor misalignment angles with the local time. However, if we explain the variation of the misalignment in such way, the repetition period of this variation should be 130D but not 260.5D, because it depends on the environment temperature. As we have mentioned, the environmental conditions of the satellite in same phase of SS are the same. Particularly, the misalignment angles are technically very stable and should not change so much. Hereby, another possibility is that an orbit dependent change of the spacecraft field is misinterpreted by the scalar calibration as a variation of misalignment angles. Namely, a time signal of f_{sat} is mismatched by the signal e.g. $\frac{B_x B_z}{|B|}$ of f_{ins}. But what is this signal? The question will be answered in the last part of the chapter.

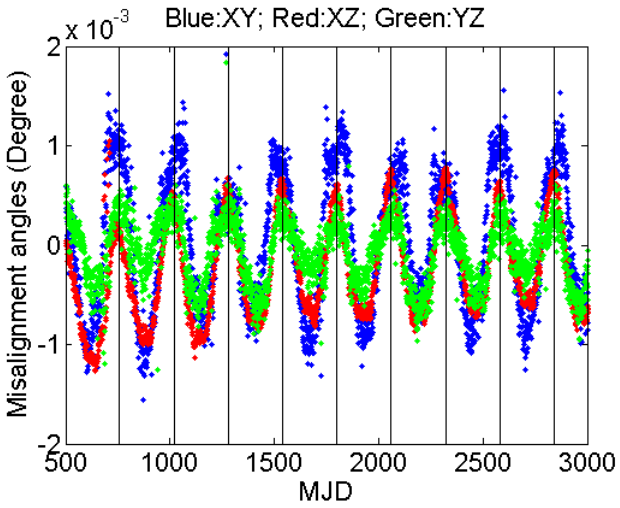

Figure 4.15: Apparent variations of the FGM sensor misalignment angles. The vertical lines indicate an ascending orbit at 12:00 LT

4.2 Cross-talk problem of calibration

In this section two cases of cross-talk that we have found in CHAMP data processing are illustrated, which indicates that cross-talk cannot be avoided in the absence of additional information about scalar error $\triangle B = |E_{fgm}| - |B_{ovm}|$.

4.2.1 Cross-talk between OVM bias and FGM scale factors calibration

So far we believe that there is not any bias in the measurements of the OVM. In order to minimize the residuals between OVM and FGM readings after scalar calibration, we had induced a 0.4 nT bias to the OVM readings in the standard processing.

$$B_{ovm} = B^{'}_{ovm} + \triangle B,\ \triangle B = 0.4nT$$

As a consequence we found this causes a deviation of the three scale factors as the result of the scalar calibration. We review our scalar calibration equation with respect to this effect.

$$B^2_{ovm} \quad = \quad P \bullet M + Q$$

$$P = \begin{pmatrix} p_1 \\ p_2 \\ p_3 \\ p_4 \\ p_5 \\ p_6 \\ p_7 \\ p_8 \\ p_9 \end{pmatrix}^{'} \approx \begin{pmatrix} k_1^2 \\ k_4^2 \\ k_6^2 \\ k_2 \\ k_3 \\ k_5 \\ E^{'}_{x0} \\ E^{'}_{y0} \\ E^{'}_{z0} \end{pmatrix}^{'}, \quad M = \begin{pmatrix} E_x^2 \\ E_y^2 \\ E_z^2 \\ 2E_xE_y \\ 2E_xE_z \\ 2E_yE_z \\ 2E_x \\ 2E_y \\ 2E_z \end{pmatrix}$$

From this equation we know that the steady component of B^2_{ovm} is mostly compensated by the terms E_x^2, E_y^2, E_z^2 which have a large constant parts. Now the equation is rewritten as,

Figure 4.16: Influence of the introduced OVM bias on the FGM scale factors: Solid line (scale factors as derived from standard processing), dashed line(scale factors after removal of OVM bias). Thin magenta line (logarithmic fit to the temporal change of the scale factors). The inserts how the details around the introduction of the OVM bias(at MJD1450)

$$\begin{aligned}(B_{ovm} + \triangle B)^2 &\approx B_{ovm}^2 + 2\triangle B B_{ovm} \\ &\approx P \bullet M + Q\end{aligned}$$

This additional term on the left side, $2\triangle B B_{ovm}$, which has a large constant parts too, will be mainly compensated by a mismatch of the scale factors. In Figure 4.16 we see clearly an abrupt change where we have began to induce 0.4 nT bias correction at MJD 1450. In fact, the conclusion we have drawn in the Chapter 3, the drift of $\triangle B(B_{fgm} - B_{ovm})$ shows a strong correlation with the scale factors, has hinted at this cross-talk problem. This means, the scalar calibration cannot distinguish a synchronous change of three scale factors from a direct bias change of the OVM readings.

4.2.2 Cross-talk between FGM/OVM time lag and FGM misalignment angles

Another strong cross-talk can occur in the calibration of misalignment angles. We see in Figure 4.17 that the variations of the product $B_x B_z$ are very similar to the signal of $\triangle B_{ovm}/\triangle t$. The correlation coefficients is approximately 0.8868. That means if they both have influences on the measurement we cannot use the scalar calibration to isolate them uniquely.

$$\begin{aligned}(B_{ovm} + t_s \frac{\triangle B_{ovm}}{\triangle t})^2 &\approx B_{ovm}^2 + 2t_s \frac{\triangle B_{ovm}}{\triangle t} B_{ovm} \\ &\approx P \bullet M + Q\end{aligned}$$

From this equation, we know that if an asynchronism between the FGM and OVM measurements occurs, due to the similarity of the two terms, the time shift t_s will be compensated by the term $E_x E_z$ via the parameter p_5. We can calculate the cross-talk quantitatively, $\triangle t_s/\triangle k_3 \approx (\frac{\triangle B_{ovm}}{\triangle t} B_{ovm})/E_x E_z \approx 0.002$, that means a 10ms time lag between the measurements of FGM and OVM will be matched by an extra $-4.1''$ misalignment angle change between the X and Z axes of FGM.

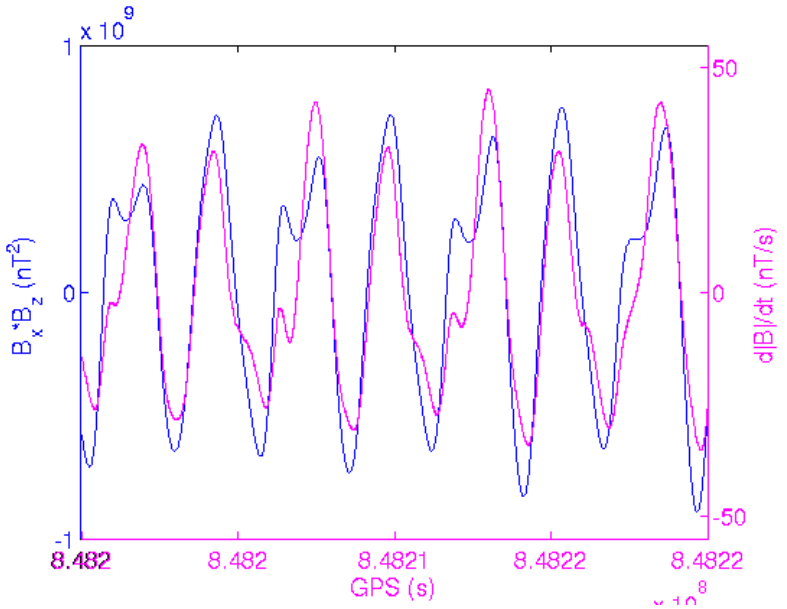

Figure 4.17: Equivalence of time shift between FGM and OVM with a misalignment angle between the X and Z axes

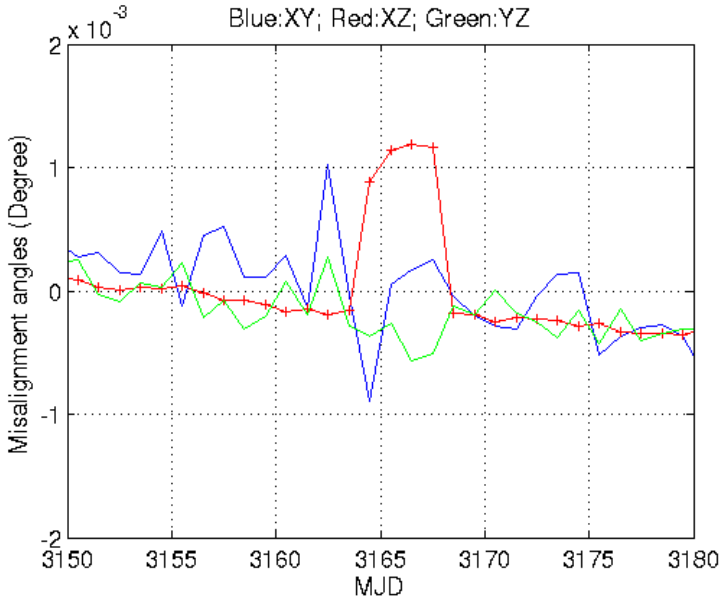

Figure 4.18: Apparent variation of the FGM sensor misalignment angles. The obvious deflection of the XZ angles (red curve) is a misinterpretation of a timing difference between FGM and OVM by 12 ms

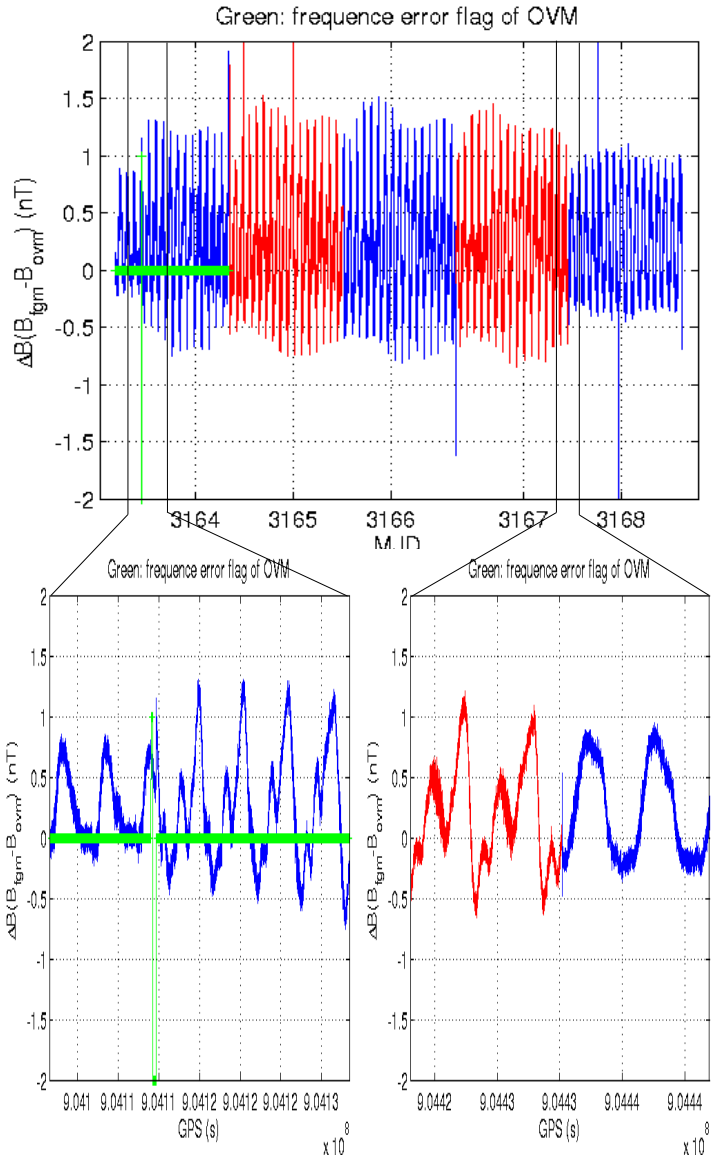

Figure 4.19: Response of the ΔB signal to a time lag of 12 ms between FGM and OVM measurements. At the time of the green curve deflection (lower left frame) the time error occurs and ΔB becomes larger. After reset of the FGM (lower right frame) the ΔB signal is restored.

An example from 2008 can disclosure the relationship between the misalignment angle calibration and the time error of the instruments. Notice in Figure 4.18 that from MJD 3164 to MJD 3167 the XZ misalignment angle of the scalar calibration shows some kind

of extraordinary values. If we look into the FGM and OVM data, we find that these are not caused by a variation of the XZ misalignment angle but a certain time error in the timing of the FGM. We can see in Figure 4.19 that on MJD3164 the pattern of $\triangle B$ shows an abrupt change when the GPS-controlled frequency of the OVM gives a error signal. Although the error flag disappeared, the strange pattern continues to the MJD3168. MJD3168 is a Wednesday. This means the disturbed GPS signal has also caused a timing error of FGM. After the FGM was synchronized to the external GPS signal by an instrument reset the pattern of $\triangle B$ was restored. But this kind of time error will be misinterpreted as a XZ misalignment angle by the scalar calibration.

4.3 Orbit synchronous disturbing magnetic fields from satellite

So far we have analyzed the recalibrated parameters and the cross-talk problem. The results show that the 9-parameter scalar calibration is somewhat unsuitable to model the errors of the magnetometers. Especially, the variation of the misalignment angles implicate that there must be some mixture of the error function f_{ins} and f_{sat} in the calibrations. In order to find f_{sat}, we review our scalar error equation,

$$\begin{aligned} \triangle B &= |E_{fgm}| - |B_{ovm}| \\ &= \frac{B_x}{|B|}(f_{insx} + f_{satx}) + \frac{B_y}{|B|}(f_{insy} + f_{saty}) + \frac{B_z}{|B|}(f_{insz} + f_{satz}) + f_{ovm} \end{aligned}$$

Because the OVM shows technically little error, and the Y component is always much smaller than the other two, we simplify the equation as follows,

$$\begin{aligned} \triangle B &= |E_{fgm}| - |B_{ovm}| \\ &= \frac{B_x}{|B|}(f_{insx} + f_{satx}) + \frac{B_z}{|B|}(f_{insz} + f_{satz}) \end{aligned} \tag{4.1}$$

Function f_{ins} gives the error of the FGM sensor itself and represents its characteristic. So f_{ins} is a function of the measured signal and the characteristic parameters, p.

$$f_{ins} \quad = \quad f_{ins}(B_x,\ B_y,\ B_z,\ p)$$

Parameters p are constant or influenced by the environmental condition. Function f_{sat} is more probably a function of time t in orbit or SD and it represents the disturbance from the satellite body.

$$f_{sat} \quad = \quad f_{sat}(t - t_0)$$

However, our measurements of the magntometer $(B_x,\ B_y,\ B_z)$ are not independent of the time t in orbit. The measurements are taken along the orbit of the satellite. The weight of the component $\frac{B_x, B_z}{|B|}$in Eq.(4.1) can be a function of $(B_x,\ B_y,\ B_z)$ as well as of t in orbit. However, if f_{sat} is absent , the $\triangle B$ is only a function of $(B_x,\ B_y,\ B_z,\ p)$. We can take an example to see whether there is f_{sat} or not. We choose the data of MJD2852(LC, 10:54) and MJD2979(LC, 23:10) which both are in the cold SS and have average CSC temperature 3.0^oC, so p should be the same. However the misalignment angles of recalibration are totally different (0.000534^o for MJD2852 and -0.000649^o for MJD2979) and located in the variation curve at maximum section and minimum section, respectively.

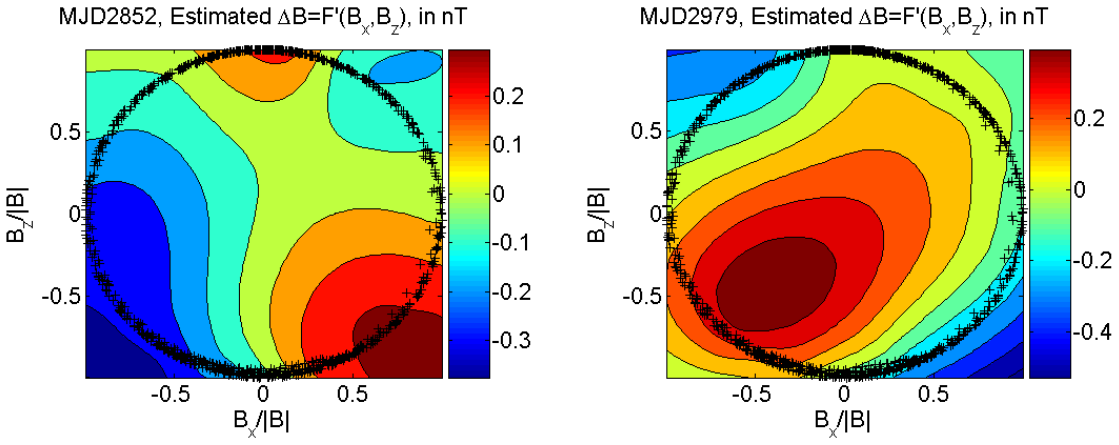

Figure 4.20: Estimated function ΔB, Black cross indicate the locations of measurement points.

We can see in Figure 4.20, the $\triangle B$ of two days are very different. This means, we need an extra f_{sat} to compensate $\triangle B$. And this $f_{sat}(t-t_0)$ is misinterpreted as misalignment angles in the recalibration. Another hint is that, if we draw a plot of $\triangle B$ versus $\frac{B_z}{|B|}$, we can see clearly two straight lines. Here we have used the conclusion of chapter3, namely, the Z offset plays important role in the disagreement between OVM and FGM, although it is not so rigid.

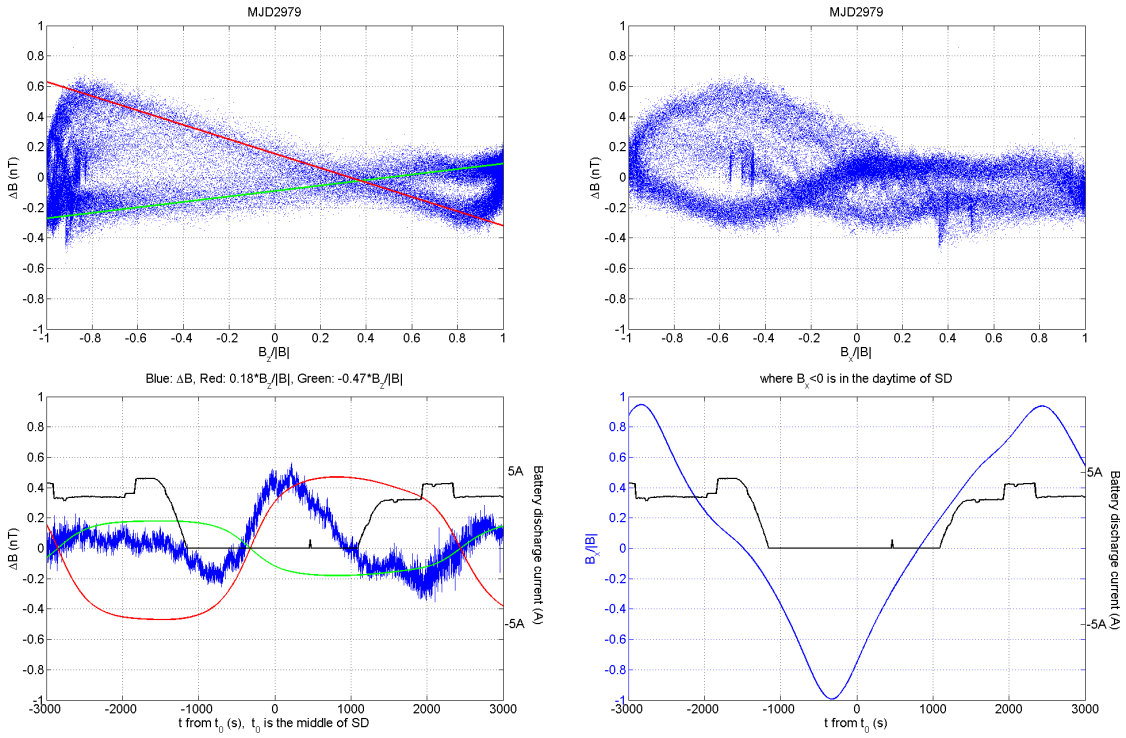

Figure 4.21: Dependence of ΔB on various parameters. upper left panel: the slope of red is -0.47nT and of green is 0.18nT; lower left: At different t, f_{sat} shows different values; upper right: the error mostly occur where $B_x < 0$; lower right: where $B_x < 0$ is also in the daytime

It seems function $f_{sat}(t-t_0)$ has a simple approximate form,

$$f_{sat}(t-t_0) = \begin{cases} O_{sat\_d} & , \ t \in daytime\ of\ SD \\ \\ O_{sat\_n} & , \ t \in nighttime\ of\ SD \end{cases}$$

Where O_{sat_d} and O_{sat_n} are constant. Therefore function $f_{sat}(\tau)$, $\tau = t - t_0$ is an even function and a quasi square wave signal due to the day-time and night-time alternation, which duty cycle is,

$$D = \frac{\tau}{T}$$

where

τ is the duration of the daytime in SD;

T is the period of the satellite orbit(SD).

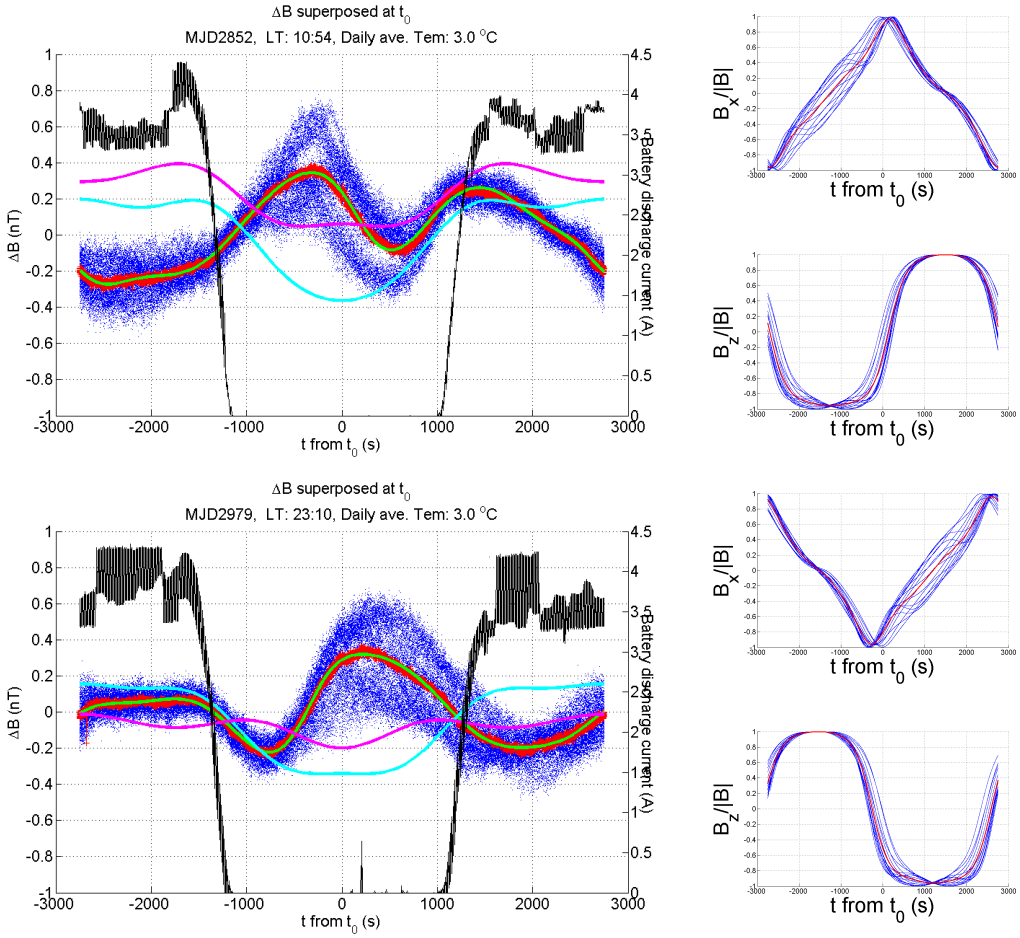

Figure 4.22: Black: Battery discharge current indicates the daytime and nighttime; Magenta: solution of f_{satx}; Cyan: solution of f_{satz}; Red on the left panel: the measured avg. scalar error; Green: the simulated scalar error with the solution; right panel: error propagation term of the components

If we simply use the group of cos functions to simulate $f_{sat}(t-t_0) = a_0 + \sum_{k=1}^{N} a_k \cos[k\frac{2\pi}{T}(t-t_0)]$, we get result showed in the left panel of Figure 4.22. We can see that the solutions of f_{satx}, f_{satz}show the same variation due to the day-night alternation. Although we have neglected the f_{saty}, we can imagine, it will show a similar variation. The right panel of Figure 4.22 shows the corresponding error propagation terms $\frac{B_x}{|B|}$, $\frac{B_z}{|B|}$. Here we take them as the function of t. Intuitively, it explains why around local time 24:00 and 12:00 the misalignment angles show respectively minima and maxima. In cold SS $D = \frac{\tau}{T} \approx 0.4$, the daytime is shortest. The dynamic part of the disturbance signal f_{sat} shows maximal similarity to the signal $\frac{B_x}{|B|}$ with positive and negative correlation. Accordingly, in the 9-parameter recalibration, e.g. the error $\frac{B_z}{|B|} f_{satz}$ is strongly compensated by the term $\frac{B_x B_z}{|B|}$ with positive and negative parameters which represents the error from misalignment angles. Obviously, when in hot SS, $D = \frac{\tau}{T} = 1$, the disturbance signal f_{satz} is constant and compensated by $\frac{B_x B_z}{|B|}$ least of all. Such cross-talk causes the regular 260.5D periodical signal with maxima at 12:00 and 18:00 in the variation of misalignment angles and offsets, respectively, which are derived in the 9-parameter recalibration. Due to the same reason, e.g. $\frac{B_x}{|B|} f_{satx}$ is prone to be compensated by $\frac{B_x B_x}{|B|}$ which represents an error in the scale factor of the X component. In section 4.1.1 we mentioned a 260.5D period of the scale factor. Here, we give the answer. However, both error models cannot separate the constant parts of the f_{ins} and f_{satz} in the absence of extra information. Actually, we can see the example in Figure 4.23, the offsets of the 9-parameter recalibration makes an average estimate of $f_{ins} + f_{satz}$. Only the dynamic part of the solution f_{satz} is certain in f_{satz}.

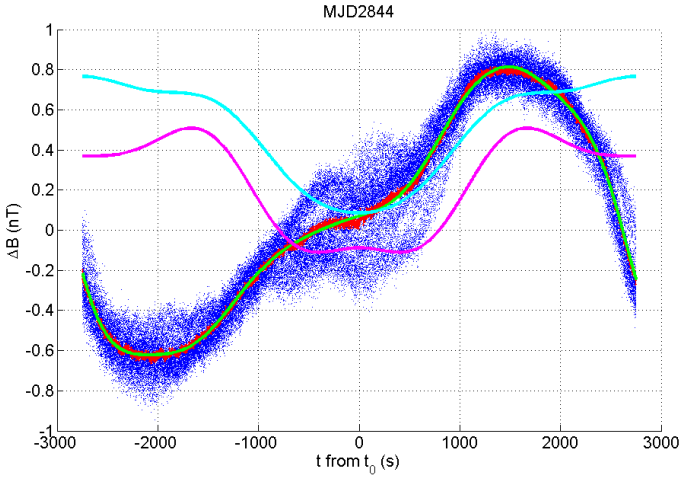

Figure 4.23: Diurnal variation of ΔB and disturbances from the X, Z component. Magenta: solution of f_{satx}; Cyan: solution of f_{satz}; Red: measured avg. scalar error; Green: the simulated scalar error with the solution; the offset of the component X and Z from the 9-parameter recalibration is respectively 0.131nT and 0.477nT

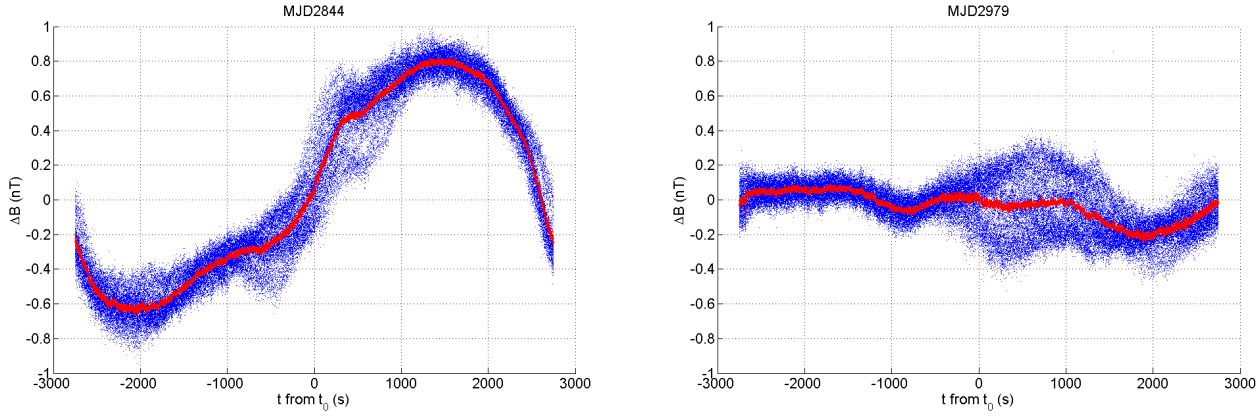

Figure 4.24: Two examples of ΔB, FGM data correted for the dynamic part of f_{sat}

Physically and technically, this dynamic part of f_{sat} is easy to explain. The daytime and nighttime alternation results in the switch of the power supply system, from solar cell to battery supply or from battery to solar cell supply, which leads to the different disturbance magnetic field from the current circuits inside of the satellite in the daytime and nighttime.

If we reevaluate Eq.(3.6) in section 3.5 with this result,

$$std^2(\triangle B) = 0.6655 Z_0^2 + 0.0390 nT^2$$

Here Z_0 should be the constant parts of the f_{ins} and f_{satz}. As regard to the term $0.0390 nT^2 (std \approx 0.2 nT)$, the dynamic part of f_{sat} contributes most of it. That means, if Z_0 and f_{sat} correction are fully achieved, the standard deviation of scalar error $\triangle B$ remains around $0.1 nT$

Chapter 5

Conclusion

The questions raised about the calibration processing of CHAMP magnetometers at the beginning of this work can be answered now. They are, for example: How is the standard calibration processing performed, why do we need 15-day scalar calibration, why don't we exercise scalar calibration everyday to achieve better data, why do the calibration parameters show some variation related to local time of the orbit, which calibration parameters play important roles in the data quality and how to quantitatively describe this relationship, finally how much is the remaining uncertain in FGM data?

We know that the OVM reading is our standard for calibration of the FGM reading. The disagreement between the OVM and the FGM readings indicates how much uncertainty is in the FGM readings. However, this disagreement shows a temporal variation, which discloses that the calibration parameters have a time dependence. For this reason, the regular scalar calibration is used to update the calibration parameters to remove this time dependence. From all the calibration parameters, the long-term behavior of the scale factors of the FGM plays a very important role. Consequently, we have found a right model (logarithmic evolution for scale factors, constant for other parameters) to describe these long-term behaviors. As a result, the disagreement between the OVM and the FGM readings during the whole mission can be limited to $\pm 1nT$ without scalar calibration. This demonstrates, our magnetometers on CHAMP exhibit a very good stability.

The scalar calibration is based on an error model of a simple linear vector magnetometer. Although, we can do daily scalar calibration, it only gives numerically the calibration parameters but doesn't provide physical explanations for the variations. We even can extend this

error model, as mentioned first in chapter 3, we take account of, for example, temperature, non-linearity, timing error etc. On account of more frequent and extended scalar calibration we can definitely get very small differences between the FGM and OVM data. The scalar calibration is robust and rough, but fails if there are cross-talk problems or short periodic (<1day) error. However, we extend the error model with the time-variation function and fix the error source on the power supply system of the satellite. The daytime and nighttime alternation results in the switch of the power supply system, from solar cell to battery or from battery to solar cell, which leads to the different disturbance fields of the currents inside of the satellite in the daytime and nighttime. Such disturbance fields are mismatched in the 9-parameter calibration, which brings the false local time related variation of the calibration parameters.

As for the CHAMP case, we have found, the Z component offset of the FGM plays a very important role in the data quality. Although many effects have influence on the Z offset and it is difficult to get a forward model to derive the Z offset, the relationship between Z offset and the standard deviation of the disagreement $\triangle B$ is established in section 3.5. This confirms that we can neglect the other effects or cross-talk problem to estimate the right daily Z offset correction from the standard deviation of $\triangle B$. If we have done a daily Z offset correction, the $\triangle B$ is limited to $\sim\pm 0.5nT$(equivalent to std $\sim 0.2nT$ for the CHAMP case). This expresses that all the uncertainty or the errors of the FGM vector data are smaller than $\sim 0.5nT$ after our reliable calibration. Furthermore, if the disturbance fields of the satellite body are fully corrected, the standard deviation of the scalar error, $\triangle B$, remains about $0.1nT$.

Finally, some thesis-induced questions and some suggestions for further satellite magnetic field observation projects are presented. The main error source of magnetic field measurement on CHAMP are temperatures, GPS time errors and the disturbance field of the satellite body, especially, the power supply system. Therefore, a more rational symmetric configuration design is desired to keep the FGM from the disturbance field of the satellite body or to decrease the disturbance field to a lower level. More stricter laboratory tests to evaluate the disturbance field of a spacecraft and thermal calibration to examine the thermal coefficients of the fluxgate sensors are worth the effort, as well for the project in the future. For the on board scalar calibration, a highly precise (<1ms) time synchronization system is needed for the combination of FGM and OVM measurement.

Bibliography

[1] B.J. Anderson, L.J. Zanetti, D.H. Lohr, J.R. Hayes, M.H. Acuna, C.T. Russell, T. Mulligan, "In-flight calibration of the NEAR magnetometer", IEEE Transactions on Geoscience and Remote Sensing, Vol. 39, No. 5, 907-917, doi:10.1109/36.921408, 2001.

[2] D.A. Lohr, L.J. Zanetti, B.J. Anderson, T.A. Potemra, J.R. Hayes, R.E. Gold, R.M. Henshaw, F.F. Mobley, D.B. Holland, M.H. Acuña, J.L. Scheifele, "Near Magnetic Field Investigation, Instrumentation, Spacecraft Magnetics and Data Access", Space Science Reviews, Vol. 82, No. 1-2, 1997.

[3] D. Gebre-Egziabher, G.H. Elkaim, J.D. Powell, B.W. Parkinson, "A non-linear, two-step estimation algorithm for calibrating solid-state strapdown magnetometers", 8th Saint Petersburg International Conference on Integrated Navigation Systems, St. Petersburg Russia, 290-297, 28-30 May 2001.

[4] Eberhard Pulz, Hans-Ulrich Auster, Monika Korte, Hans-Joachim Linthe, "Experiences with a New Method for the Absolute Component Determination of the Earth's Magnetic Field", Journal of Electrical Engineering, Vol. 55. No. 10/S, 53-57, 2004.

[5] Fritz Primdahl, Torben Risbo, J.M.G. Merayo, Peter Brauer, Lars Tøffner-Clausen, "In-flight spacecraft magnetic field monitoring using scalar/vector gradiometry", Measurement Science and Technology, Vol. 17, No. 6, 1563-1569, doi: 10.1088/0957-0233/17/6/038, 2006.

[6] K. Gödderz, H. Lühr, M. Rother, R. Bock, "CHAMP Optical Bench Star Camera/Vector Magnetometer Inter-Calibration", Workshop on Calibration of Space-Borne Magnetome-

ters, TU-Braunschweig, March 9 1999, in: "Ground and In-Flight Space Magnetometer Calibration Techniques", eds: A. Balogh and F. Primdahl, ESA SP-490, 2002.

[7] J.M.G. Merayo, F. Primdahl, P. Brauera, T. Risbo, N. Olsen, T. Sabaka, "The orthogonalization of magnetic systems", Sensors and Actuators A: Physical, Vol. 89, 185-196, doi:10.1016/S0924-4247(00)00515-X, 2001

[8] J.M.G. Merayo, P. Brauer, F. Primdahl, J.R Petersen, O.V. Nielsen, "Scalar calibration of vector magnetometers", Measurement Science and Technology, Vol. 11, 120-132, doi: 10.1088/0957-0233/11/2/304, 2000.

[9] J.M.G. Merayo, P. Brauer, F. Primdahl, J.R. Petersen, "Absolute magnetic calibration and alignment of vector magnetometers in the Earth's magnetic field", Workshop on Calibration of Space-Borne Magnetometers,TU-Braunschweig, March 9 1999, submitted to ESA-SP 1999A.

[10] John Crassidis, Kok-Lam Lai, Richard Harman, "Real-Time Attitude-Independent Three-Axis Magnetometer Calibration", Journal of Guidance, Control, and Dynamics, Vol. 28, No. 1, 115-120, 2005.

[11] Mario H. Acuña, "Space-based magnetometers", Review of scientific instruments, Vol. 73, No. 11, 2002.

[12] Martin Rother, Sungchan Choi, Wolfgang Mai, Hermann Lühr, David Cooke, "Status of the CHAMP ME data processing", Earth Observation with CHAMP(Results from three years in orbit), ISBN: 3-540-22804-7, Springer, 2005.

[13] Nils Olsen, Lars Tøffner-Clausen, Terence J. Sabaka, Peter Brauer, Jose M. G. Merayo, John L. Jørgensen, J.-M. L´eger, Otto V. Nielsen, Fritz Primdahl1, Torben Risbo, "Calibration of the Ørsted vector magnetometer", Earth Planets Space, Vol. 55, 11–18, 2003.

[14] Nils Olsen, T. Risbo, P. Brauer, J.M.G. Merayo, F. Primdahl, T. Sabaka, "In-flight Calibration Methods Used for the Ørsted Mission", Workshop on Calibration of Space-Borne Magnetometers, TU-Braunschweig, March 9 1999, in: "Ground and In-Flight

Space Magnetometer Calibration Techniques", eds: A. Balogh and F. Primdahl, ESA SP-490, 2002.

[15] P. Brauer, J.M.G. Merayo, O.V. Nielsen, F. Primdahl, J.R. Petersen, "Transverse field effect in fluxgate sensors", Sensors and Actuators A: Physical Vol. 59, Issues 1-3, 70-74, 1997.

[16] P. Brauer, J.M.G. Merayo, T. Risbo, F. Primdahl, "Magnetic calibration of vector magnetometers: linearity, thermal effects and stability", Workshop on Calibration of Space-Borne Magnetometers, TU-Braunschweig, March 9 1999, in: "Ground and In-Flight Space Magnetometer Calibration Techniques", eds: A. Balogh and F. Primdahl, ESA SP-490, 2002.

[17] P. Brauer, T. Risbo, J.M.G. Merayo, O.V. Nielsen, "Fluxgate sensor for the vector magnetometer onboard the Astrid-2 satellite", Sensors and Actuators A, Vol. A81, 184-188, 2000

[18] Robert C. Snare, "A History of Vector Magnetometry in Space", Measurement Techniques in Space Plasmas-Fields: Geophysical Monograph, Vol. 103. 101-104, 1998.

[19] Y.V. Kim, K.J. Di Filippo, A. Ng, "On the Calibration of Satellite On-Board Magnetometer", Control and Automation, 2003. ICCA apos;03. Proceedings. 4th International Conference, 947 - 951, ISBN: 0-7803-7777-X, June 10-12 2003.

CHAMP Internal Documentations

[20] H. Lühr, L. Grunwaldt, Ch. Förste, CHAMP Reference Systems, Transformations and Standards, CH-GFZ-RS-002, 2002.

[21] H. Lühr, M. Rother, R. Bock, Magnetic Calibration of the CHAMP Boom Instrumentation Report and Results, CH-GFZ-TR-2602, 2000.

[22] H. Lühr, R. Bock, M. Rother, CHAMP Magnetic Test Report, CH-GFZ-TR-2000, 2000.

[23] H. Lühr, R. Bock, M. Rother, Overhauser Magnetometer Performance Test Report, CH-GFZ-TR-2501, 1999.

Acknowledgements/Danksagungen

An erster Stelle möchte ich ganz herzlich Herrn Prof. Dr. Hermann Lühr für die enthusiastische Betreuung danken!

Mein Dank gilt auch den Kolleginnen und Kollegen von GFZ Sektion 2.3, insbesondere der CHAMP-Magnetfelddaten Processing Gruppe, darunter Dr. Martin Rother, Wolfgang Mai, Dr. Choi, Sungchan, Jan Rauberg, Ingo Michaelis.

Bei Herrn Prof. Dr. Matthias Holschneider und Frau Prof. Dr. Mioara Mandea möchte ich mich für die Vorschläge und Mithilfe bedanken.

Darüber hinaus gebührt mein Dank Dr. Stefanie Rentz, Dr. Zou, Yong, Kathrin Häusler, Teti Zubaidah für die vielen praktischen und pragmatischen Tips and Erfahrungen!

Prof. Ma, Shuying hat mich unterstützt und motiviert. Hierfür bedanke ich mich sehr.

Für die finanzielle Unterstützung möchte ich, an dieser Stelle, der Hanns-Seidel-Stiftung, China Scholarship Council, Helmholtz-Zentrum Potsdam Deutsches GeoForschungsZentrum GFZ meinen Dank aussprechen.
Von ganzem Herzen bedanke ich mich meinen Eltern, die mich stets tatkräftig unterstützt haben!

Abschließend geht mein Dank an den Chinesischen Akademikerchor Berlin für die wunderschöne gemeinsame Freizeit während meines wissenschaftlichen Aufenthalts in Deutschland.